Development of pH-responsive multi-layered membranes based on flavylium salts and marine-origin polysaccharides for food spoilage monitoring

Mariana Salomé Nunes da Cunha
Chemistry Masters degree
Department of Chemistry and Biochemistry
2023

Supervisor
Professor Doctor Luís Miguel Neves Ferreira Serra Cruz, REQUIMTE/LAQV researcher, Faculdade de Ciências da Universidade do Porto

Co-supervisor
Professor Doctor Nuno Filipe da Cruz Batista Mateus, Associate Professor, Faculdade de Ciências da Universidade do Porto


U.PORTO
FACULDADE DE CIÊNCIAS
UNIVERSIDADE DO PORTO

Dedicated to my furry life partner

Acknowledgements

I would like to thank to everyone involved in this work and to everyone who supported me during all these years.

To my advisor, Professor Doctor Luís Cruz, for all the support and knowledge, and above all, I appreciate the opportunity and trust offered by allowing me to collaborate with him on this project.

To my co-advisor, Professor Doctor Nuno Mateus for having given me the confidence to carry out this work.

To professor João Rodrigues of CICECO, University of Aveiro, for all the help and support in the membranes fabrication and for the QCM-D and SEM analysis.

To Dr. Zélia for her assistance during the mass spectrometry analysis. To Mariana Andrade for all the NMR analysis she performed, to Claúdia Alves for all help and patience in all FTIR-ATR experiments.

To all elements of FoodPhenoLab, for the warm reception and for all the laughs. A special thanks to Sofia, my co-worker. Thank you for everything that you taught me and for your tolerance with me over the last almost two years.

To the friends that FCUP brought me, and to those I met throughout my life: you are the family that I chose. Thank you for being in my life and for making it a more beautiful story to tell.

To Afonso. Thank you always being there for me, for always adding joy to my daily boring life, for everything.

To my brothers and to my parents, for giving me the opportunity to enter in a Chemistry degree and for the councils. Without you, this journey would not have been possible. I hope I made you proud with this.

Resumo

A comunidade científica mundial apresenta cada vez mais interesse em embalagens inteligentes, que é uma nova aplicação que fornece aos consumidores informações visuais e rápidas sobre o estado de conservação de um determinado produto. Tendo isto em conta, foram sintetizados pigmentos, derivados de antocianinas, nomeadamente pirano-3,7-desoxiantocianinas, que têm a capacidade de mudar a sua cor em função do pH do ambiente em que estão inseridos, através dos diferentes estados de equilíbrio das espécies. Assim, ao conjugar covalentemente esses pigmentos com uma matriz polimérica natural, é viável a criação de membranas indicadoras de pH que podem ser incluídas em embalagens de alimentos.

Na primeira parte deste trabalho efetuaram-se as sínteses de pigmentos derivados de antocianinas (Flavílio e Piranoflavílio) contendo um grupo azida, 4'-azido-5,7-dihidroxi-4-metilflavílio, com um rendimento superior a 2% e 10-azidopropil-4'-hidroxipiranoflavílio, com um rendimento de 10%. Posteriormente realizou-se a funcionalização química em Quitosano modificado com grupos alcino terminais através da reação de cicloadição azida-alcino catalisada por cobre (CuAAC), também conhecida como "Química de *Click*". Todos os compostos e conjugados sintetizados foram totalmente caracterizados utilizando análises de HPLC, LC-DAD/ESI-MS, e espectroscopia FTIR-ATR, RMN, UV-VIS. Estas estratégias foram também essenciais para monitorizar todas as sínteses realizadas e determinar as suas condições ótimas de reação.

A segunda tarefa deste projeto passou pela construção de membranas multicamada indicadoras de pH usando a tecnologia de montagem camada-a-camada, (do inglês *Layer-by-Layer* (*LbL*)) através de um robot. Para a síntese das membranas foi utilizado Quitosano modificado (4 e 25% com grupos alcino terminais) funcionalizados com os pigmentos e o polímero Alginato (ALG), que atuou como polímero de carga superficial negativa, e crucial para formação de membranas através de interações eletrostáticas. A formação de filmes multicamada foi primeiramente monitorizada *in situ* através da técnica de Microbalança de Cristais de Quartzo com Dissipação (QCM-D) onde através da diminuição da frequência de ressonância e aumento do fator dissipação, foi possível concluir que a adsorção dos polieletrólitos ao substrato de ouro foi bem sucedida. Efetuaram-se ainda ensaios de DLS (*Dynamic Light Scattering*), verificando, dessa forma, as cargas dos conjugados: Quitosano modificado a 25 % apresentou um valor de 23,3 ± 0,7 mV, o Alginato apresentou um valor de -24,5

± 0,4 e o conjugado Quitosano-Flavílio um valor de 32,9 ± 3,1. O conjugado Quitosano-Piranoflavílio apresentou um valor de 21,8 ± 0,5 e o Quitosano modificado a 4 %, 20,6 ± 0,5 permitindo aferir que a fabricação desse tipo de membrana seria favorável. As membranas multicamada Quitosano-Flavílio/Alginato foram obtidas com auxílio de um robot de deposição automático usando polipropileno como substrato e seguindo condições de construção descritas em trabalhos publicados na literatura. As membranas destacadas foram submetidas a uma variedade de testes de morfologia, durabilidade e robustez, incluindo SEM (*Scanning Electron Microscopy),* espessura, teor de humidade e solubilidade em água.

Palavras-chave: Polifenóis, antocianinas, tecnologia *Layer-by-Layer*, embalagens inteligentes, pigmentos sensíveis a pH, membranas.

Abstract

The scientific community worldwide is becoming more and more interested in smart packaging, which is a new application that provides customers with visible and practical information on the conservation state of a certain product since consumers are increasingly concerned about the conservation and physical-chemical state of the foods. Taking this into consideration, anthocyanin-derived pigments, namely pyrano-3,7-deoxyanthocyanins, were produced, which have the capacity to change colour based on the pH of the environment in which they are present, displayed by different equilibrium species. Thus, by combining these pigments with a natural polymeric matrix, it is feasible to create pH indicator membranes that may be included into packaging and provide visual information of the conservation state of foods.

The aim of this work was to rationally design flavylium-type and pyranoflavylium-type containing an azide group, 4'-azide-5,7-dihydroxyflavylium with a > 2 % yield and 10-azidepropyl-4'-hydroxypyranoflavylium with a 10 % yield, for further functionalization onto alkyne-modified Chitosan through copper-catalyzed azide-alkyne cycloaddition (CuAAC), also known as "Click Chemistry". Through that methodology, a triazole group was formed acting as a covalent linker between the synthesized dyes and the naturally polymer Chitosan (modified with 4 and 25 % with terminal alkyne groups), whose proved to be very well succeeded. All synthesized compounds and conjugates were fully characterized using HPLC, LC-DAD/ESI-MS, FTIR-ATR, NMR and UV-VIS spectroscopy. All these strategies were also essential to monitoring all performed synthesis and to determine the optimal reaction conditions.

The second major task of this project was to built-up pH indicator membranes using Layer-by-Layer (LbL) assembly technology through a home-made robot using both synthesized conjugates (Chitosan-Flavylium and Chitosan-Pyranoflavylium) and Alginate, acting as negatively charged biopolymer. QCM-D (Quartz Crystal Microbalance with Dissipation) technique and Dynamic Light Scattering (DLS) analysis were performed to verify if the deposition processes were feasible: the 25 % modified Chitosan presented a potential value of 23.3 ± 0.7 mV, 4 % modified Chitosan presented a 20.6 ± 0.5 mV value and ALG, -24.5 ± 0.4 mV. With the Chitosan-Flavylium conjugate was obtained a 32.9 ± 3.1 mV and the with Chitosan-Pyranoflavylium, 21.8 ± 0.5 mV. The results obtained were satisfactory, concluding that the fabrication of this kind of membranes was achievable. Attending to previously published work, the build-up conditions were followed, and the Chitosan-Flavylium/Alginate membranes were fabricated and

submitted to morphology, durability, and robustness studies, including analyses of SEM (Scanning Electron Microscopy), Thickness, Moisture Content, and Water Solubility.

Keywords: Polyphenols, Anthocyanins, *Layer-by-Layer* assembly technology, Smart Packaging, pH sensor dyes, Membranes.

Table of Contents

List of Tables

List of Figures

Communications in Scientific events

‘‘**Chitosan-flavylium conjugates towards construction of pH-responsive multilayer membranes for food spoilage detection’’**, Cunha, M., de Freitas, V., Rodrigues, J. M. M., Cruz, L., XXVIII Encontro Nacional da SPQ, 24-26th July 2023, Aveiro, Portugal, poster presentation.

‘‘**Chitosan-flavylium conjugates towards construction of pH-responsive membranes for food spoilage detection’’**, Cunha, M., de Freitas, V., Rodrigues, J. M. M., Cruz, L., IJUP 2023 - Encontro de Jovens Investigadores 2023, 10-12th May 2023, Porto, Portugal, poster presentation.

Articles in preparation

Cunha, M., de Freitas, V., Mano J., Borges, J., Rodrigues, J. M. M., Cruz, L., ‘‘**Fabrication of smart and free-standing multilayered membranes based on alginate and pyranoflavylium-modified chitosan for food spoilage monitoring**’’, 2023.

List of Abbreviations

ALG	Alginate
CHT	Chitosan
CHT4%	4% Modified Chitosan with terminal alkyne groups
CHT25%	25% Modified Chitosan with terminal alkyne groups
DLS	Dynamic Light Scattering
DMF	Dimethylformamide
DMSO	Dimethylsulfoxide
ESI-MS	Electrospray Ionization – Mass Spectrometry
Flav	Flavylium
FTIR-ATR	Fourier transform infrared spectroscopy – attenuated total reflectance
HPLC-DAD	High-Performance Liquid Chromatography with Diode Array Detection
J	Coupling Constant
LC-DAD	Liquid Chromatography with Diode-Array Detection
NMR	Nuclear Magnetic Resonance
PP	Polypropylene
PyFlav	Pyranoflavylium
QCM-D	Quartz Crystal Microbalance with Dissipation monitoring
TFA	Trifluoroacetic Acid
TMS	Tetramethylsilane
m/z	Mass/Charge ratio
SEM	Scanning Electron Microscopy
UV-VIS	Ultraviolet/Visible Spectroscopy
δ	Chemical Shift
λ	Wavelength

ζ	Zeta-potential

I. Introduction

1. Polyphenols

Polyphenols are a numerous group of plant synthesized compounds (secondary metabolites) having important functions as UV protector of plants and also as other threats such as microbial agents and herbivores [1]. As they are present in natural products such as plants, red fruits and wine, polyphenols end up being present in human's diet. Some fruits, such as apple, pear, grapes, or cherries contains up to 300 mg polyphenols/100 gr and the products manufactured from them also present high levels of these compounds in its composition such as a glass of wine or a cup of coffee or tea present approximately 100 mg of polyphenols [2]. They also act as antioxidants in human and animal metabolism since they can combat UV radiation damage, pollution, and have anti-inflammatory properties that could prevent cancer, obesity, cardiovascular and neurodegenerative disorders, and have signal transduction properties through interaction with receptors or enzymes, which pharmaceutical industries are very interested in. In fact, polyphenols are thought to be the most abundant dietary antioxidants, with an average daily consumption of around 1 g per person [3]. Responsible for color, odor and astringency of several foods relying on the content of different polyphenolic compounds [2], polyphenols have some properties that the scientific community have found relevant: they are activated with external stimulus such as pH, different concentration of molecular oxygen, water, among others. Their colour changes due to pH and, therefore, polyphenols can be used as potential biosensor molecules for food degradation marking which is the aim of this work. They also have been studied as preventors of several diseases in particularly cancer [4], cardiovascular diseases [5], diabetes [6], obesity [7], infectious and neurodegenerative diseases [8].

Polyphenolic compounds can present many different structures: they are characterized by a monomer - a phenolic ring capable of housing several substituents [9] however the most common one is one or more hydroxyl substituents directly linked to aromatic or benzene rings [10]. That way, they can be divided in two major groups: flavonoids and non-flavonoid compounds.

1.1. Flavonoids

As shown in Figure 1, flavonoids are constructed by two benzene rings (A and B) connected by a chain of three carbons creating a closed pyrano-ring with one of the benzene rings. The primary structure is C6-C3-C6, which is also known as 2-phenylbenzopyran.

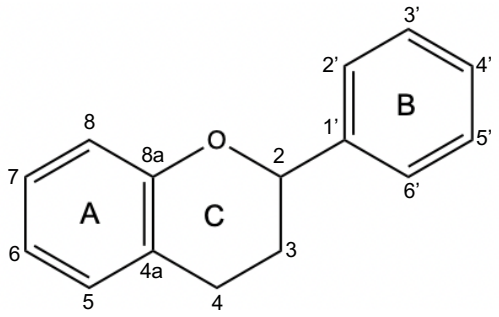

Figure 1: Basic structure of flavonoid compounds.

The flavonoid-compounds subgroups are flavanones, flavones, flavonols, dihydroflavonols, flavan-3-ols, isoflavones, anthocyanins and proanthocyanidins. Flavones have present in their molecular structure carbonyl groups at C-4 position while the rest of flavonoids have an extra hydroxy group in C-3 [11]. Flavanones are known by their characteristic three-carbon chain and an oxygen atom in C-4 [9]. Figure 2 presents different types of flavonoids and their molecular structures.

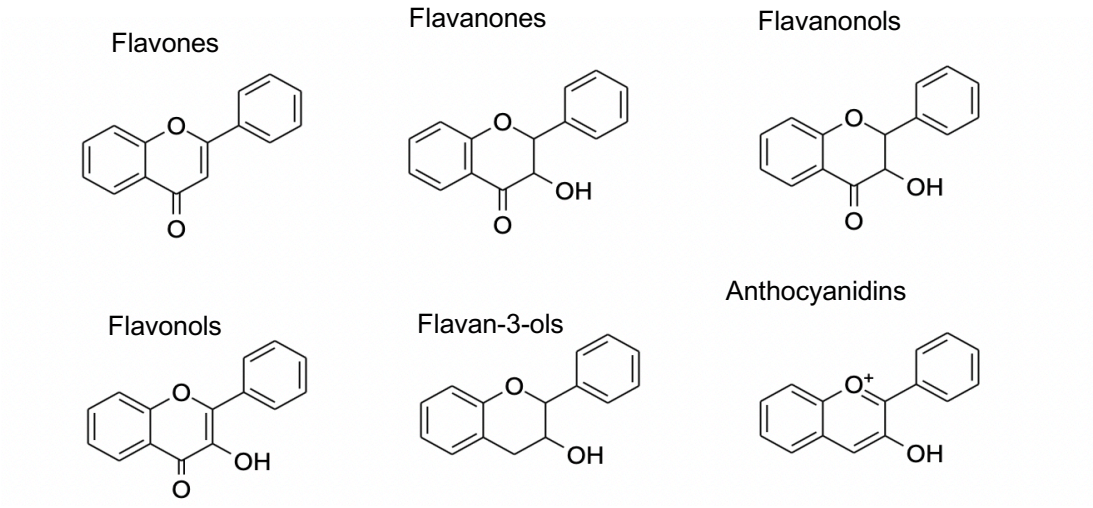

Figure 2: Different types of flavonoid chemical structures.

Nevertheless, the nonflavonoid compounds are characterized by the differences in the number of carbons that they are associated with. The main groups are phenolic acids, stilbenes and lignans, which the common basic structure is an aromatic ring [9].

1.2. Anthocyanins

Anthocyanins, who derived from 2-phenylbenzopyrylium cation, are colourful and water-soluble pigments frequently found in plants, fruits, and tubers [1213]. These compounds are constituted by an aromatic ring attached to a heterocyclic ring and containing oxygen which is also connected by a carbon-carbon bond to a third aromatic ring (B). They are also the basic structures of anthocyanidins and are normally found in the form of glycosides and the most common sugars encountered are glucose, galactose, fructose, xylose, rhamnose and arabinose. Sugars often link themselves at C-3 position of anthocyanins as glycosides and C-3 and C-5 as diglycosides, as shown in figure 3 [9].

As a result of the insaturation of the C-ring of the basic structure base of anthocyanins (flavylium cation), several conjugated double bonds appear and become responsible for spectral absorption in the visible range (520 - 540 nm), granting a range of colours from red to purple and even some blue hues. The anthocyanins differ from one another based on their degree of hydroxylation and methylation in B-ring, as well as the number, type, and position of the linked sugars to it.

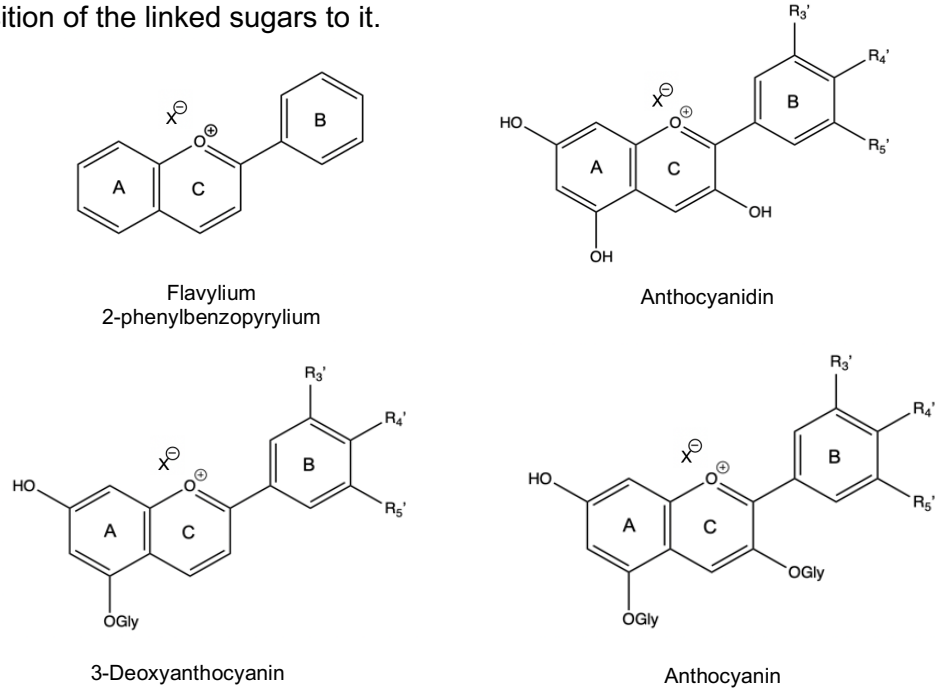

Figure 3: Anthocyanin compounds and flavylium chromophore (Gly = glycoside). Reprinted from [15].

1.2.1. pH equilibria network of anthocyanins

The only found species in an acidic environment at pH ~ 1, is the flavylium cation, AH^+, which is red coloured. As the pH values increases two events start to occur: (i) acid-base proton transfer reaction, forming the neutral quinoidal base (A) shifting its color from red to purple. It can also happen event (ii) which is hydronation, giving rise to the hemiketal carbinol base (B) [14] almost instantly. The B species can also suffer a keto-enolic tautomerization producing cis-chalcone or trans-chalcone through thermal or photochemical isomerization of the previous structure which may appear yellow in aqueous solution [15].

However, at basic pH levels (pH > 7) the neutral quinoidal base (A) originates an anionic quinoidal base (A^-) through the deprotonation of the hydroxyl group in the B-ring originating a shift of the visible maximal wavelength absorbed by the molecules, resulting in a colour change in aqueous environment from purple to dark blue [14, 16].

Figure 4 illustrates the chemical equilibrium network of anthocyanins and each one of the formed species differ in their charge and electronic distribution [16].

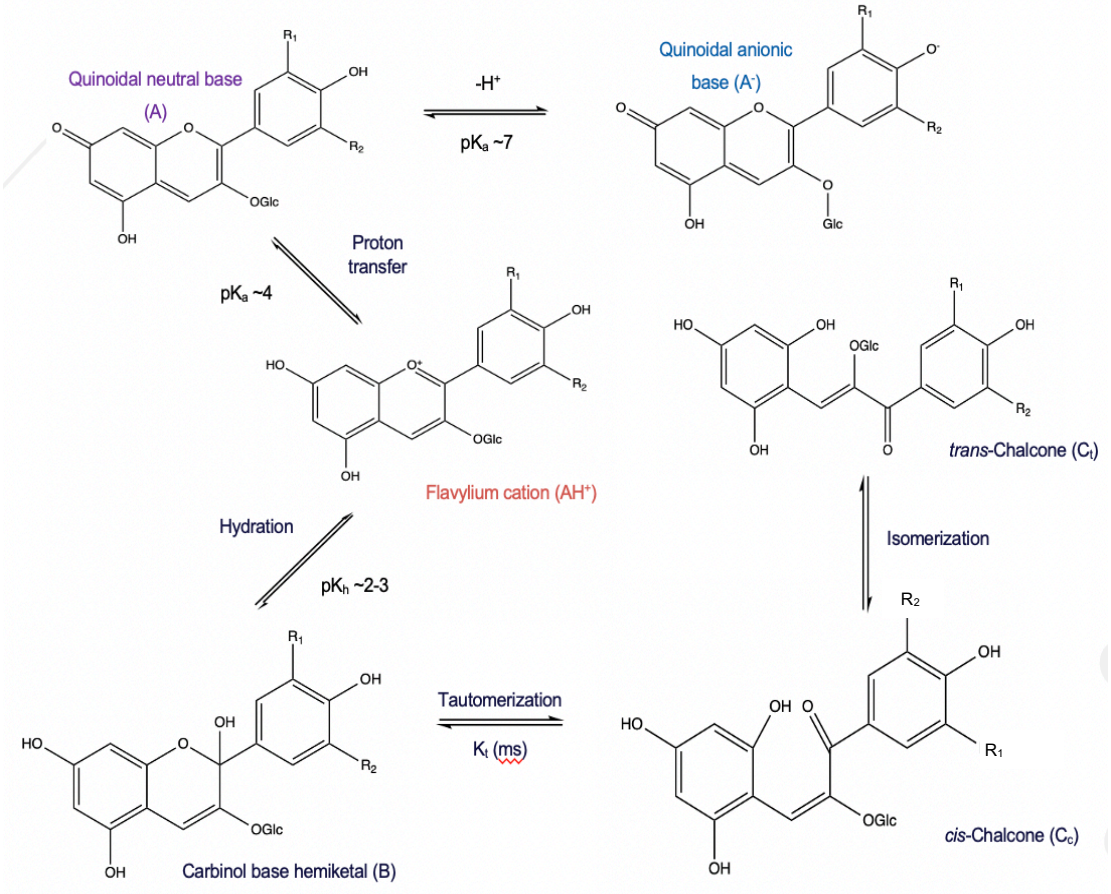

Figure 4: pH-dependent chemical equilibria multistate of anthocyanins.

Is it known that the OH-groups in the C-4', C-5 and C-7 positions are acidic, with OH-groups at C-7 being the most acidic of them all, meaning that this is the group that most promotes the acidic-base equilibrium of a molecule [16] originating pigments with more diversified colour variation. Also, it is important to note that the colour of the anthocyanins can vary with the number of OH-groups in the B-ring of the molecule [12].

Anthocyanin stability are also affected by the nature of the pigment but also of other external factors, such as temperature, light, oxygen, and antioxidants [17] and its solubility in water also depend on pH values – solubility increases in acidic environments since strong protonation occurs.

Anthocyanidins, figure 5, are aglycons and are instable in water and much less soluble than their corresponding glucosides (anthocyanins), and for that reason it is thought that glycosidation provides stability and solubility to these pigments. There are several anthocyanidins in nature, but the most abundant are summarized in Table 1, where they only differ from one another by the number and position of the hydroxyl and methyl groups that are linked to the B-ring, also resulting in a wide range of colours. These solely vary in the substitution of the groups in 3' and 5' positions [18, 19].

Table 1: Different types of anthocyanins

Anthocyanidin	R_1	R_2	Colour*	λ_{max} (nm)
Cyanidin	OH	H	Pink	535
Delphinidin	OH	OH	Purple	546
Malvidin	OCH_3	OCH_3	Purple	542
Pelargonin	H	H	Red	520
Peonidin	OCH_3	H	Red	532
Petunidin	OCH_3	OH	Purple	543

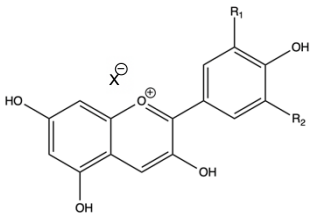

Figure 5: Basic structure of anthocyanidins.

*In aqueous environment, with 0.01% HCl

1.2.2. Colour stability of anthocyanins

These are very insoluble in food matrix and easily degraded - the colour stability of anthocyanins is easily influenced by factors such as pH values, SO_2, solvents, temperature, oxygen, light, enzymes, ascorbic acid, and sugars. However, there is the

possibility of making them more stable by copigmentation phenomena in which anthocyanins and other non colored organic compounds form complexes in solution via noncovalent interactions (such as hydrophobic and Van der Waals interactions). As a result, a hyperchromic effect (increase in colour intensity) is observed and in certain cases, there is also a bathochromic shift in the maximum wavelength absorption [20]. Due to the potential oxidation reactions of these pigments, oxygen is a significant factor giving rise to uncoloured or brown products. Also, the increase of temperature causes a decrease in stability that can be explained by delocalization of the equilibrium turning the species into a hemiketal. The colour of anthocyanins in solution changes according to the physical-chemical conditions of the medium in which they are inserted, or, according to the pH values in the medium, since changes in the equilibrium of these pigments occur, resulting in different species with different colours at different pH ranges [21].

1.2.3. Reactivity of anthocyanins

The presence of hydroxylated aromatic rings promotes anthocyanin reactivity, as these groups have an acidic character, as previously mentioned. As shown in figure 6, A-ring has two nucleophilic sites, one in C-6 and the other one in C-8, which are activated by OH groups in surrounding carbons (C-5 and C-7). The B-ring has a reducer character if R_1 and/or R_2 = OH, which is the typical catechol structure. On the other hand, C-ring has a naturally positive charge due to the natural form of the flavylium cation, affecting C-2 and C-4 of the C-ring.

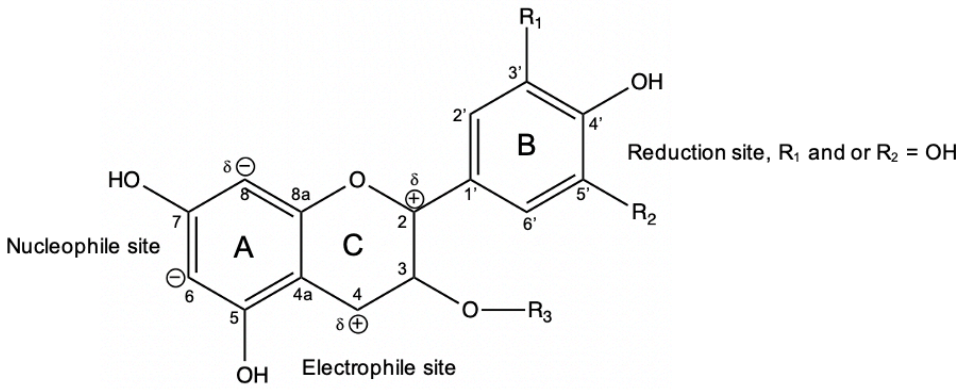

Figure 6: General reactivity sites of anthocyanins.

It is crucial to note that the activity of anthocyanins is stimulated by the presence of an OH group in C-5 that, when combined with C-4, forms pyranoantocyanins, which will be explored further in this work [22].

1.3. Different types of polyphenols in foods

Anthocyanins have been applied as a food additives - E163. This additive is one of the most used commercial additives, derived from grape skin, among other sources. It is often a purple culinary colorant used in the production of jam, coloured drinks, and pastries [12]. As there has been a whole controversy about the excessive use of food colours in marketed foods, many industries have shown an interest in anthocyanins as food dyes, because these are natural compounds and have the potential, as previously stated, to reduce oxidative stress and neutralize the appearance and/or progression of various other diseases, and thus their consumption can be beneficial to the consumer [23].

Tannins, are also phenolic compounds, are responsible for taste (astringency), which in enology plays a critical role in wine quality. The main source of these compounds are the grape skin and seeds. They can undergo chemical alterations as they age due to association, complexation, or oxidation-reduction interactions with other substances such as proteins, polysaccharides, and even metals. The wide range of these modifications produces new anthocyanins stable derivate pigments with distinct physicochemical characteristics, affecting numerous organoleptic properties of wines [24–26].

1.4. Pyranoanthocyanins

Flavylium derivates from pyranoanthocyanins and other pyranoflavylium compounds and can also be found in processed foods such as wine and red fruit juices. These pigments undergo cycloaddition events between the flavylium cation's C-4 and 5-OH and a double bond from another molecule, such as pyruvic acid [27, 28], vinylcatechin [28], vinylcatechol [29] or even acetone [30] resulting in the production of an extra pyran D ring, as described elsewhere (figure 7).

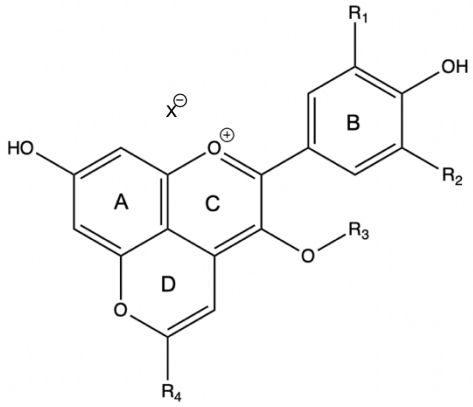

Figure 7: General structure of pyranoanthocyanins.

The additional ring improves stability, allowing these molecules to keep their colour and some other beneficial characteristics (intensity, bioavailability and antioxidant properties) for a longer amount of time, however anthocyanins can lose their shades between pH 1 and 5, due to the development of colourless hemiketal form through hydration (pK_h 2 and 3), pyranoanthocyanins are still very coloured stable molecules [31]. This stability can be explained by the fact that the D-ring protects the chromophore group from nucleophilic attacks of water specifically on C-4 of the C-ring, preventing the formation of hemiketal (colourless) species as well as cis and trans chalcones (yellow), figure 8.

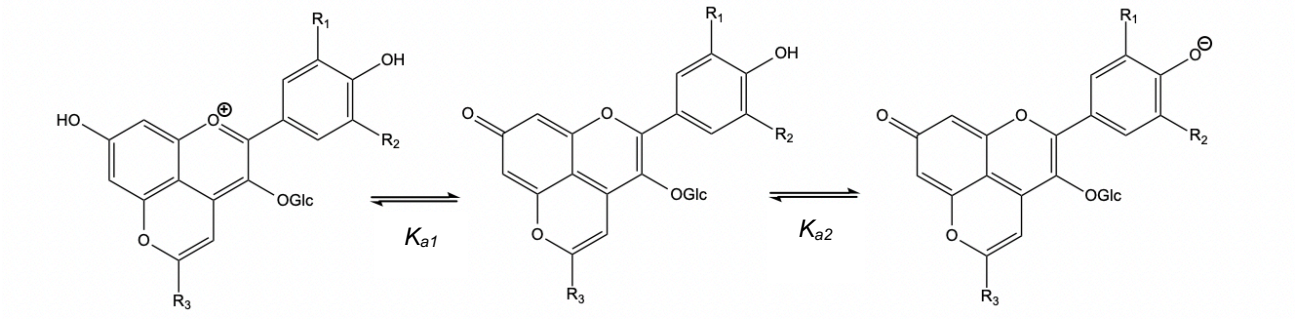

Figure 8: Equilibrium forms of pyranoanthocyanins at different pH values in aqueous solutions.

Comparing to anthocyanins, pyranoanthocyanins present a hypsochromic difference in the UV-VIS spectrum (478-510 nm) when compared to its precursor (520-540 nm), originating a colour shift (from red-purple to orange). Also, pyranoanthocyanins do not suffer degradation overtime: their amount just increases while anthocyanins degrade through storage and processing of the foods in which they are present [32].

2. Click Chemistry reaction – Copper catalyzed Azide-Alkyne Cycloaddition (CuAAC)

Kolb, Finn, Sharpless and their colleagues introduced the term invented ‘‘Click Chemistry’’ in 2001, and it has since become a reliable and selective methodology for attaching probes or substrates of interest to specific molecules, yielding novel and significant chemical compounds. It describes a current chemical topic that enables the coupling of small units to create functional molecular materials [33].

Click Chemistry is a simple and versatile chemical reaction due to its several advantages: i) high yields, ii) readily available reactants, and iii) can be used in mild conditions (e.g., green solvents and low temperatures). Furthermore, the formed by-products during the reaction are not hazardous, and they can be easily removed using non-chromatographic methods [34–36]. In 2022, the approach pioneered by Carolyn R. Bertozzi, Morten Meldal and K. Barry Sharpless earned them the Noble Prize in Chemistry for their contributions to Click Chemistry processes and biorthogonal chemistry. In the work present in this thesis, Click Chemistry was used to conjugate the synthesized N_3-containing pigment to the alkyne-modified biopolymer. This was achieved through copper-catalyzed azide-alkyne cycloaddition reactions, resulting in the formation of a triazole group.

Figure 9 depicts one of the proposed mechanisms of Click Chemistry, in which species **1** is activated by deprotonation promoting their binding to the Cu(I) species, forming species **2**. Afterwards, substitution of azide for one of the ligands takes place, which binds to the copper atom through the nitrogen proximal to carbon, generating intermediate **3**. The terminal nitrogen of the azide in **3** attacks the C-2 carbon of acetylide (derived from **2**), resulting in the uncommon six-membered copper (II) metallacycle **4**. Ring contraction results in the triazolyl-copper derivative and the triazole product is released from compound **5**, completing the catalytic cycle [37–39].

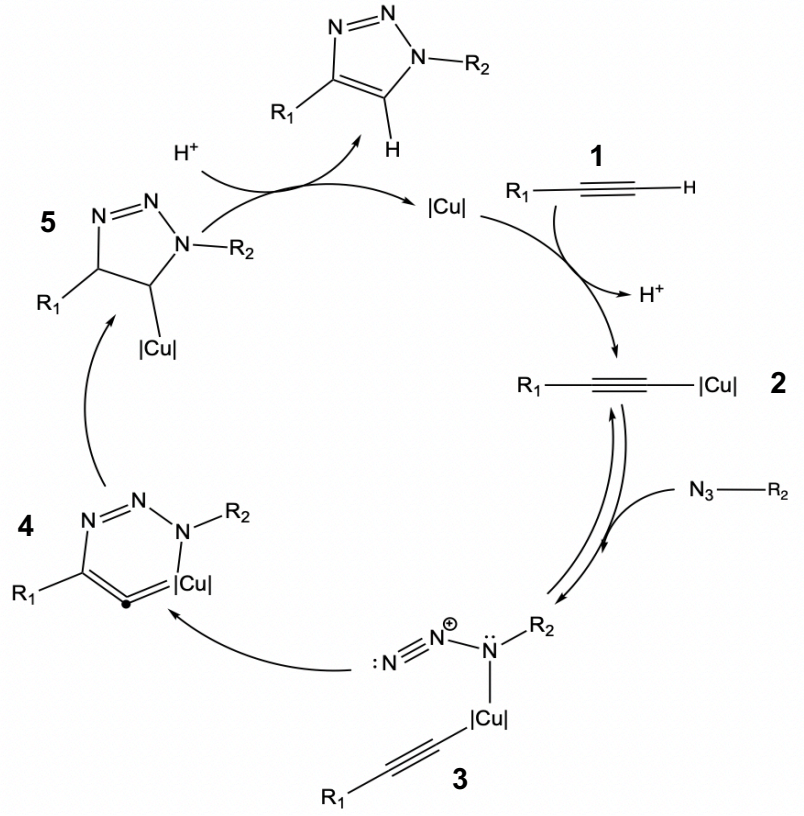

Figure 9: Copper catalysed Azide-Alkyne Cycloaddition (CuAAC) scheme example. Reprinted from [37, 38].

Click Chemistry reactions offer advantages, including the fact that they are very selective, do not require high temperatures allowing them to be done under atmospheric circumstances, and are able to work on unprotected molecules giving us direct access to simply synthesize triazole groups with medium to high yields (~43-99%) [40].

3. Smart packaging

3.1. The importance of the smart packaging

Nowadays, the consumers are increasingly paying particular attention to the quality of the food they consume. The labelling and expired dates of the products are increasingly consulted and more considered at the time of purchase. Taking this into account, the aim of this work would be to create colorimetric membranes that can be incorporated in food packaging and can be responsive to pH changes that food undergoes during their spoilage. Consumers may determine food freshness status by

witnessing chromatic change during microbial infection or chemical changes on packaged food. Recently, the food packaging trend has shifted toward more environmentally friendly and biodegradable materials, with natural components being preferred over synthetic ones. It is critical to underline that polysaccharides and proteins are popular biopolymers used in the production of smart packaging membranes. The primary causes of food degradation are oxidation and microbial contamination. Anthocyanin-based membranes have been lately used for food packaging purposes both in active and smart packaging. These are able to extend foods shelf life giving its strong antioxidant and antibacterial capabilities: foods can be protected from food-borne microbes and several pathogens, particularly Gram-positive bacteria [4142]. However, anthocyanins stability issues are not promising to develop pH-freshness labels. Bearing this, other flavylium derivates have been early described by our group as outstanding alternatives for these applications [31,43,44].

3.2. Membranes

The formation of membranes entails the inclusion of manufactured pigments in natural origin substrates that are appropriate for incorporation into smart packaging, i.e., non-toxic and biodegradable, and it must be a ductile substance in order to be easily worked with. To that purpose and based on prior published work by the same research group, the Chitosan and Alginate polymers were chosen as the natural origin substrates.

3.2.1. Polymers

Polymer is derived from Greek where *poly* means ‘many’ and *meres* means ‘parts’. These materials are build-up from several tiny molecules, which are known as monomers bonded covalently together in order to create extensive chains of molecules. They are also known as macromolecules and present a molecule weight in the range of 10000 to 1000000 Da. In this work, the polymers used were modified Chitosan (in 4 and 25 % with terminal alkyne groups, CHT4% and CHT25%) and Alginate (ALG), which present opposite superficial charges, which are essential characteristics for the formation of the desired membranes. Polymers are found in nature but can be artificially manufactured as well. They have an important role in human life, and it can be stated that these are

responsible for life itself, medication, nourishment, communication, transportation, irrigation, clothing, buildings, and roadways [45] and so, the scientific community ends up revealing interest in working with these compounds, as they end up being extremely versatile materials.

3.2.1.1. Alginate

Alginate is an anionic polymer found in brown seagrass generally Phaeophyceae which includes *Laminaria hyperborea*, *Laminaria digitata*, *Laminaria japonica*, *Ascophyllum nodosum*, and *Macrocystis pyrifera* through treatment with Sodium Hydroxide (NaOH) or another alkali aqueous solution, and it is a water-soluble polysaccharide.

The obtained extract can be filtered, followed by the addition of either sodium chloride or calcium chloride. This procedure promotes the precipitation of alginate. Afterwards, the precipitated alginate salt it is transformed into alginic acid through the addition of HCl, and after its purification and conversion, water-soluble sodium alginate salt is produced [46]. Alginate possesses biodegradable and biocompatible characteristics hence it can be used for food applications. Alginate salts are usually composed by alternating blocks of 1-4 linked *α*-L-glucuronic acid (G) and *β*-D-mannuronic acid (M) residues as showed in figure 10 [4748].

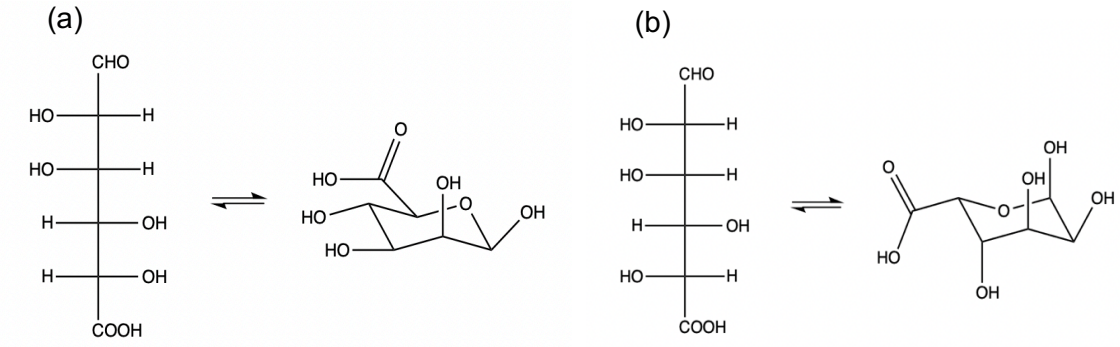

Figure 10: Chemical structures of two the two monomeric units of alginate. (a) D-mannuronic acid (b) L-glucuronic acid.

The M and G block distribution depends on the origin of the algae and sequentially the functional properties of these polymers strongly depend on the M/G

ratio. They can be combined as MM, GG and MG blocks; however, MG blocks promotes residues chain flexibility and reduce solution viscosity [49], and GG dimers provides greater solubility compared to MM dimers. It is also reported that the solubility and stiffness of the chains are affected with the presence of G residues (increasing stiffness solubility). These blocks are linked to each other through glycosidic bonds, figure 11 [50].

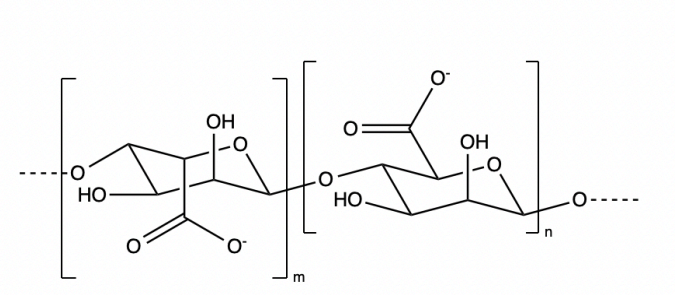

Figure 11: Representation of general structure of alginate.

Alginate has been widely used as an inert and not biological interactive biomaterial for the purpose of drug delivery [51], catalysis [52], water treatment [53], food industry [54], among others. Its biocompatibility, low cost and low toxicity are main reasons why these polymers have been used in so many applications [55].

3.2.1.2. Chitosan

Chitosan is a linear, polycationic polysaccharide of β–(1-4) linked 2-acetamide-2-deoxy-D-glucose and 2-amino-2-deoxy-D-glucose derived from the partial deacetylation of chitin [56]. Chitin is also a linear polysaccharide and is the second most abundant in nature, only behind cellulose, found in the exoskeletons of some crustaceans such as shrimp and crabs. It is often used as biomaterials in several applications, even in food applications because of their biocompatibility, biodegradability, their non-toxicity and non-allergenicity. To obtain chitin, it is required the use of some treatments such as enzymatic processes or fermentation after demineralization and deproteinization of several compounds found in the shells. After the processes of acquiring chitin, follows the deacetylase using NaOH, obtaining chitosan, figure 12 [5758].

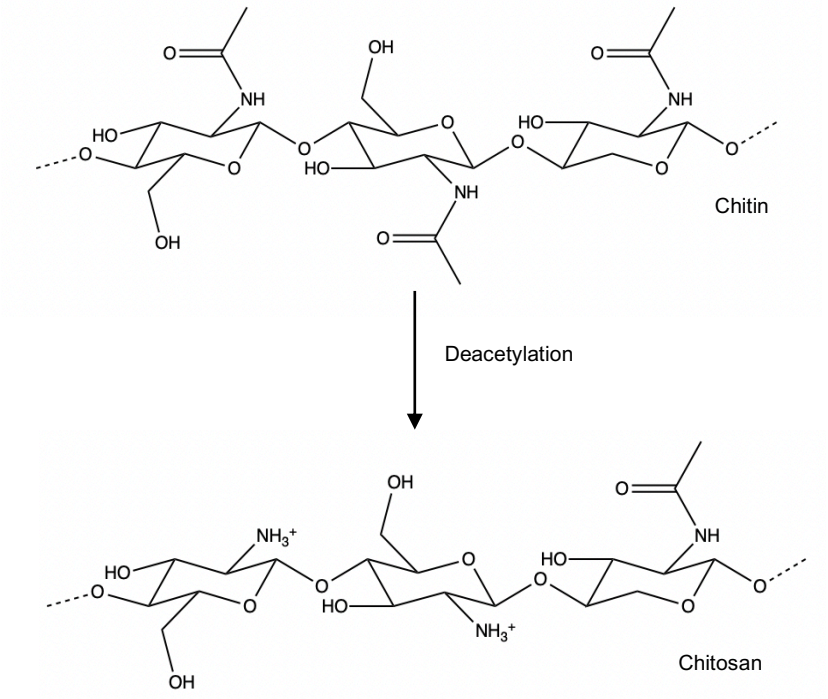

Figure 12: Representative scheme of deacetylation of Chitin to form Chitosan.

The degree of deacetylation (DD) is the parameter that indicates the molar percentage of glucosamine monomeric units in the polymer chain and varies from 0 (chitin) to 100 (fully deacetylated chitin). These charges provide interactions with neutral species through ion-dipole interactions or with negatively charged species, such as anionic polymers or lipids by electrostatic forces. The greater the degree of deacetylation, the greater is the insolubility of this polymer. The fact that it presents in its structure primary amino groups allows chitosan to have a great interest in terms of chemical modifications through covalent bonds and may have promising applications in several areas of organic chemistry such as pharmacology, cosmetics, and food chemistry [58–61].

As they have values of pK_a below 6.5, the amine groups are positively charged at pH under this value. This feature will be valuable because with that, it is possible to build membranes using synthesized pigments coupled with chitosan [62,63]. However, if the pH value increases, the amino groups turn deprotonated causing the polymer chain to lose its positive charge and therefore a loss of its solubility. It is also important to emphasise that the solubility of these polymer chains increases with the degree of deacetylation [58].

3.2.2. Procedures towards production of membranes

3.2.2.1. Casting

Most of the chitosan/alginate based membranes described in literature are formed by classical solvent casting. This method consists in dissolving 1.0 - 3.0 % (w/v) CHT on an acidic solution, such as acetic acid and the functionalization occurs through non-covalent interactions [43]. That solution is then poured onto a mold, evaporated and left to dry at a set temperature. The dried film is then peeled off and immersed in NaOH, which renders chitosan insoluble in water and neutralizes the excess of acid. Before final drying, the membranes are thoroughly washed with deionized water.

There are numerous protocols for solution casting chitosan membranes, many of which are restricted to the use of a specific degree of deacetylation [6465]. Although solution casting is the most widely used method for forming membranes, due to its low cost and ease of preparation, this technique does not offer control of thickness and architectures which could compromise the properties and efficiency of the membrane [66].

3.2.2.2. Layer-by-Layer technique

Layer-by-Layer (LbL) assembly technology has proven to be a simple, cost-effective, and highly versatile technology for coating surfaces and developing a diverse range of (multi)functional multi-layered assemblies with tunable compositions, structures, properties, and functions. LbL is a technique used to create thin membranes or coatings with precise control over their thickness and composition [67]. Hydrophobic interactions, hydrogen bonding, van der Waals forces, and electrostatic interactions between charged polymers could all be used towards deposition of materials [66]. In general the electrostatic interactions are the main driving force for LbL, involving sequential deposition of alternating layers of positively and negatively charged materials, over an inert substrate (PP, polypropylene) as shown in figure 13.

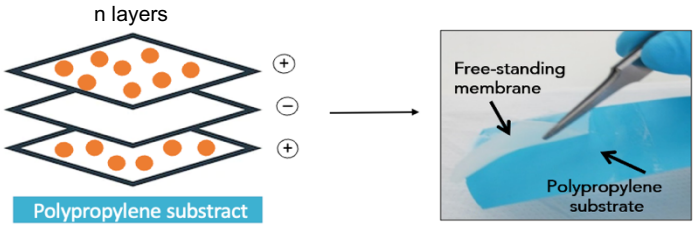

Figure 13: Layer-by-Layer assembly technique sketch on a polypropylene substrate.

3.2.2.2.1. Free-standing membranes fabrication

The membranes were fabricated using Layer-by-Layer processes, which includes deposition steps intercalated with rising steps between dips of positively and negatively charged polymers, in order to remove the excess of polymer solution not attached to the substrate. This procedure of layer deposition and rising processes is repeated until de desired number of layers is reached, and freestanding membranes are obtained. In this work, as a negatively charged polymer it was used Alginate (ALG) and as a positively charged polymer it is used the Chitosan-Flavylium (CHT25%-Flav) conjugate, and the manufacturing was achieved using a home-made Robot, at University of Aveiro (figure 14).

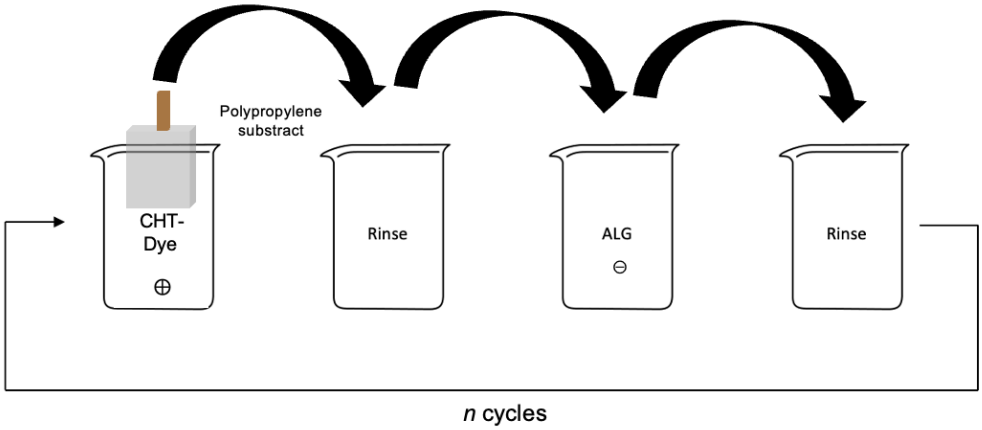

Figure 14: Operational mode of Layer-by-Layer technique for charged polymers deposition.

3.2.2.2.2. Polyelectrolytes

Polyelectrolytes are polymers with polymeric and electrolytic properties containing a large number of ionizable groups and can carry an electrical charge in solution. These polymers can be synthetic or natural, as well as positively or negatively charged. These can be classified as cationic, anionic, or amphiphilic based on the functional group load present in the polymer structure after ionization (if positive and negative charged functional groups are present).

The charged groups on the polyelectrolyte interact with ions of opposite charge in a solution, forming a complex that can have significant effects on the physical and chemical properties of the solution. Because of their unique properties, polyelectrolytes are used in a wide range of industrial applications, including water treatment, biotechnology, and drug delivery, but the ability of producing functional and nanostructured membranes using Layer-by-Layer assembly technology is the most relevant application for this project [68].

II. Experimental section

1. Reagents and solvents

All regents used are presented in table 1.

Table 1: List of used reagents

Reagent	Brand	Molecular weight /g·mol^{-1}
4'-Hydroxyacetophenone	Aldrich	136.15
2',6'-dihydroxyacetophenone	Aldrich	152.15
2',4',6'-trihydroxyacetophenone	Aldrich	168.15
Sodium azide	Sigma-Aldrich®	65.01
Dichloromethane	Carlo Erba	84.93
Methanol	Honeywell	32.04
Diethyl Ether	Honeywell	74.12
Ethanol absolute	Sigma-Aldrich®	46.06
Silicon tetrachloride	Sigma-Aldrich®	169.90
Acetone	LabChem	58.08
Acetonitrile	LabChem	41.05
Hydrochloric acid 37% (v/v)	Sigma-Aldrich®	35.46
Reverse phase silica gel C18, LiChroprep® RP18 (25-40 µm)	Merck®	-
Trimethylsilyl chloride	Sigma-Aldrich®	108.64
Trichloroacetic Acid	PanReac AppliChem	163.39
Sodium Phosphate dibasic dihydrate	Sigma	177.99
Sodium phosphate monobasic dihydrate	Sigma	156.01
Sodium acetate trihydrate	Sigma	136.08
Glacial Acetic Acid		60.03
L-Sodium ascorbate	Sigma	198.11
Copper sulfate pentahydrate	PanReac AppliChem	249.68

Chitosan	Primex	Aprox. 100 000
Tris(benzyltriazolylmethyl)amine	Aldrich	530.640
Alginate	Sigma-Aldrich®	10 000 – 600 000
Dimethyl sulfoxide	Acros organics	78.14
5-chloro-2-pentanone	Aldrich	120.58

2. Materials and instrumentation

- Analytic balance by KERN ABT 120-5DM;
- Micropipette P10, P20, P100, P200 and P1000 and respective tips by Eppendorf Research plus;
- Quartz cuvette by Starna scientific, Type: 9-F/Q/10, Path Leng: 10 and Match Code: 6;
- Disposable cuvettes by BRAND® PMMA (12.5 x 12.5 x 45 mm);
- Rotary evaporator by LABOROTA 4001 – efficient, Heidolph WB, BUCHI Vac V-500;
- Automatic rotary evaporator by BUCHI Interface I-100, Vacuum Pump V-100, Rotavapor R-100, Heating Bath B-100.
- Velocity 14R Refrigerated centrifuge by Dynamica Scientific
- pH Meter pH 538 by WTW

3. Purification and identification techniques

3.1. Column chromatography

Purification of the synthesized flavylium-based compounds was performed using column chromatography using as C18 reverse phase silica gel (LiChroprep® RP18, with a particle size of 25-40 μm) as stationary phase. The stationary phase used was previously suspended in the eluent, used as the mobile phase, Methanol. To help the elution flow, it was used a pump and the eluate fractions collection was performed manually. The compounds were separated and isolated by using the ratio of methanol (MeOH) and water solutions.

3.2. HPLC-DAD technique

High-performance liquid chromatography analysis were performed using two equipment sets: a Merck® Hitachi L-7100 composed by a DAD Merck® L-7450ª diode detector, a Merck® L-7360 furnace, a Merck® L-7100 pump and a Merck® L-7612 solvent degasser and a VWR Hitachi Elite LaChrome equipped with a VWR Hitachi L-2455 Diode Array Detector, a VWR Hitachi L-2200 Autosampler, a Merck® Hitachi L-2130 Pump a Merck® Hitachi L-2300 Column Oven. These analysis took place in the Chemistry and Biochemistry department of Faculty of Sciences of University of Porto.

It was injected 20 µL of all samples in a reverse phase column C18 (150 x 4.6 mm i.d., 5 µm, Thermo Scientific), thermostated at 25ºC. Elution solvents were prepared according to the following instructions: Solvent A – 10% Formic acid in Milli-Q H_2O (v/v) and Solvent B – 10% Formic acid in Acetonitrile (v/v), using an elution flow of 0.5 mL/min. The gradients are presented in table 2. Data acquisition was performed using HSM D-7000 software.

Table 2: Flow gradient of HPLC-DAD analysis

Time (min)	% A solvent	% B solvent
0.0	90.0	10.0
50.0	35.0	65.0
51.0	0.0	100.0
55.0	0.0	100.0
56.0	90.0	10.0
60.0	90.0	10.0

3.3. LC-DAD/ESI-MS technique

All analyses were performed on a Finnigan Survevor with dual photodiode detection and mass spectrometry LC-DAD/ESI-MS supplied with an LCQ DECA XP MAX mass detector (Finnigan Corp., San Jose, California), an ionizing source (at atmospheric pressure – API) using and electrospray ionization (ESI). The capillary temperature was set at 325 ºC, and vaporizer and capillary voltages were 5 and 4 kV, respectively. As

carrier and auxiliar gas it was used nitrogen with a 90 and 25 flow, respectively. It was also used a reverse phase column (150 × 4.6 mm i.d., 5 µm, C18) by Thermo Finnigan (Hypersil Gold) thermostatized at 25 ºC. Elution solvents were prepared according to the following instructions: Solvent A – 10% Formic acid in Milli-Q H_2O (v/v) and Solvent B – 10 % Formic acid in Acetonitrile (v/v), using an elution flow of 0.5 mL/min and all acquired spectra were obtained in positive mode with the range between 250 and 1500 of *m/z*. The equipment was set to do three scans: a complete mass scan (MS), a scan where the most intense ion in the initial scan is shown (MS^2) and MS-MS which is the most intense ion using relative collision energies of 30 and 60 (MS^3). LC-DAD/ESI-MS analysis were performed at Chemistry and Biochemistry Department in Faculty of Sciences of University of Porto.

4. Structural characterization techniques

4.1. NMR analysis

NMR analyses were performed on a Bruker-advance 600 obtaining a proton spectrums ^1H (600.13 MHz) and the temperature was set at 303 K. The used solvents were deuterated DMSO-d_6/TFA (9:1), containing TMS as internal standard. Coupling constants (J) were obtained in Hertz (Hz) and chemical shifts (δ) in parts per million (ppm). Signal multiplicities were designated as singlets (s), duplets (d), double duplets (dd) and multiplets (m). Chemical shifts were assigned using 1D (^1H) and 2D techniques (COSY). All analyses were made at CEMUP – Centro de Materiais da Universidade do Porto, in Faculty of Sciences of University of Porto.

4.2. FTIR-ATR analysis

The usual range of the analysis were between 4000 and 500 cm^{-1} [69]. All obtained analyses were performed using a PerkinElmer device, Spectrum two model, with 4 to 20 scans. The analysis were made at Chemistry and Biochemistry Department in Faculty of Sciences of University of Porto (FCUP).

4.3. UV-VIS spectroscopy

UV-VIS spectra were obtained using a UV-VIS Evolution Array spectrophotometer from Thermo Scientific. The software used to gather and analyse the spectra was Scientific VISIONcollect. Later on, it was also used a Cary 60 UV-VIS spectrophotometer from Agilent and the software used is powered by the same company. The data was obtained in a 200-800 nm range using a quartz cuvette with 1 cm of optical path. The analysis were performed in the Chemistry and Biochemistry Department of FCUP.

4.4. Dynamic light scattering (DLS)

The zeta-potential, ζ, of the conjugates, as well as native polymers, CHT and ALG, were assessed at 25 ºC using a Malvern Instruments Ltd. Zetasizer Nano-ZS (Royston, Hertfordshire, UK). Each component was analysed in Acetate Buffer pH 5.5 at 0.2 mg/mL. The intensity of light scattered was measured by an avalanche photodiode at an angle of 173º and the solution was illuminated using a laser of 633 nm. The information given is based on the particle size and polydispersity, measured in triplicate [70]. The analysis were performed at Chemistry and Biochemistry Department in Faculty of Sciences of University of Porto, in an Analytical Chemistry laboratory.

4.5. Quartz-crystal microbalance with dissipation monitoring (QCM-D)

The CHT25%-Flavylium conjugate as well as the ALG polymer were assessed through QCM-D analyzes to determine their ability to produce multi-layered membranes by a QSense equipment, from Biolin Scientific from Gothenburg, Sweden. It was used a Gold-coated 5 Mz AT-cut quartz sensor from Q-Sense, model QSX301 Gold as subtract which was previously cleaned with a 1:1:5 (v/v) solution of NH_4OH (25%), H_2O_2 (30%) and ultrapure water. The solution was prepared in an ultrasonic bath set at 70ºC for 10 minutes and then rinsed using ultrapure water and finally dried using a soft stream of nitrogen. The conjugate and the alginate were analyzed dissolved in 0.1 M Acetate Buffer Solutions at pH 5.5 [67], producing 0.2 mg/mL solutions. The formation of multi-layered thin membranes is often demonstrated by dropping 50 μL of each solution at each

minute. The solutions containing the polymers (CHT and ALG) were deposited for 6 minutes and the rising processes took 4 minutes. All analysis were made in CICECO, at University of Aveiro.

4.6. Scanning electron microscopy (SEM)

Scanning electron microscopy (SEM) analysis of the CHT25%-Flavylium was performed in a field emission gun (FEG-SEM from Hitachi, model SU-3800, Tokyo, Japan) operated in high vacuum in the secondary electrons mode at an acceleration voltage of 10 kV and working distances between 4.7 and 5.4 nm. The analytes were bound to a metal stub with double-sided carbon conductive tape to provide electrical contact, and then sputtered coated with a conductive carbon layer using a Polaron E5000 sputter coater (Quorum Technologies, Laughton, UK) [67]. This analysis were carried out at CICECO located at University of Aveiro.

5. Pigment synthesis

5.1. Synthesis of 4'-azide-5-hydroxy-4-methylflavylium

To synthesize 4'-azide-5-hydroxy-4-methylflavylium (**3**) it was initially dissolved 125 mg (0.82 mmol) of 2',6'-dihydroxyacetophenone (**1**) and 1 eq. of *p*-azideacetophenone (**2**) (132 mg; 0.82 mmol) in 2 mL of absolute ethanol (EtOH) and silicon tetrachloride ($SiCl_4$) (30 eq.; 500 μL) at room temperature during 2 h in constant stirring. This is the result of an aldolic condensation of two acetophenones (figure 15). The reaction progression was followed by HPLC-DAD and LC-MS analysis to determine the optimal reaction time, resulting in two reaction products.

Because other unwanted reaction products were detected, after the reaction is completed, the mixture was washed 3 times using diethyl ether (Et_2O) and H_2O. The aqueous phase was evaporated and isolated using an C18 reverse phase silica gel column whereas the fraction containing the desired pigment was collected using 50 % - 60% MeOH acidified (HCl 2%). After lyophilization processes, it was obtained a dark orange solid. Yield = 7 %. $[M]^+$ *m/z* 278, λ_{max} = 413 nm.

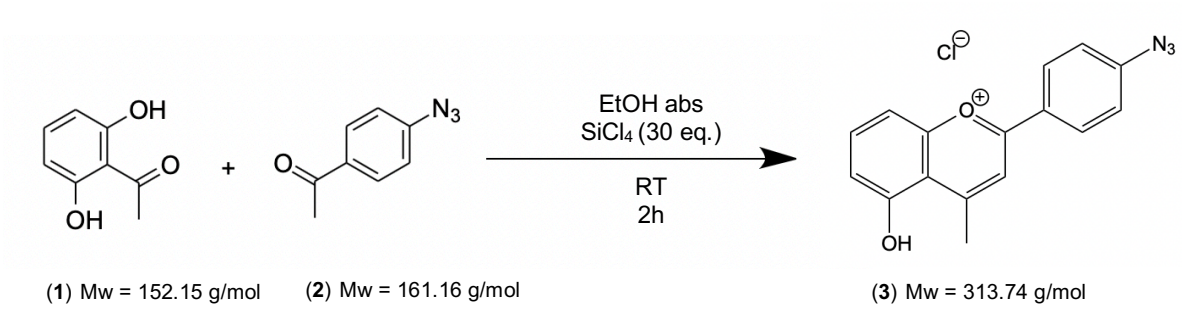

(**1**) Mw = 152.15 g/mol (**2**) Mw = 161.16 g/mol (**3**) Mw = 313.74 g/mol

Figure 15: Synthesis reaction of 5-hydroxy-4-methyl-4'azideflavylium (**3**).

5.2. Synthesis of 4'-azide-5,7-dihydroxy-4-methylflavylium

The purchased compound 2',4',6'-trihydroxyacetophenone (**4**) (130 mg; 0.78 mmol) and 1 eq. (125 mg; 0.78 mmol) of *p*-azideacetophenone (**2**) were also dissolved in 2 mL of absolute ethanol and 500 μL (30 eq.) of silicon tetrachloride ($SiCl_4$) at room temperature during 2 h in constant stirring (figure 16). This reaction was also monitored using HPLC-DAD and LC-MS analysis and after 2h the mixture was washed down 3 times using Et_2O and the aqueous phase was saved and evaporated. Isolation of the same phase was performed using an C18 reverse phase silica gel column and the desired product was eluted using 60% of MeOH. It was obtained a dark orange solid after lyophilization processes. Yield = 2%. LC-DAD / ESI-MS: $[M]^+$ *m/z* 294, λ_{max} = 407/455 nm.

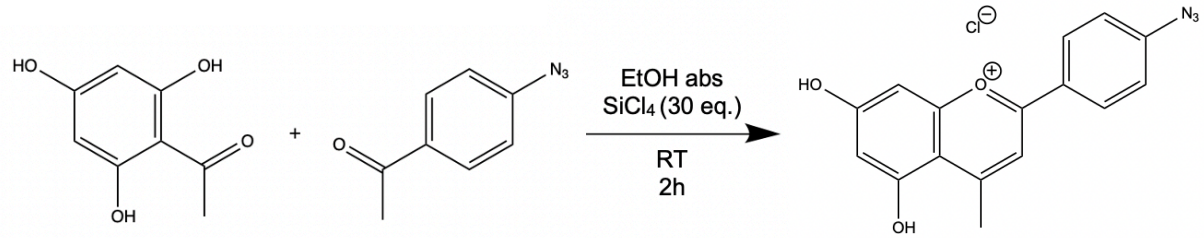

(**4**) Mw = 168.15 g/mol (**2**) Mw = 161.16 g/mol (**5**) Mw = 329.74 g/mol

Figure 16: Synthesis reaction of 4'-azide-5,7-dihydroxy-4-methylflavylmethylflavylium (**5**).

4'-azide-5,7-dihydroxy-4-methylflavylium (**5**): ^{1}H NMR (600.13 MHz, DMSO-d_6/TFA 9:1) δ (ppm): 8.47 (d, 2H, *J* = 8.77 Hz, H-3'/H-5'), 8.32 (s, 1H, H-3), 7.45 (d, 2H, *J* = 8.71 Hz, H-2'/H-6'), 7.03 (d, 1H, *J* = 2.05 Hz, H-6), 6.80 (d, 1H, *J* = 1.94 Hz, H-8), 3.10 (s, 3H, H-4).

5.3. Synthesis of 4',5-dihydroxyflavylium

The 4',5-dihydroxyflavylium compound works as a precursor to synthesize the desired pyranoflavylium product. As a first step, it was performed an acidic aldol condensation between a benzaldehyde and an acetophenone, using Trimethylsilyl chloride (TMS-Cl) in excess to generate HCl in situ, that will work as a catalyst of this reaction, as previously reported by the same research group [71]. For this purpose, in a round bottom flask it was added 100 mg (0.72 mmol) of 2,6-dihydroxybenzaldyde (**6**) and 1 eq. (0.72 mmol; 97.9 mg) of 4-hydroxyacetophenone (**2**) dissolved in mixture of ethyl acetate (AcOEt) and MeOH (2:1) with total volume of 4 mL. Then, it was finally added 20 eq. of TMS-Cl (91 μL). The reaction was kept in constant stirring at 0 ºC during 1 h, thus forming the product described in figure 17.

The product was precipitated by the addition of AcOEt athwart liquid-liquid extraction. The compound was purified through C18 reverse phase silica gel column where the desired product is eluted using a MeOH:H_2O 40:60 solution yielding an impure dark orange solid powder after lyophilization. Yield = 60%. ^{1}H NMR. LC-DAD / ESI-MS: $[M]^+$ *m/z* 239, λ_{max} = 442 nm.

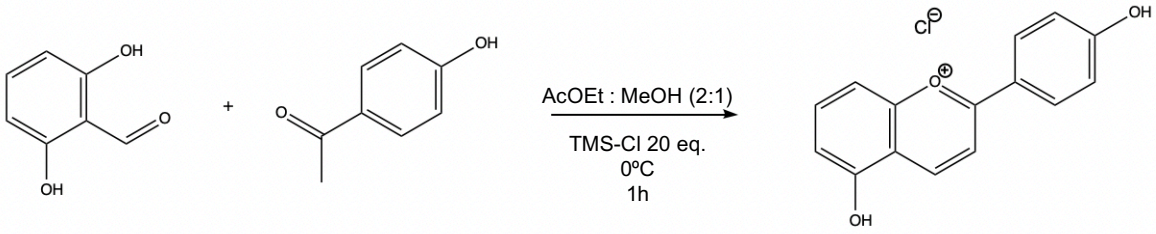

(**6**) Mw = 152.15 g/mol (**2**) Mw = 136.05 g/mol (**7**) Mw = 274.70 g/mol

Figure 17: Synthesis reaction towards production of 4',5-dihydroxyflavylium (**7**).

4',5-dihydroxyflavylium (**7**): ^{1}H NMR (600.13 MHz, 9:1 DMSO-d_6/TFA): δ (ppm): 9.29 (d, *J* = 9.1 Hz, 1H, H-4), 8.53 (d, *J* = 9.1 Hz, 1H, H-3), 8.50 (d, *J* = 8.8 Hz, 2H, H-2′, H-6′), 8.00 (t, *J* = 8.3 Hz, 1H, H-7), 7.61 (d, *J* = 8.5 Hz, 1H, H-6 or H-8), 7.20 (d, *J* = 8.1 Hz, 1H, H-6 or H-8), 7.11 (d, *J* = 8.8 Hz, 2H, H-3′, H-6′).

5.4. Synthesis of 5-azidopentan-2-one

The S_N2 reaction was performed between 5-chloropentan-2-one (**8**) (2 mL, 17.6 mmol) and 3 eq. of Sodium Azide, NaN_3 (3.4 g, 52.2 mmol), as showed in figure 18. The reactants were dissolved in 10 mL Dimethylformamide (DMF) and left in constant stirring at 80 ºC overnight. As catalyst, 10 mg of Tetrabutylammonium Iodide (TBAI) was added, which corresponds to 0.1% m/v of the used volume of DMF.

After the reaction was completed, the reaction was filtered to remove NaN_3 and NaCl. Following that, a liquid-liquid extraction was performed, to which equal volumes of H_2O and AcOEt were added, recovering the organic phase. As a result, the DMF is eliminated as it is soluble in the aqueous phase. The organic phase was dried over anhydrous sodium sulphate, then filtered again using a pleated funnel and evaporated to dryness, yielding a brown-coloured oil at the end. After AcOEt evaporation, a mass of 1,41 g was obtained, which was weighted by difference. Yield = 50%.

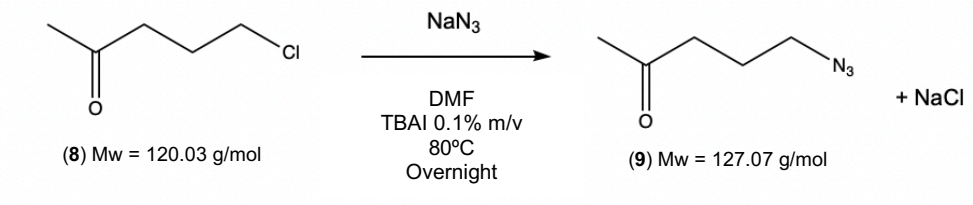

Figure 18: Synthesis reaction towards product formation of 5-azidopentan-2-ona.

5.5. Synthesis of 10-azidepropyl-4'-hydroxypyranoflavylium

Using 60.8 mg (0.2 mmol) of 4',5-dihydroxyflavylium (**7**) previously synthesized and 50 eq. of 5-azidopentan-2-one (**9**) (1.41 g, 11.1 mmol) were mixture in a 50 mL round bottom flask with 10 mL of H_2O:EtOH (4:3) as solvent. The pH levels was set at 2.9 and the reaction is left to stir for 1 day at room temperature (figure 19). The reaction was followed by HPLC analysis, and the mixture was also analysed by LC-MS. After maximum formation of the desired product, EtOH was evaporated using a rotary evaporator. Following that, a liquid-liquid extraction is performed 3 times using AcOEt and H_2O. The aqueous phase was collected, which is then reduced to a smaller volume by rotative evaporation in order to purify through column chromatography using C18

silica. The 10-azidepropyl-4'-hydroxypyranoflavylium (**10**) was recovered with 40% MeOH, and after lyophilization processes it was obtained a dark orange powder. Yield = 10%. LC-DAD / ESI-MS: $[M]^+$ *m/z* 346, λ_{max} = 463 nm.

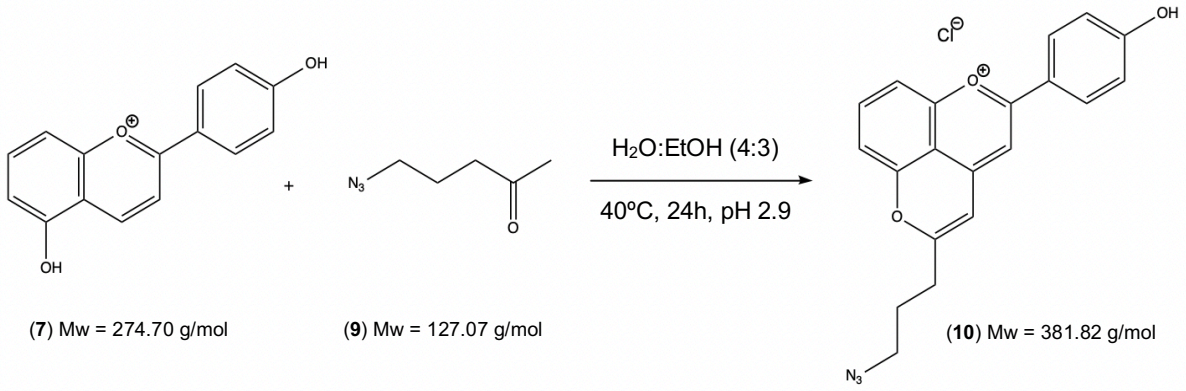

(**7**) Mw = 274.70 g/mol (**9**) Mw = 127.07 g/mol (**10**) Mw = 381.82 g/mol

Figure 19: Reaction scheme of 10-azidopropyl-4'-hydroxypyranoflavylium.

10-azidepropyl-4'-hydroxypyranoflavylium (**10**): ^{1}H NMR (600.13 MHz, DMSO-d_6/TFA 9:1) δ (ppm): 8.25 (t, 2H, *J* = 9.04 Hz, H-3' and H-5'), 8.22 (d, 1H, *J* = 8.39 Hz, H-7), 7,90 (s, 1H, H-3 or H-9), 7,89 (d, 1H, *J* = 8.35 Hz, H-6 or H-8), 7.76 (d, 1H, *J* = 8.35 Hz, H-6 or H-8), 7.11 (s, 1H, H-3 or H-9), 7.08 (t, 2H, *J* = 8.93 Hz, H-2' or H-6'), 3.51 (t, 2H, *J* = 7.07 Hz, H-11), 3.01 (t, 2H, *J* = 7.07 Hz, H-13), 2.04 (q, 2H, *J* = 7.10 Hz, H-12).

6. Pigments and polymers conjugation

6.1. Click Chemistry reactions – Copper-catalyzed Azide-Alkyne Cycloaddition (CuAAC)

For the Click Chemistry reactions, chitosan functionalized with hex-5-ynoyl groups (with 4 and 25% of DD) was kindly provided by COMPASS Group of CICECO, University of Aveiro.

6.1.1. Experimental process

In a 50 mL round bottom flask were added 1.5 mg of the pigment, (**5**) or (**10**), and 75 mg of dialysed CHT (either 4 or 25% substituted), which is approximately 52 equivalents of CHT. These two compounds were dissolved in 10 mL of Dimethylsulfoxide (DMSO). A solution of copper sulfate pentahydrate, $CuSO_4{\cdot}5H_2O$, (0.2 eq) was dissolved in 1 mL of water and added to an ice-cold solution of Sodium Ascorbate (0.4 eq) also dissolved in 1 mL of water and a yellow precipitate appeared. The resulting Cu(I) solution was transferred to the reaction vessel, along with 1.5 mg of Tris(benzyltriazolylmethyl)amine, TBTA, dissolved in 2 mL of H_2O. This mixture was then allowed to stir at room temperature overnight and kept in the dark (figures 20 and 21). The 4'-azide-5-hydroxy-4-methylflavylium (**3**) dye was not covalently attached to the modified chitosan since it did not showed to be a promising candidate for the development of pH-responsive membranes, as there was no colour change in response to pH variations.

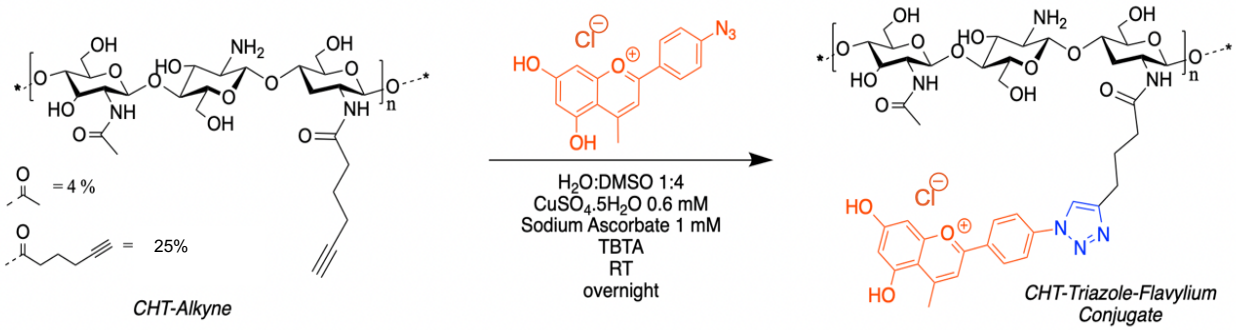

Figure 20: Click Chemistry reaction to obtain Chitosan-Flavylium conjugate.

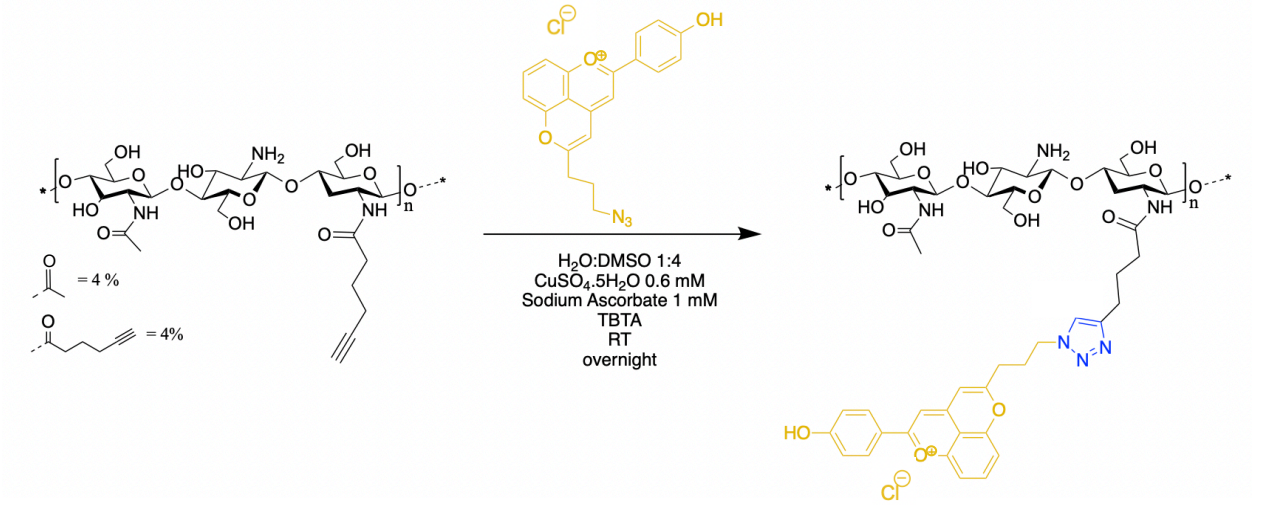

Figure 21: Click-Chemistry reaction to obtain Chitosan-Pyranoflavylium conjugate.

The reaction mixture solution was after transferred and purified by dialysis using a membrane with molecular weight cutoff of 3.5 kDa. After that, the dialysis bag containing the reaction mixture was stirred in a beaker filled with deionized water for 24 hours (water was changed twice every day).

The solution was then taken out from the dialysis bag and lyophilized to get a final dark dried material. The chemical modification of CHT was assessed by proton nuclear magnetic resonance spectroscopy (^{1}H NMR) and FTIR-ATR analysis to confirm the proton and respective bands of the triazole group.

The conjugates used in this project were CHT25% with Flavylium dye and CHT4% with the Pyranoflavylium dye.

6.1.2. Degree of dye conjugation to polymer

In order to determine the degree of dye conjugation, the released dye into the dialysis water was quantified. A calibration curve was calculated using the maximum absorbances of several pigment stock solutions at different concentrations: 0.005, 0.01, 0.02, 0.04, 0.06, 0.08 mM. The used conjugate to this study was the CHT25%- Flavylium, therefore, the study of pigment release into dialysis water concerns the pigment 4'-azide-5,7-dihydroxy-4-methylflavylium (**5**). A stock solution of pigment (6.94 mM) was prepared in EtOH 0.001 M HCl (pH 3). The several stock solutions were analysed in a UV-VIS spectroscopy equipment, using a glass cuvette and after in a HPLC-DAD equipment resulting into calibration curves.

7. Determination of the acidity constant (pK_a) of the synthesized compounds

All acidity constants were determined through spectrophotometric titrations which consists in successive additions of NaOH solutions, of different molarities to a dye stock solution previously prepared using a 75% (v/v) Ethanol (0.1 M HCl) solution.

In a quartz cell, equal volumes (1 mL) of Universal Buffer solution at pH = 1, aqueous NaOH solution (0.1 M) and the Dye stock solution were used to give the final

concentration of 0.1 mM for pigment (**5**) and 0.09 mM for pigment (**10**) as well as 25% ethanol (EtOH). Afterwards, a titration using successive addition of NaOH solutions is performed in order to obtain pH values between 1 and 12. At each addition, the solution is mixed, and a UV-VIS spectrum was taken and finally, the pH value was measured.

The universal buffer solution used was prepared according to previous studies and according to the method stablished by Theorell and Stenhagen. Preparation is performed by dissolving phosphoric acid (2.25 mL, 85% w/w), boric acid (3.54 g), monohydrated citric acid (7.00 g), and NaOH (343 mL, 1 M) solution diluted in distilled water until a total volume of 1 L is reached [7230].

However, the Chitosan-Pyranoflavylium conjugate determination of acidity constants was performed a little differently: To dissolve the conjugate, a stock solution in acetate buffer at pH 3.5 was previously prepared, with 8 mg of conjugate diluted in 1 mL of acetate buffer. The stock solution was transferred to the cuvette, and 2 mL of buffer solution was added to a concentration of 2.7 mg/mL. The titration was made with NaOH solution as well.

Acetate Buffer solution was prepared according to the following reference: [73]. Initially, a 0.2 M Acetic Acid (solution A) was created by dissolving 11.5 mL of Acetic Acid in 1 L of H_2O. The sodium acetate (solution B) was then made by dissolving 27.2 g in 1 L of H_2O, followed by the preparation of a 0.2 M solution in the same way. After that, the following volumes were withdrawn from each of solutions, A and B: 463 mL and 37 mL, respectively. To those volumes was added 500 mL of H_2O making up a Sodium Acetate Buffer solution 0.1 M at pH = 3.6.

The pK_a values were determinated by adjusting the experimental absorbance values to the theorical calculated absorbance values. The sum of the minimum square method was diminished through application of the solver function available on Excel.

8. Membranes fabrication

The experiment consists in the fabrication of three distinct membranes: one with the produced CHT25%-Flavylium conjugate and two additional control membranes - one with modified with 25% alkyne terminal groups chitosan (CHT25%) and another one with native CHT. The robot had a mechanical arm with a PP substrate at the tip, which was immersed in the various solutions successively according to the scheme depicted in figure 14. The polymeric solutions (CHT and ALG, 1mg/mL each) are submerged for 6 minutes and then rinsed for 4 minutes. The robot was programmed to accomplish 200 cycles throughout this operation and all solutions were prepared using Acetate Buffer solution as solvent, with a concentration of 0.1 M and pH 5.5, as shown in figure 22.

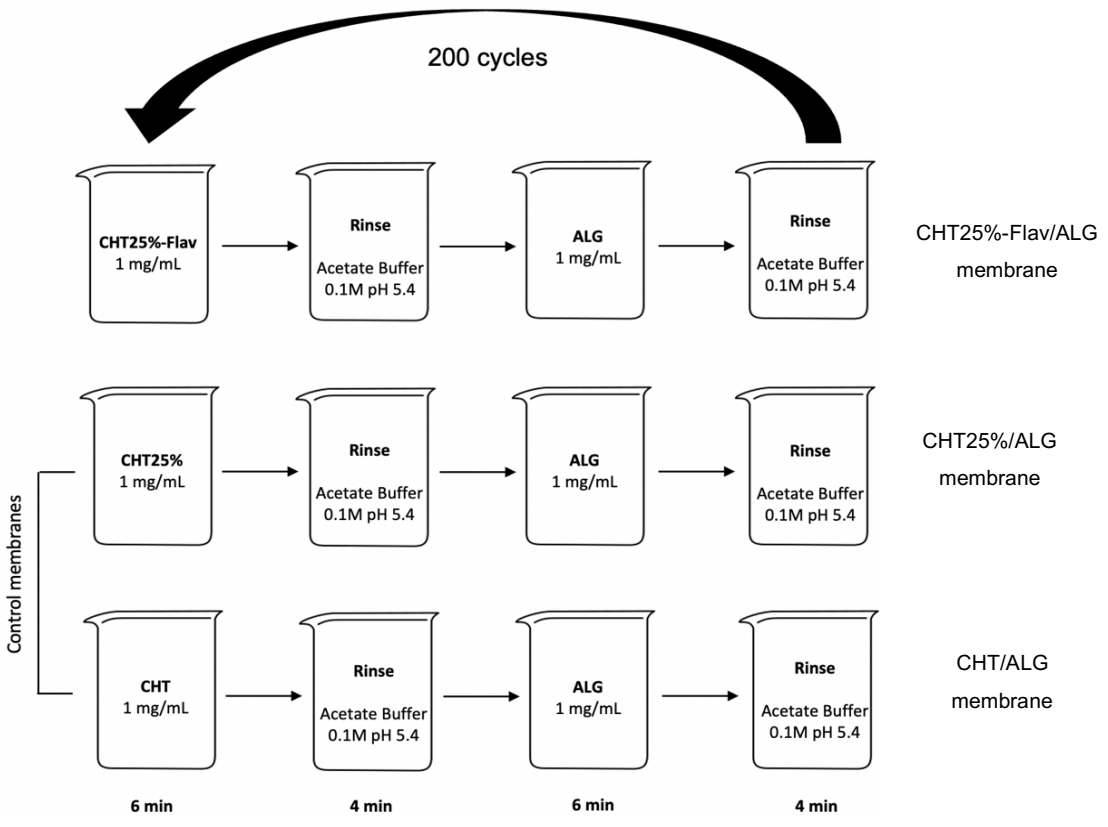

Figure 22: Fabrication scheme of CHT25%-Flavylium/ALG, CHT25%/ALG and CHT/ALG membranes.

9. Membranes characterization

2.1.1. Thickness

This analysis was carried out using a digital coating thickness meter model TE 1250-0.1 F, Sauter. The measurements were taken with 3 replicates in which each membrane thickness was measured in 10 random positions.

2.1.2. Moisture content

Moisture content is defined as the quantity of taken up water by the previously dried membrane until an equilibrium of the moisture content and the surrounding air it is reached.

To accomplish this study, the membranes were cut in 2 x 2 cm pieces, weighed (W1) and then dried in a 105 ºC set oven for 24 h. after that time, the membranes were weighed again (W2). The moisture content is then estimated, using the equation presented below. The studies were all carried out using triplicates.

$$MC\% = \left(\frac{W1-W2}{W1}\right) \times 100 \qquad \text{(Equation 1)}$$

2.1.3. Water solubility

Water solubility tests were done after letting the membranes in separated containers filled with water during 24 h at a 25 ºC environment in constant stirring using a mechanical shaker. After that time the membranes were carefully dried in a paper towel. They were then re-dried as previously done (105 ºC oven, during 24 h) and weighed one last time (W3). The equation below allows the determination of the water solubility of the membranes.

$$WS\% = \left(\frac{W2-W3}{W2}\right) \times 100 \qquad \text{(Equation 2)}$$

III. Results and discussion

1. Synthesis of 4'-azide-5-hydroxy-4-methylflavylium

The synthesis of the 4'-azide-5-hydroxy-4-methylflavylium (**3**) was accomplished through the reaction between two acetophenones - 2',6'-dihydroxyacetophenone (**1**) and *p*-azideacetophenone (**2**) - catalysed by acidic conditions and it is known as aldol condensation (figure 23).

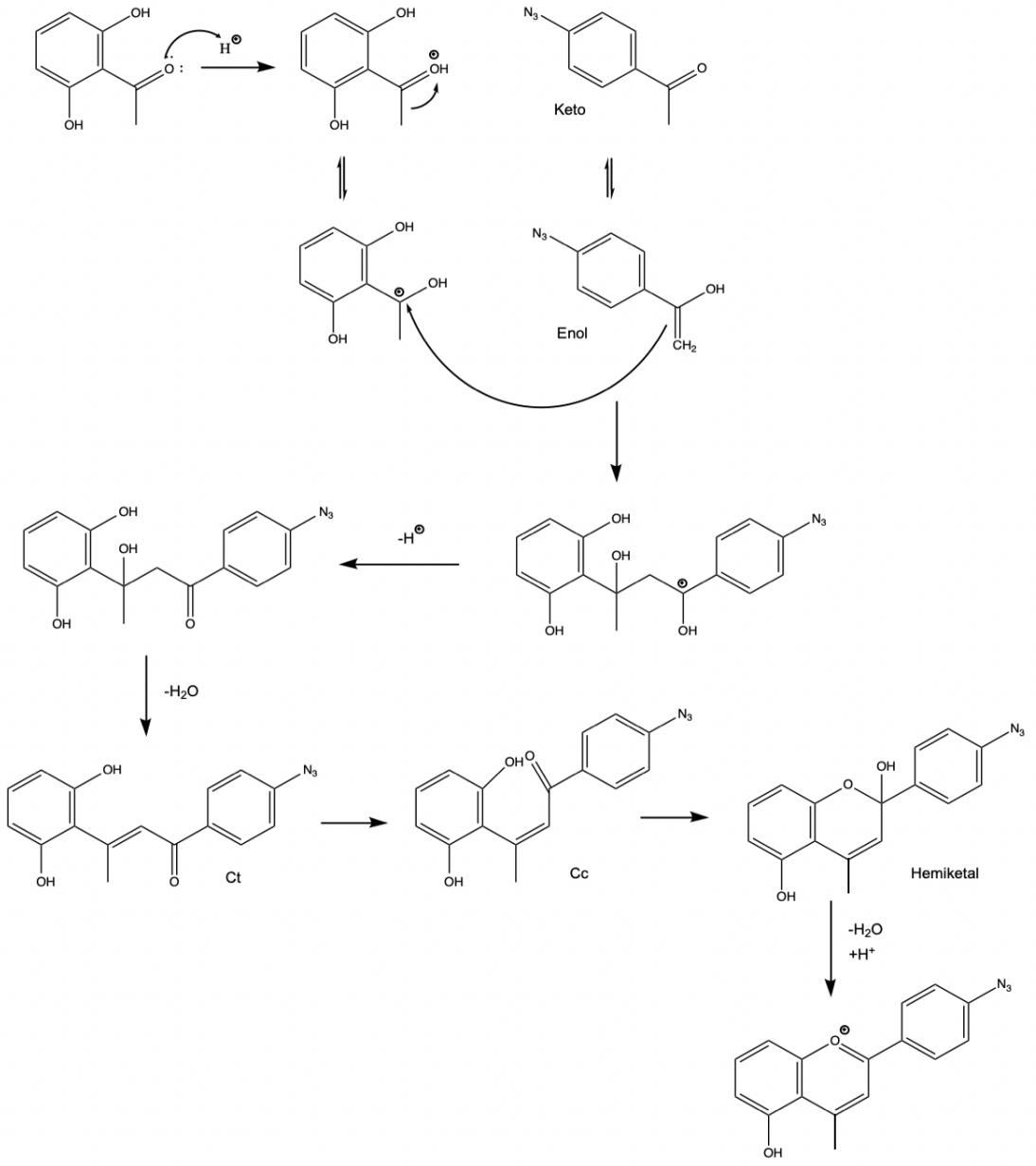

Figure 23: Reaction mechanism of 4'-azide-5-hydroxy-4-methylflavylium (**3**) synthesis.

The aldol reaction involves the use of two carbonyl compounds, one as an electrophile and the other as a nucleophile, to generate a new carbon-carbon single or double bond. It is a type of condensation reaction in which two carbonyl moieties (of aldehydes or ketones) combine to generate a β-hydroxyaldehyde or β-hydroxyketone, which is subsequently dehydrated to yield a conjugated enal or enone, respectively [74]. After purification, the pigment was obtained with yield of 7%. λ_{max} = 413 nm; t_r = 31 min; $[M]^+$ *m/z* 278; MS^2: $[M - 278]^+$ *m/z* 250 (figure 24).

The procedure used in this study is based on several works published by the same research group, although in a process of aldol condensation between a ketone and an aldehyde [26][27][76].

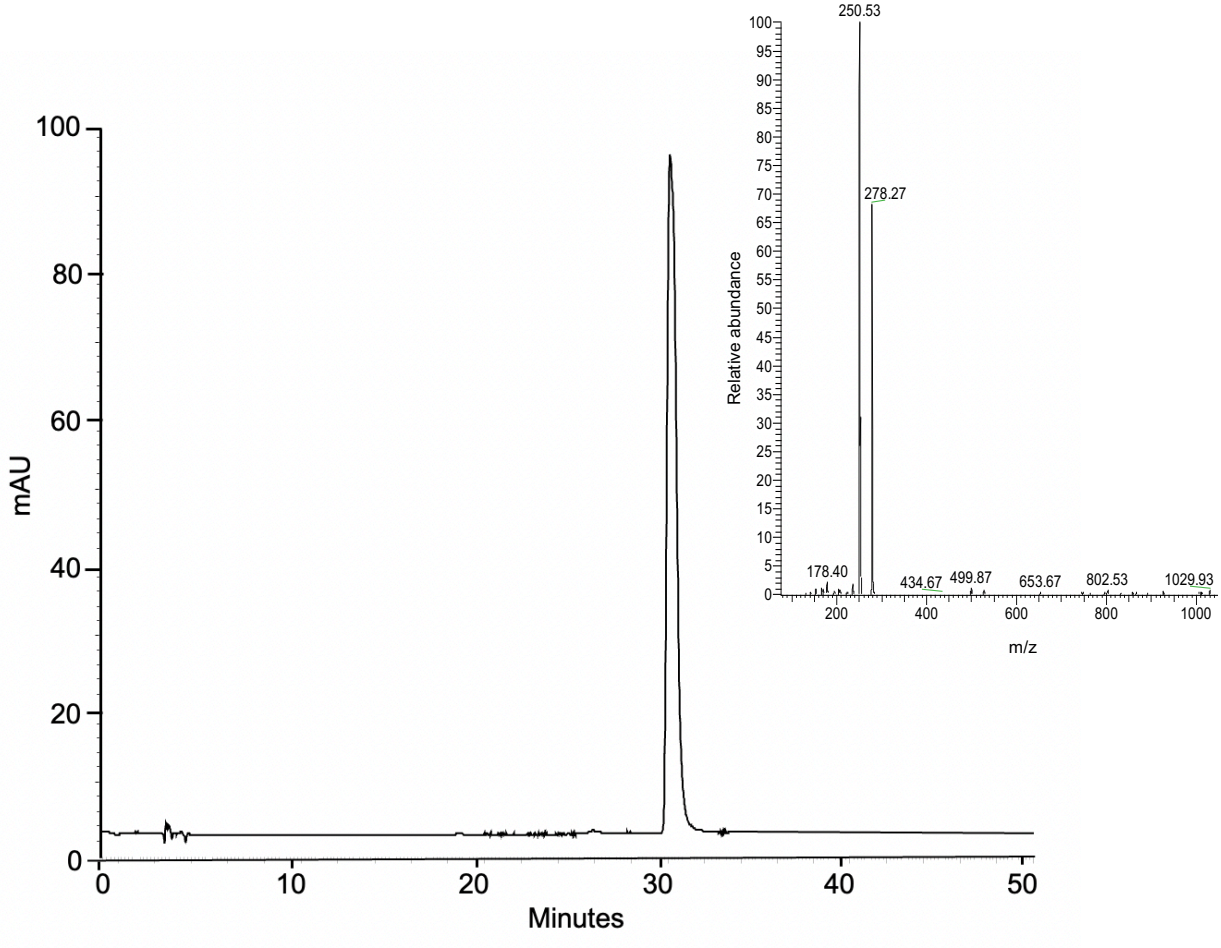

Figure 24: HPLC Chromatogram of fraction which corresponds to the desired product. Inset: Full MS spectrum of 4'-azide-5-hydroxy-4-methylflavylium (**3**).

1.1. Physical - chemical equilibria of 4'-azide-5-hydroxy-4-methylflavylium

To carry out this study, 1 mL of universal buffer solution at pH = 1, 1 mL of 1 M NaOH solution and 1 mL of pigment stock solution are inserted into a quartz cuvette, making up a volume of 3 mL in the cuvette, containing a concentration of 0.1 mM pigment and 25% EtOH, at pH 1, as shown in figure 25. The titration to obtain different pH values was performed using solutions of NaOH (1 M and 5 M), and at each value, the absorbance of the mixture in the cuvette was measured.

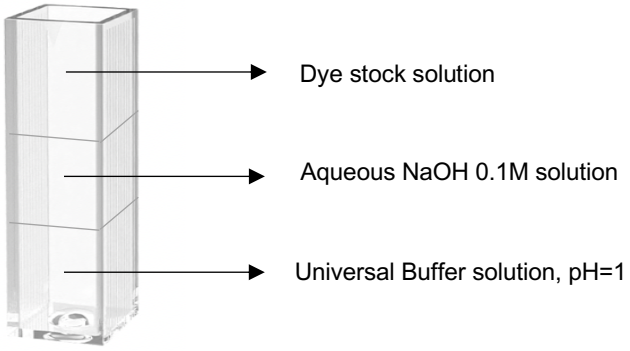

Figure 25: Representation of the different contents in the cuvette used for the titration of stock solution.

The absorbance spectra were after duly corrected taking in account the dilution factor caused by the successive increase of the solution by the titration inside the cell.

$$A_{corrected} = A_{experimental} \times \frac{V_{ad\ NaOH\ 1M} + V_{inicial}}{V_{inicial}} \quad \text{(Equation 3)}$$

The acid-base equilibrium of the synthesized dyes is summarized in the following equations:

$$AH^+ + H_2O \leftrightarrow A + H_3O^+ \qquad K_{a1} \quad \text{(Equation 4)}$$

$$A + H_2O \leftrightarrow A^- + H_3O^+ \qquad K_{a2} \quad \text{(Equation 5)}$$

$$A^- + H_2O \leftrightarrow A^{2-} + H_3O^+ \qquad K_{a3} \quad \text{(Equation 6)}$$

And,

$$K_{a1} = \frac{[A] \cdot [H_3O^+]}{[AH^+]} \qquad K_{a2} = \frac{[A^-] \cdot [H_3O^+]}{[A]} \qquad K_{a3} = \frac{[A^{2-}] \cdot [H_3O^+]}{[A^-]}$$

(Equation 7). (Equation 8) (Equation 9)

The total concentration of the individual species, C_0, is given by equation 7.

$$C_0 = [AH^+] + [A] + [A^-] + [A^{2-}] \quad \text{(Equation 10)}$$

Molar fraction distribution of the different species is calculated by:

$$\chi_{AH+} = \frac{[AH^+]}{C0} = \frac{[H_3O^+]^3}{[H_3O^+]^3 + K_{a1} \cdot [H_3O^+]^2 + K_{a1} \cdot K_{a2} \cdot [H_3O^+] + K_{a1} \cdot K_{a2} \cdot K_{a3}}$$

(Equation 11)

$$\chi_A = \frac{[A]}{C0} = \frac{K_{a1} \cdot [H_3O^+]^2}{[H_3O^+]^3 + K_{a1} \cdot [H_3O^+]^2 + K_{a1} \cdot K_{a2} \cdot [H_3O^+] + K_{a1} \cdot K_{a2} \cdot K_{a3}}$$

(Equation 12)

$$\chi_{A^-} = \frac{[A^-]}{C0} = \frac{K_{a1} \cdot K_{a2} \cdot [H_3O^+]}{[H_3O^+]^3 + K_{a1} \cdot [H_3O^+]^2 + K_{a1} \cdot K_{a2} \cdot [H_3O^+] + K_{a1} \cdot K_{a2} \cdot K_{a3}}$$

(Equation 13)

Synthesized dyes absorbance at a given wavelength is pH dependent and is defined by the equation:

$$A_{calc} = \varepsilon_{AH}+ + \chi_{AH}+ + \varepsilon_A \cdot \chi_A + \varepsilon_{A}- \cdot \chi_{A}- \quad \text{(Equation 14)}$$

Where ε_{AH}^{+}, ε_{A} e ε_{A}^{-} are the molar absorption coefficients of the individual species at the considered wavelength.

By tracing the UV-VIS spectra of this compound, it was observed an isosbestic point that is identified in figure 26 concerning a specific wavelength at which a sample's total absorbance does not change during a chemical reaction. However, this compound does not show colour change, instead, it becomes a colourless compound with the pH increase, which for the purpose of this project will not be useful. In figure 27 is shown the achieved fitting of the equilibrium constant of this pigment, using the solver function available on Excel.

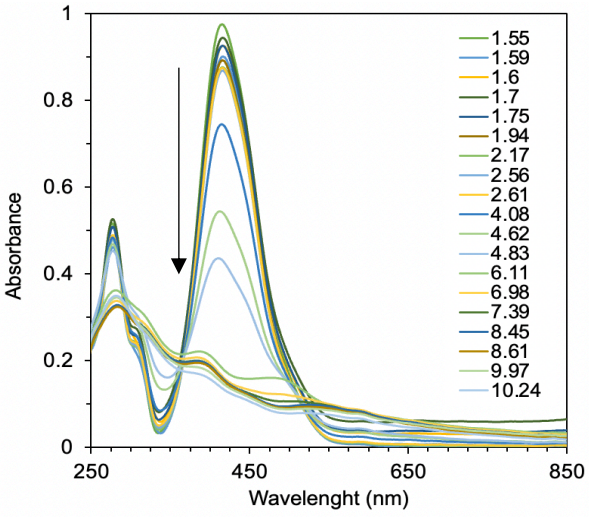

Figure 26: UV-Vis spectra of the 4'-azide-5-hydroxy-4-methylflavylium (**3**) at different pH values.

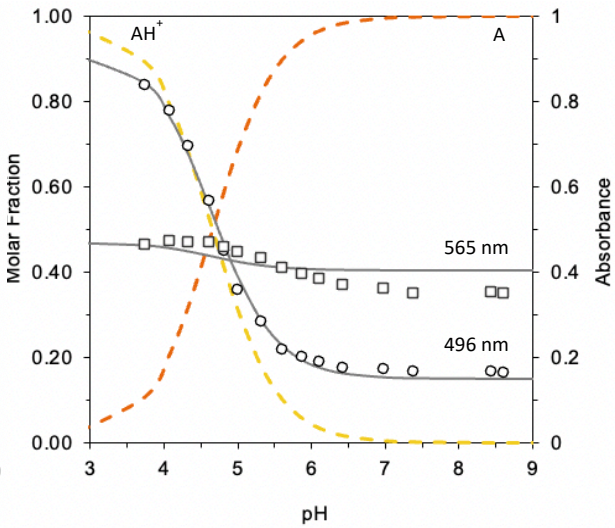

Figure 27: Experimental data fitting to achieve pK_a values of 4'-azide-5-hydroxy-4-methylflavylium (**3**).

What is suggested to have happened is a hydration of the flavylium, giving rise to the opening of the C-ring, resulting in the cis-chalcone form. However, anthocyanins present high isomerization barrier into cis and trans-chalcone which makes it more conducive to the formation of a hemiketal, which is colourless (figure 28). These forms could not be analysed by NMR or other techniques of characterization due to its short lifetime [77].

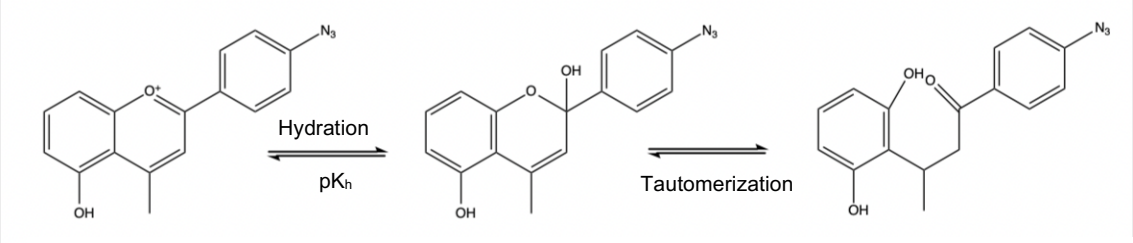

Figure 28: Possible chemical equilibria which may have caused the loss of pigment colouring.

2. Synthesis of 4'-azide-5,7-dihydroxy-4-methylflavylium

The procedure to synthesize this compound is similar to the one described to synthesize the 4'azide-5-hydroxy-4-methylflavylium: an aldol condensation is performed again between two acetophenones, 2',4',6'-trihydroxyacetophenone (**4**) and *p*-azideacetophenone (**2**).

The purification steps involve liquid-liquid extraction with Et_2O and water and subsequently, purification in a C18 glass column (figure 29).

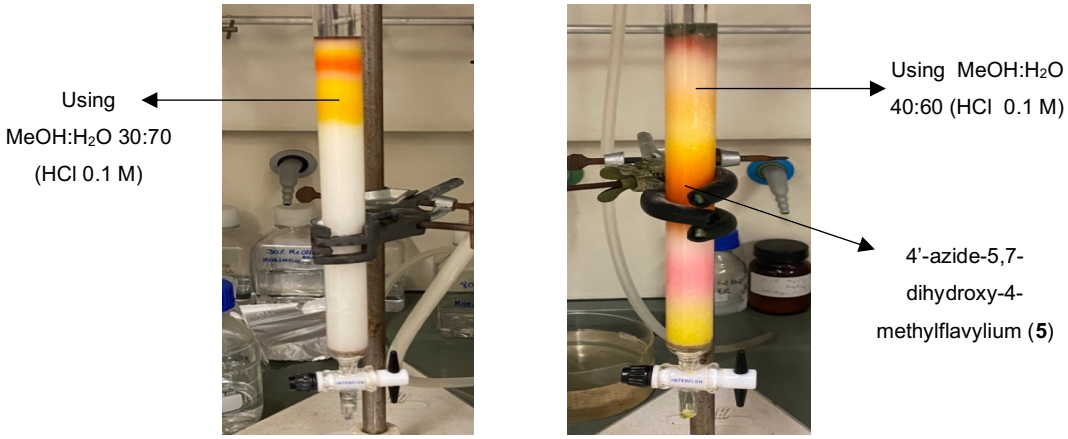

Figure 29: Purification of 4'-azide-5,7-hydroxy-4-methylflavylium (**5**) through flash chromatography.

Later, it was found that performing the same reaction under 0 ºC stirring for 6 hours exhibited a larger yield and its purification proved to be easier. Despite this, the yield is still very low, and in this way, we continue to try to improve it.

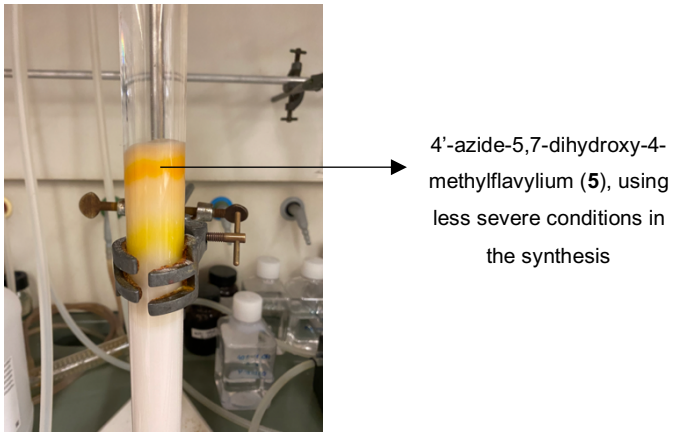

Figure 30: Purification of 4'-azide-5,7-hydroxy-4-methylflavylium (**5**) through flash chromatography using less severe conditions.

Figure 29 depicts the various impurities found in the produced substance, when synthesized at room temperature. It is clear that the amount of impurities has decreased significantly in figure 30, when the reaction occurs under low temperatures (on ice) and the reaction goes on for a longer period of time. This not only increases the yield of the reaction, but also turns the purification steps less labour-intensive and cheaper: the reaction is slower and there is less formation of secondary products which favours the formation of the desired pigment. The isolation procedure was similar, and the desired product was eluted with 60% MeOH. After lyophilization it was obtained a dark orange solid with a yield of 10%. The compound was later analysed and characterized by HPLC, LC-MS, FTIR-ATR and ^{1}H NMR.

After all the steps of purification and separation, the results are very satisfactory: the HPLC-DAD analysis shows only a peak at approximately 33 minutes of retention time (figure 31) which corresponds to the peak of the 4'-azide-5,7-dihydroxy-4-methylflavylium (**5**) dye. This statement can be confirmed through mass spectrometry analysis that was performed.

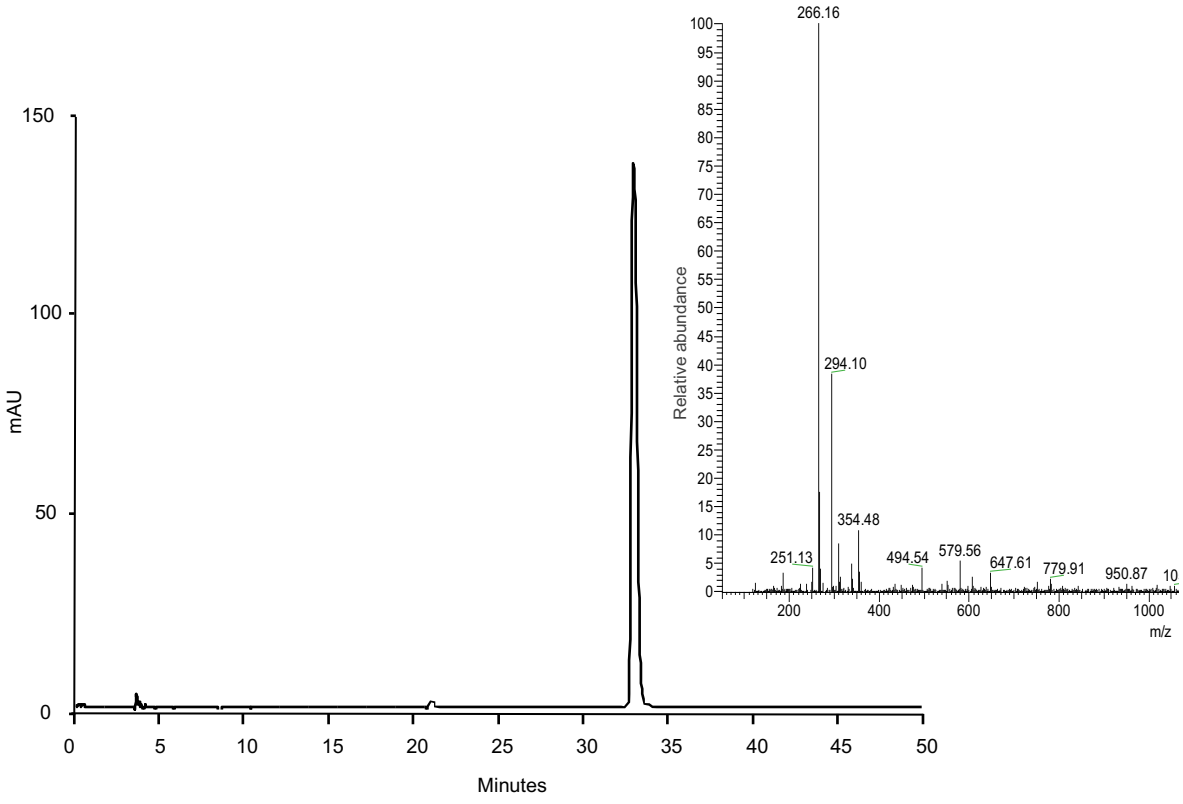

Figure 31: HPLC chromatogram of fraction which corresponds to the desired product. Inset: Mass spectrometry spectrum of 4'-azide-5,7-dihydroxy-4-methylflavylium (**5**).

2.1. FTIR-ATR analysis

The purpose of this analysis would be to understand if the 4'-azide-5,7-dihydroxy-4-methylflavylium synthesis was successful, as well as the characterization of this new compound. The only evidence that can be taken from this analysis is the appearance of the azide band found in this new compound, which together with other techniques could give us information on the success of this reaction method. Based in figure 32, it can be actually stated the existence of an azide group, located at 2090 cm^{-1} in the molecule.

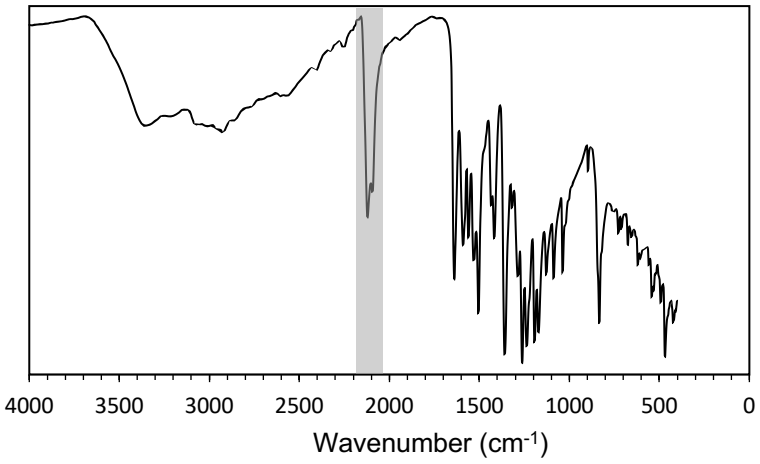

Figure 32: FTIR-ATR analysis of the 4'-azide-5,7-dihydroxy-4-methylflavylium (**5**) pure compound.

Unfortunately, no other groups could be evidently located through this analysis and so ^{1}H NMR analysis was used to further characterize the synthesized molecule.

2.2. ^{1}H NMR analysis

The obtained ^{1}H NMR analysis carried out in CEMUP are presented below in figure 33. The aromatic zone it is the most important area to analyse. Therefore, is presented a zoom in this specific area, as well as the identification of the relevant peaks. It is also important to note that the peak at 2.6 and at 14 ppm corresponds to the peak from the solvent in which the analysis was performed: DMSO-d_6 (deuteration degree minimum is 99.9%) and TFA, respectively.

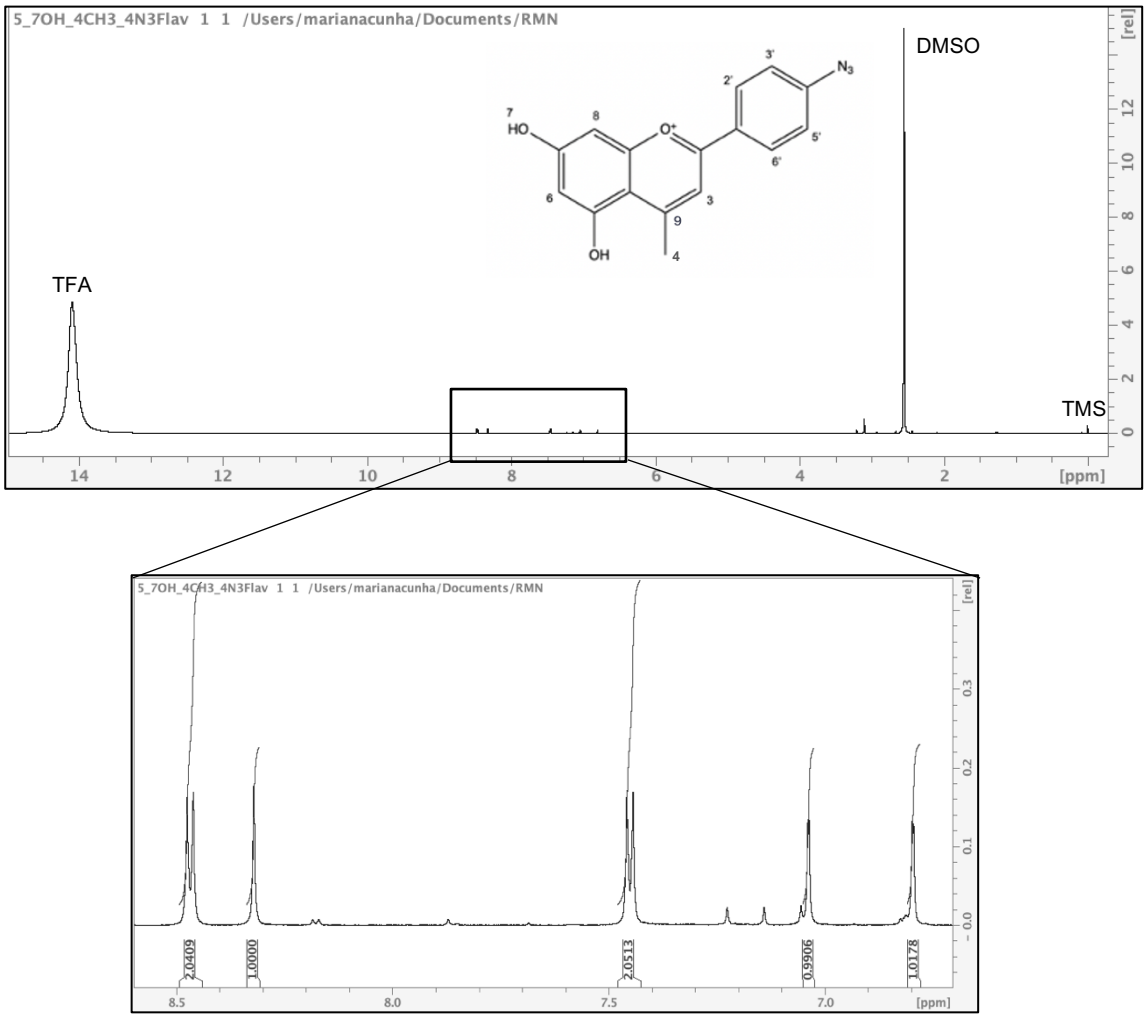

Figure 33: ^{1}H NMR spectrum of the isolated 4'-azide-5,7-dihydroxy-4-methylflavylium pigment.

The aromatic zone is the most relevant zone to analyze this compound, as most of the protons are located in this area. At 8.5 ppm, approximately, it can be seen a duplet which integrates to 2 protons and may correspond to H-3' and H-5'. Next, is seen a singlet integrating to one proton, at 8.32 ppm that integrates to H-3 followed by another duplet and two more singlets, which integrates to 2, 1 and 1 protons respectively. These are probably related to H-2' and H-6', H-6 and H-4 of the Flavylium dye. Outside of the aromatic zone there is another singlet at 3.10 ppm which integrates to 3 protons and has to correspond to H-4. A 2D COSY analysis was also conducted to confirm interactions between the protons.

2.3. Physical - chemical equilibria of 4'-azide-5,7-dihydroxy-4-methylflavylium

The UV-VIS spectra of the pigment at different pH values was recorded, according to the methodology previously stated, figure 34. A graph of the molar fractions was also subsequently plotted (figure 35). The first value of pK_a corresponds to the deprotonation of the OH group of flavylium at C-5. This transition of the flavylium cation (AH^+) originates the neutral quinoidal base (A) followed by a colorimetric visual transition in which the solution changes from yellow to darker yellow. The second value of pK_a corresponds to the deprotonation of another group OH this time in position 7 of the flavylium originating the anionic quinoidal base (A^-) which is orange coloured (figure 36).

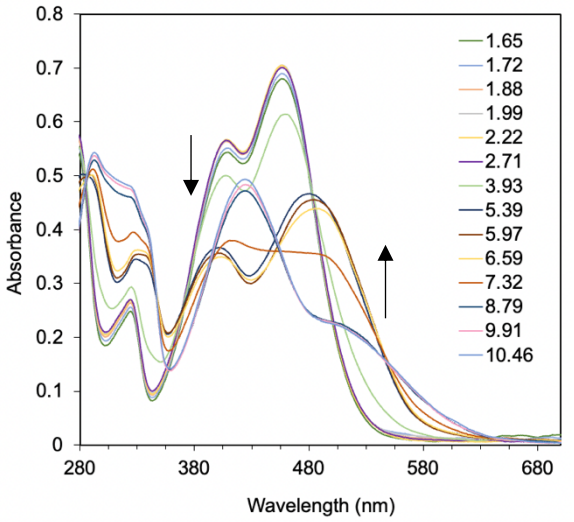

Figure 34: UV-VIS spectra of the 4'-azide-5,7-dihydroxy-4-methylflavylium (**5**) at different pH values.

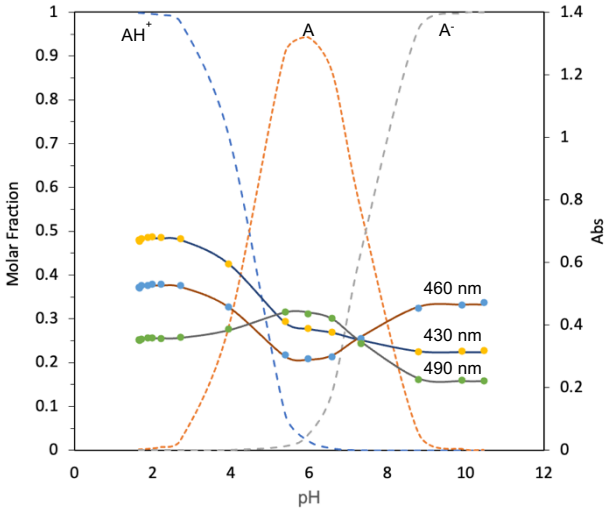

Figure 35: Experimental data fitting to achieve pK_a values of 4'-azide-5,7-dihydroxy-4-methylflavylium (**5**).

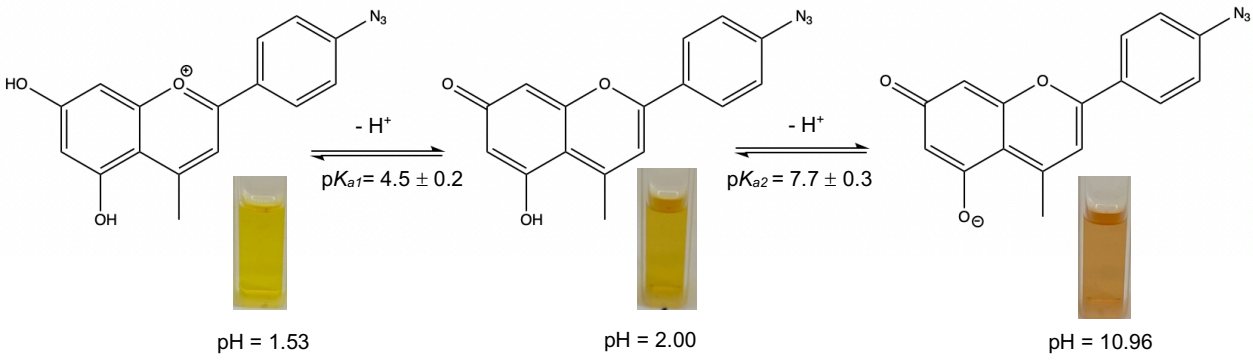

Figure 36: Equilibrium forms of pigment (**5**) in aqueous solutions with pH variation.

3. Synthesis of 10-azidepropyl-4'-hydroxypyranoflavylium

3.1. Synthesis of 4',5-dihydroxyflavylium

The synthesis mechanism of this reaction is presented below, in figure 37. Similar to other reactions reported in this work, this one also involved an acidic aldol condensation between a benzaldehyde, 2,6-dihydroxybenzaldehyde (**6**) and an acetophenone, *p*-hydroxyacetophenone (**2**) using as solvent a AcOEt:MeOH (2:1) mixture. This compound has already been thoroughly studied by the same research group, as has its full characterization is well established [71].

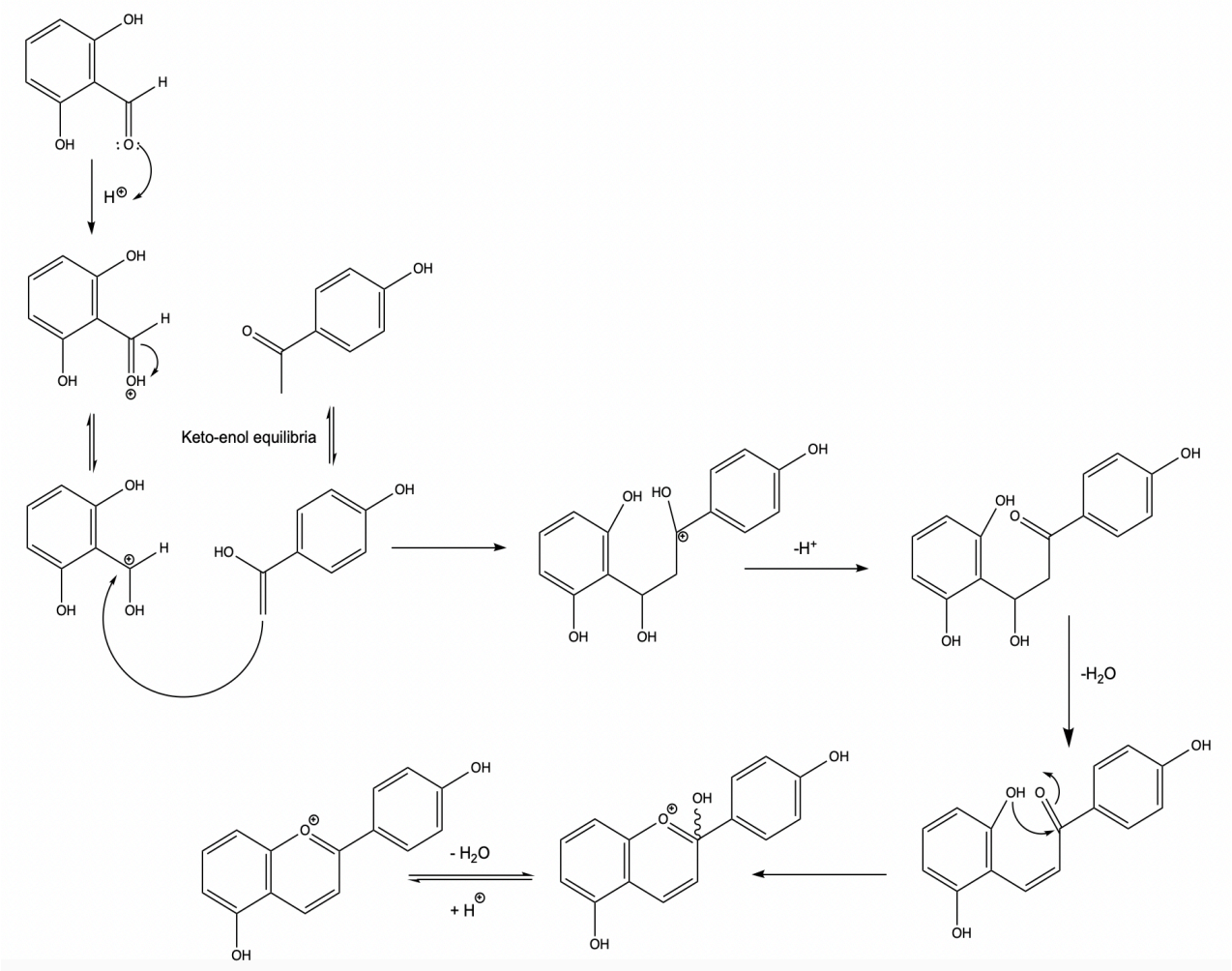

Figure 37: Reaction mechanism towards production of 4',5-dihydroxyflavylium (**7**).

3.2. Synthesis of 5-azidopentan-2-one

To synthesize 5-azidopentan-2-one (**9**) it was necessary to dissolve 5-chloropentan-2-one (**8**) and sodium azide in DMF. This reaction occurs by S_N2 mechanism, in which the N_3^- group of the NaN_3 acts as a nucleophile and the leaving group is chloride, as shown in Figure 38. It is also used TBAI, which performs as a catalyser of SN_2 reactions: the iodide contained in the catalyst replaces the chloride by an iodide anion which is a better leaving group, turning the S_N2 mechanism more suitable. The reaction was monitored through FTIR-ATR analysis, in order to determine whether or not an azidation had occurred.

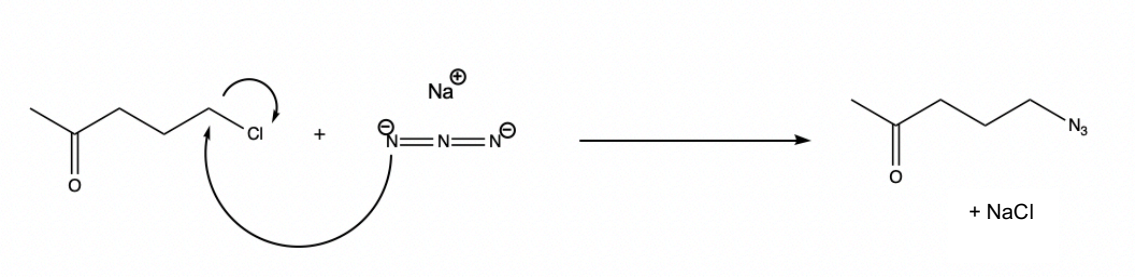

Figure 38: Reaction mechanism in order to obtain 5-azidopentan-2-one (**9**).

3.2.1. FTIR-ATR analysis

The goal of this analysis is to determine if azidation took place by visualizing the appearance of a characteristic band of the azide group (N_3). It can be stated that the reaction actually occurred, as shown in figure 39, since at 2090 cm^{-1}, a lengthy and visible band, typical of this identical group, appeared. This band was not present when compared to the reagent, 5-chloropentan-2-one (**8**), as predicted. Looking at the two spectra, they are quite similar, which is to be anticipated given the similarities in the structures of the two molecules.

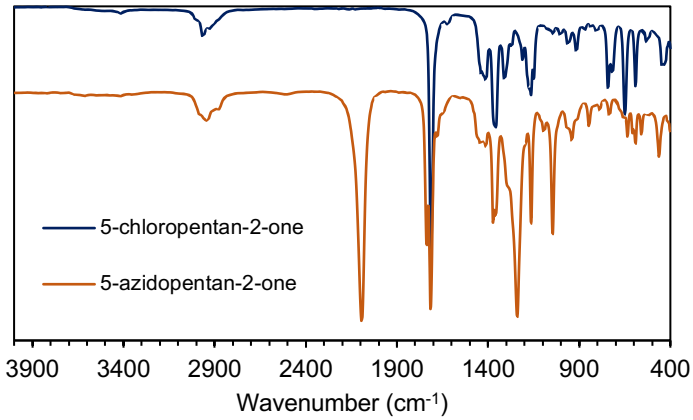

Figure 39: FTIR-ATR analysis results of the S_N2 reaction.

3.3. Annelation reaction between 4',5-dihydroxyflavylium and 5-azidopentan-2-one

This synthesis represents an annelation reaction between C-4 of the flavylium cation, the hydroxyl group of C-5, and the enolic form of the acetone as predicted in figure 40. This mechanism was already described in other works of our research group [7178].

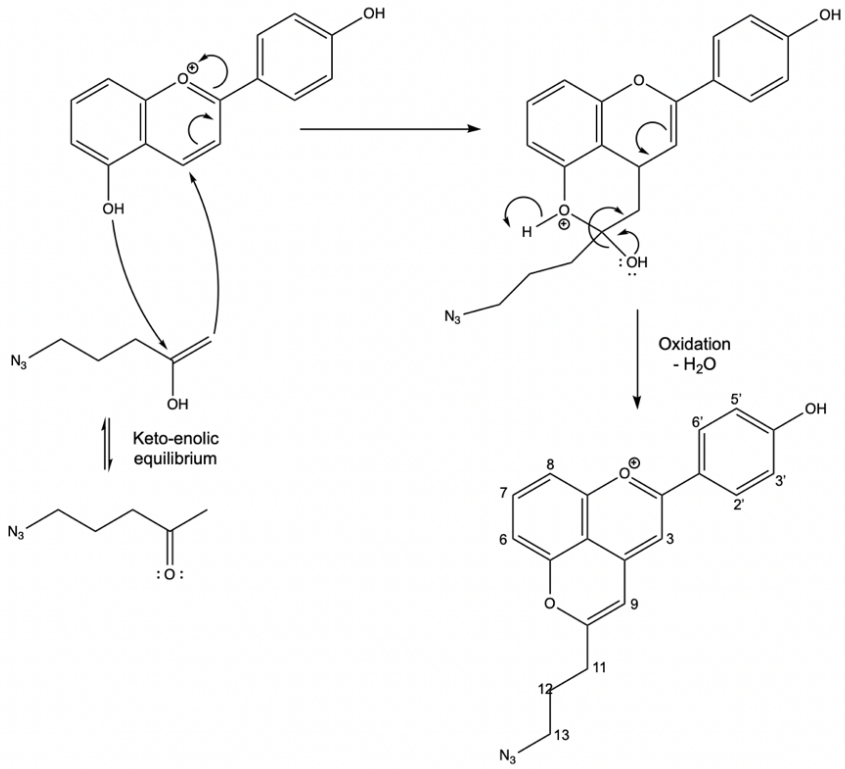

Figure 40: Proposed mechanism to obtain 10-azidepropyl-4'-hydroxypyranoflavylium (**10**).

For the reaction to occur, the molecule 5-azidopentan-2-one (**9**) must undergo a keto-enolic equilibrium. As previously mentioned, it is important to maintain the pH levels of the media at 2.9 in order to maintain that keto-enolic equilibria.

To perform this reaction, it was crucial to follow the reaction, to ensure the optimal conditions. The HPLC chromatogram in the beginning of the reaction and after 1 day is presented in figure 41. After that time, the corresponding peak of the desired product did not evolve. Besides, the impurities of this reactions increased, so it was possible to conclude that the optimal time to perform this reaction was 24 h.

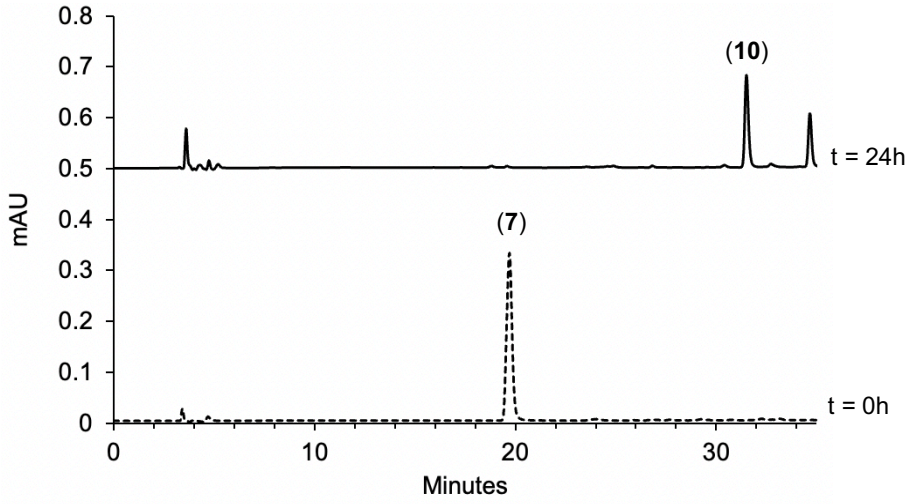

Figure 41: HPLC Chromatogram in the beginning of the reaction and 24 h after the beginning of the reaction.

The purification of this compound involves performing liquid-liquid extraction using ethyl acetate and water and subsequently, a C18 silica purification column, where the desired compound is recovered using a 40% MeOH solution. This method must be repeated twice, as seen in Figure 42, in order to properly isolate the compound.

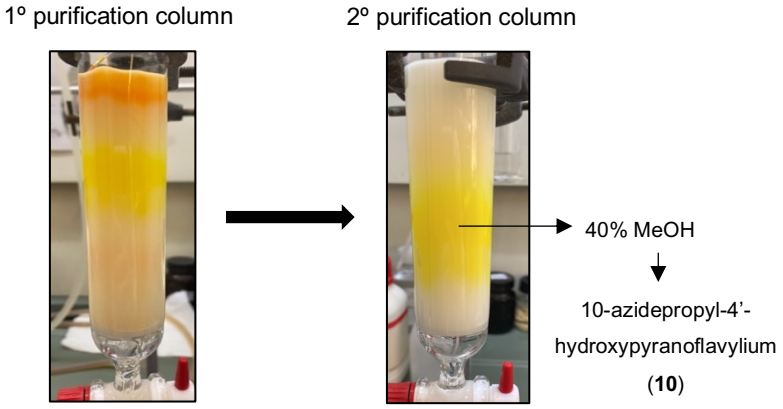

Figure 42: C18 silica columns towards 10-azidepropyl-4'-hydroxypyranoflavylium (**10**) purification.

After column chromatography purification, the pigment was obtained with yields around 10%. Through HPLC analysis it was possible to witness that this compound has a maximum absorbance at 463 nm and appears at 31 minutes of retention time, as seen in figure 43. This chromatogram shows that the pigment was effectively separated. Furthermore, it is known that this peak belongs to the desired pigment, as this was confirmed by injection in a mass spectrometry (LC-DAD/ESI-MS), which yielded a molecular ion $[M]^+$ *m/z* 349 with a typical fragment $[MS^2]$ *m/z* 318, which is confirms the tendency of the loss of two nitrogen atoms, the typical fragmentation of the N_3 group.

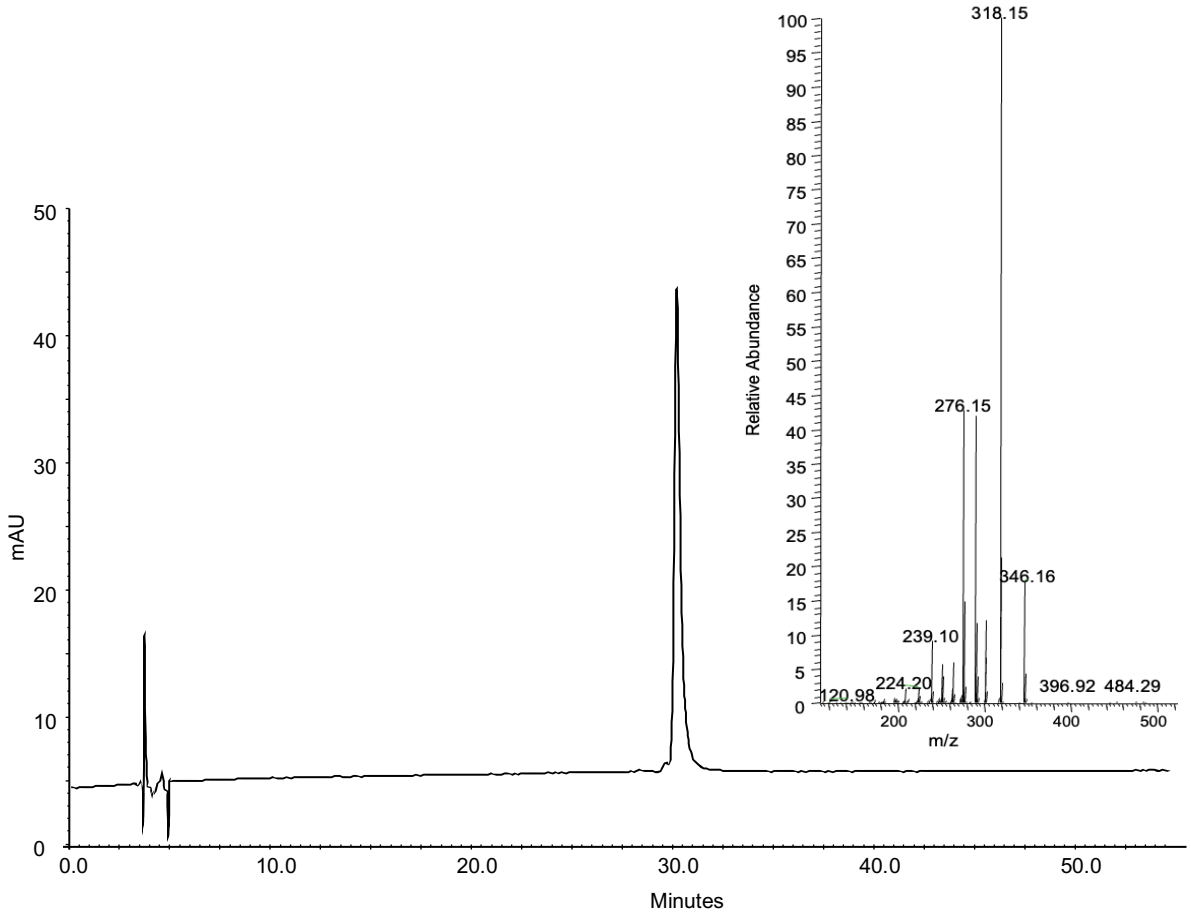

Figure 43: Chromatogram of the 10-azidepropyl-4'-hydroxypyranoflavylium (**10**) reaction after purification steps. Inset: Mass spectrometry of the pure pigment.

The molecule's structure was also confirmed using ^{1}H NMR, that is described further down. Previously, the synthesis of this dye was attempted for three days in a 40 ºC oven, but with those conditions the compound can suffer degradation and increasing the percentage of the impurities in the mixture.

3.3.1. FTIR-ATR analysis

Based on figure 44, FTIR-ATR results demonstrate the presence of the azide group in the molecule because of the presence of a band at 2090 cm^{-1}. Besides that, there is also the presence of an OH group in the form of a broad peak around 3350 cm^{-1}. Actually, the two key groups of the molecule in study are well defined in FTIR, therefore, the reaction was well succeeded.

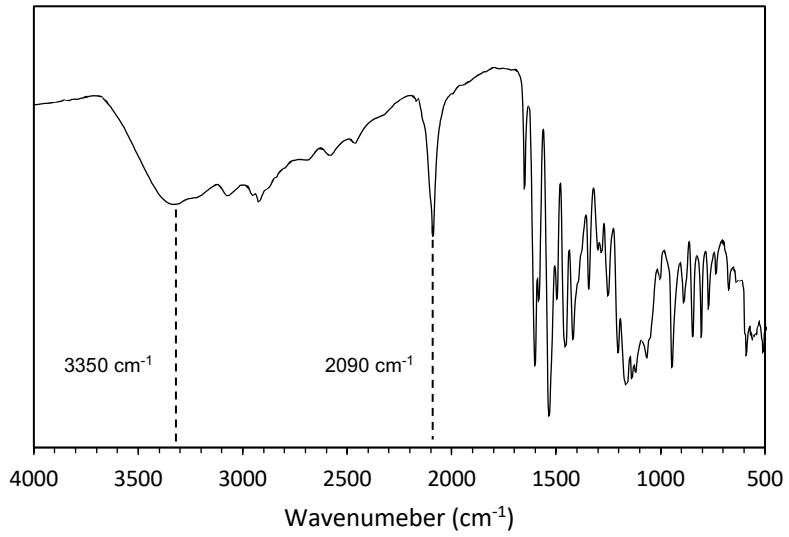

Figure 44: FTIR-ATR analysis results of the pure 10-azidepropyl-4'-hydroxypyranoflavylium (**10**) pigment.

3.3.2. ^{1}H NMR analysis

In order to fully characterize the synthesized 10-azidepropyl-4'-hydroxypyranoflavylium (**10**) pigment, a ^{1}H NMR analysis was carried out where 1 mg of pigment was dissolved in a mixture of 600 μL of DMSO-d_6:TFA (9:1). The obtained results are shown in figures 45, 46 and 47.

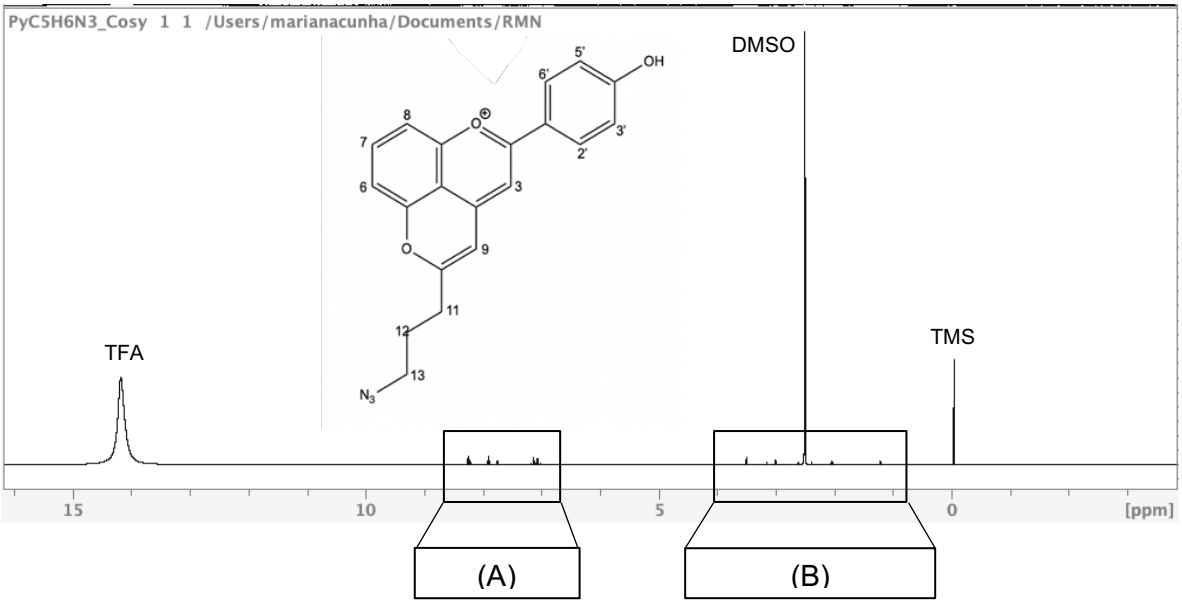

Figure 45: 1H NMR 600 MHz spectrum of 10-azidepropyl-4'-hydroxypyranoflavylium (10) recorded in DMSO-d6:TFA (9:1).

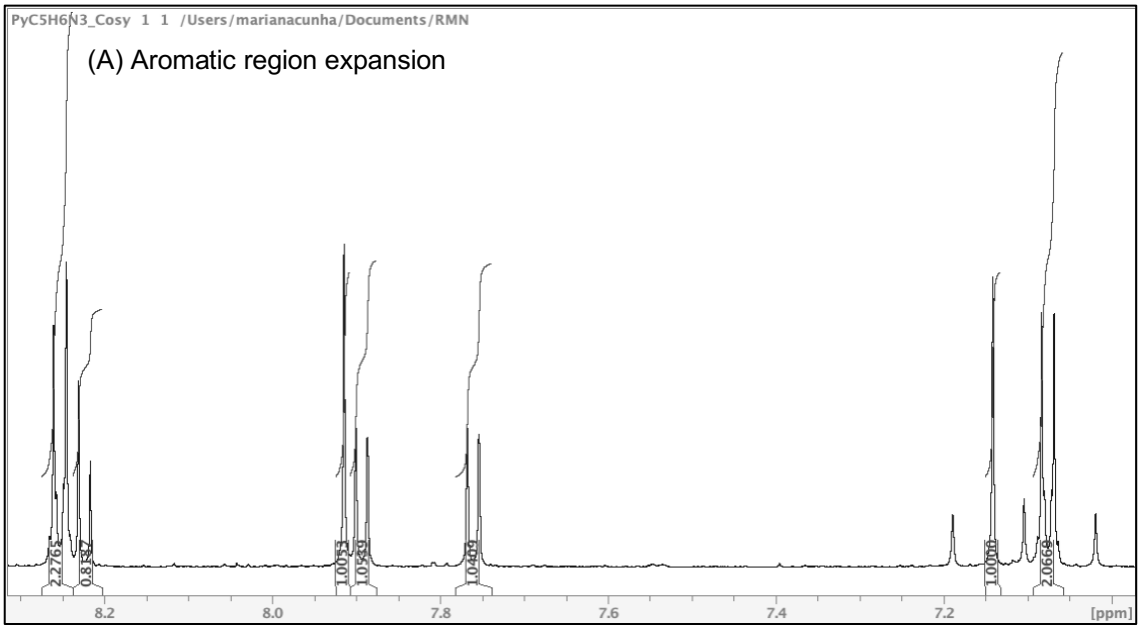

Figure 46: Expansion of the aromatic region of the 1H NMR spectrum presented in figure 45 (A).

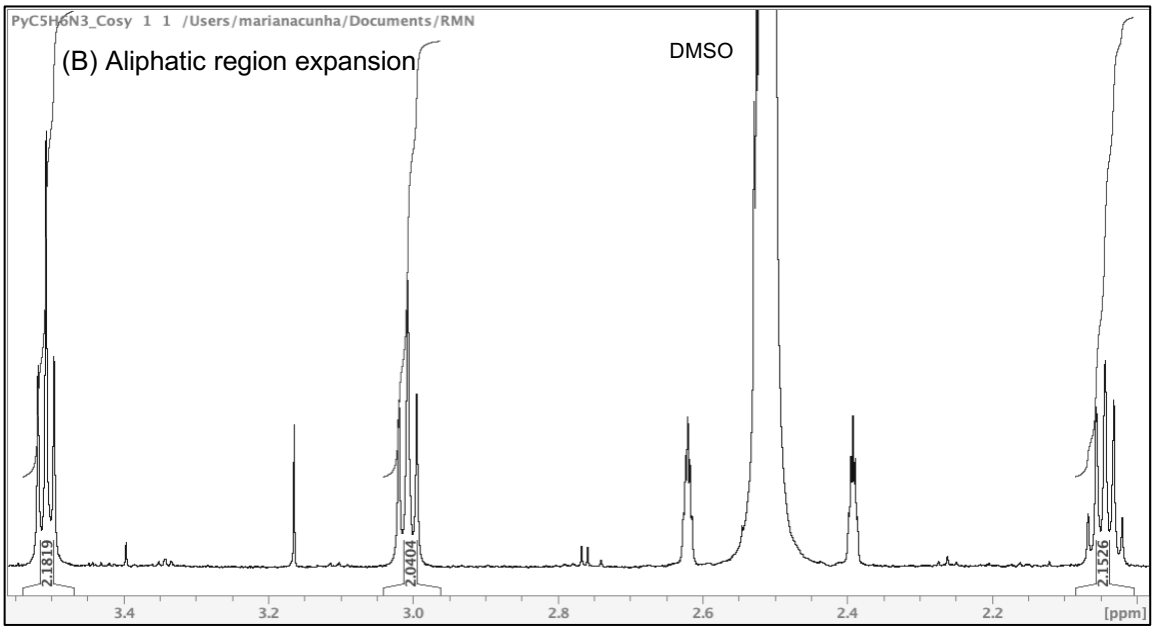

Figure 47: Expansion of the aliphatic region of the 1H NMR spectrum presented in figure 45 (B).

Starting this analysis at the 8.3 ppm peak, it is noticeable a triplet and a doublet which integrates to one and two protons respectively. The doublet was assigned to the H-2' and H-6' protons or H-3' and H-5' protons, however H-3' and H-5' protons are close to an oxygen atom and because of that, they might be more unshielded thus appearing more in the downfield zone. The triplet might correspond to H-7. After that, it is presented a singlet (7.9 ppm) integrating to one proton that may correspond to H-3 or H-9, followed by two doublets that may correspond to protons H-6 and H-8, which each one of them integrates to 1 proton. At 7.15 ppm, there is another singlet that integrates to 1 proton which corresponds to one of the following protons: H-9 or H-3 and following that, there is the appearance of a doublet at around 7.1 ppm that integrates to two protons and should relate to the protons H-2' and H-6'. Finally, in the aliphatic region, there are two triplets, at 3.5 and 3.0 ppm integrating to two protons, and a quintuplet at around 2.1 ppm, which also integrates for two protons. The triplets correspond to H-11 and H-13 whereas the quintuplet corresponds to H-12. It was also performed a 2D COSY analysis to confirm the correlations of protons.

3.3.3. Physical and chemical equilibria of 10-azidepropyl-4'-hydroxypyranoflavylium

In order to study the chemical equilibria of this compound, an acidic solution of the pigment was titrated with successive additions of NaOH solutions, and the UV-VIS spectrum was taken for each pH value. The UV-VIS spectra are presented in figure 48. Using fitting of experimental data using the mathematical described in section 2.2. The pK_a values were determinated through least-squares method and the solver function of Microsoft Excel.

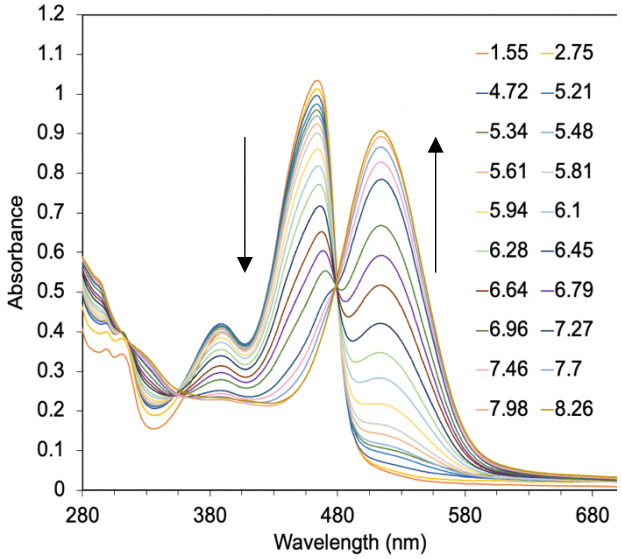

Figure 48: UV-VIS spectra of the 10-azidepropyl-4'-hydroxypyranoflavylium (10) at different pH values.

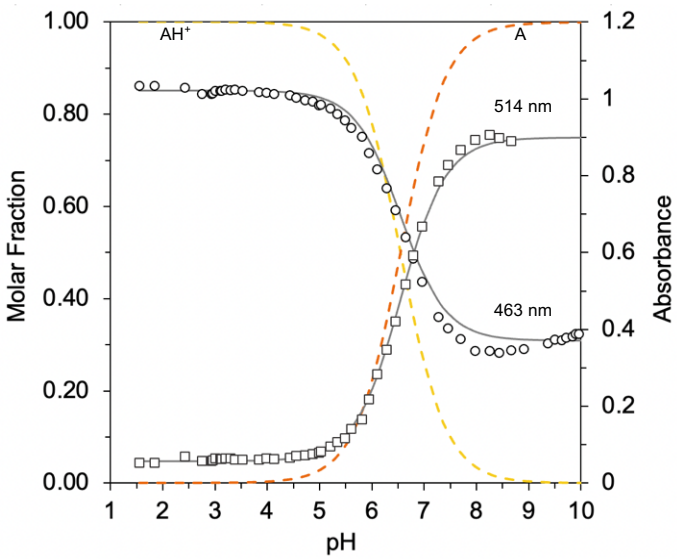

Figure 49: Experimental data fitting to achieve pK_a values of 10-azidepropyl-4'-hydroxypyranoflavylium (**10**).

As expected, it can be observed an absorbance shift, as pH values increase. This means that when these values rise, the flavylium cation give rise to the neutral quinoidal base (A) by deprotonation of the OH group found in the C-4' of the B-ring of pyranoflavylium. It was noticeable an isobestic point at 476 nm in figure 48 which is a certain wavelength value at which two (or more) chemical species (in this case AH^+ and A) have the same absorptivity and identical molar extinction coefficients.

Figure 49 allowed the determination of pK_a values, through least-squares method and the solver function of Excel. With that, it was possible to determine the acidity constant of this pigment (6.6 ± 0.5). Figure 50 shows the chemical balance that is established when the pH values of the mixture are increased, resulting in a colour change of the pigment: from yellow to dark pink.

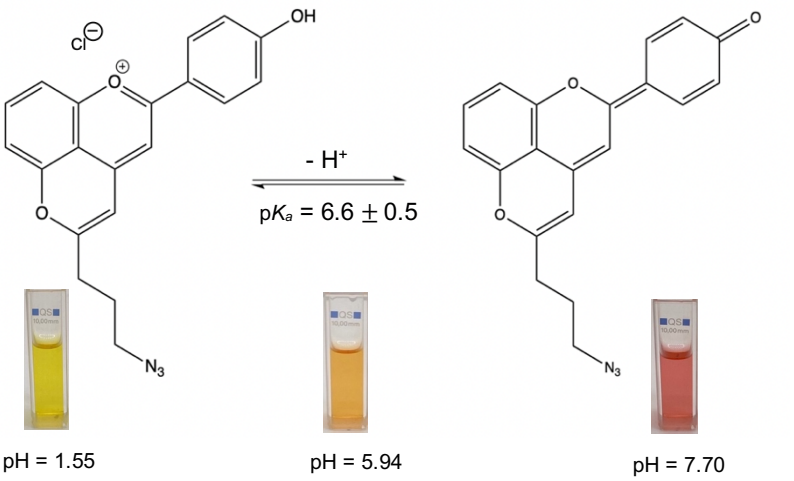

Figure 50: Chemical equilibria of the 10-azidepropyl-4'-hydroxypyranoflavylium (**10**) dye with pH variation.

4. Click Chemistry

In order to covalently bind dyes to chitosan, Click Chemistry strategy was followed. After all synthesizing and purification steps are concluded, we proceeded to structural characterization by several techniques presented below as well as determining the degree of dye conjugation to Chitosan.

4.1. Chitosan-Flavylium conjugation

4.1.1. Degree of dye conjugation to polymer

As stated before, one of the purification steps of the conjugation reaction is the dialysis, were the conjugated is poured to a 3.5 cut-off membrane, where several impurities with a smaller cut-off are transferred to the water, as shown in figure 51.

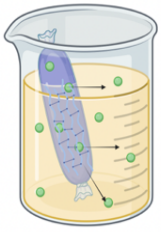

Figure 51: Illustration of the dialysis procedure.

After some time, the dialysis water became coloured, indicating that the pigment that was not covalently bonded to the CHT polymer had been transferred to the water. The release of this pigment in the dialysis water was firstly quantified through UV-VIS spectroscopy analysis. The calibration curve was plotted using pigment stock solutions of 0.005, 0.01, 0.02, 0.04, 0.06 and 0.08 mM, which were prepared using a previously prepared stock solution of Flavylium pigment of 6.94 mM in an EtOH 0.001 M HCl solution.

The stock solution of 0.005 mM was withdrawn from the calibration curve as it had very low absorbance. Following that, the dialysis water was lyophilized and redissolved in a known volume of the solvent to quantify the amount of pigment release. To finally determine the total pigment realising to the dialysis water, the maximum absorbance of lyophilized dialysis water was measured at 455 nm, which corresponds to the maximum wavelength typical of this pigment. Taking this into consideration, as well as the previously determined values of the slope (m) and intercept (b) through the calibration curve, the pigment's lost mass in the dialysis water may be estimated (figure 52).

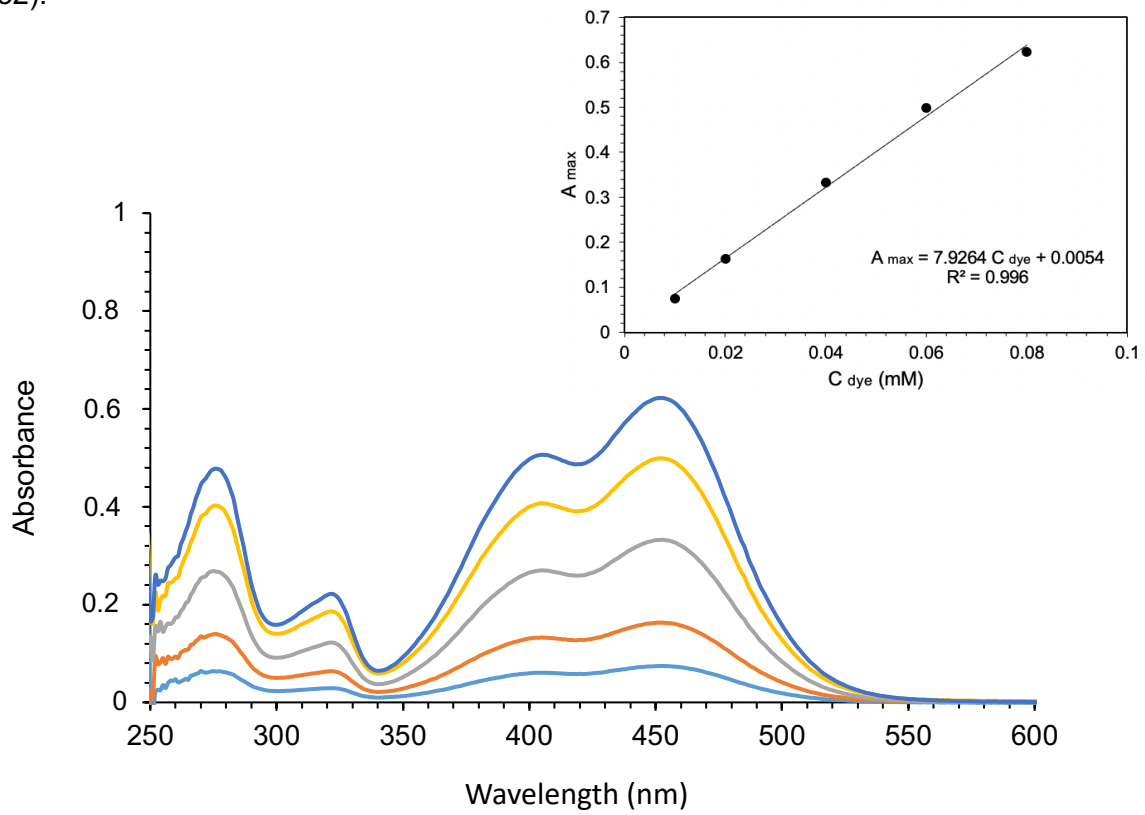

Figure 52: Maximum absorbance spectra obtained in several concentrations of the 4'-azide-5,7-dihydroxy-4-methylflavylium (**5**). Inset: Calibration line using stock solutions of several concentrations of the 4'-azide-5,7-dihydroxy-4-methylflavylium (**5**) pigment.

The sample of lyophilized dialysis water then was analysed through UV-VIS spectroscopy and the obtained spectrum does not correspond to the typical spectrum of pure flavylium, and its maximum absorption wavelength also does not correspond to the observed one in the pure flavylium solutions, leading us to believe that there will be more components in the sample than the flavylium dye, so the results from this technique cannot be fully trusted. Thus, the dialysis water was injected in a HPLC-DAD equipment, and the conclusion obtained is that there are more components in the lyophilized sample that absorb in the visible zone, interfering with the spectrum obtained in the UV-VIS, probably degradation products of the Flavylium.

Considering that, a calibration curve was created, once again using a HPLC-DAD equipment in triplicate, so that the pigment released in the dialysis water after the CHT25%-Flavylium conjugation reaction can be quantified from the areas of the peak of interest.

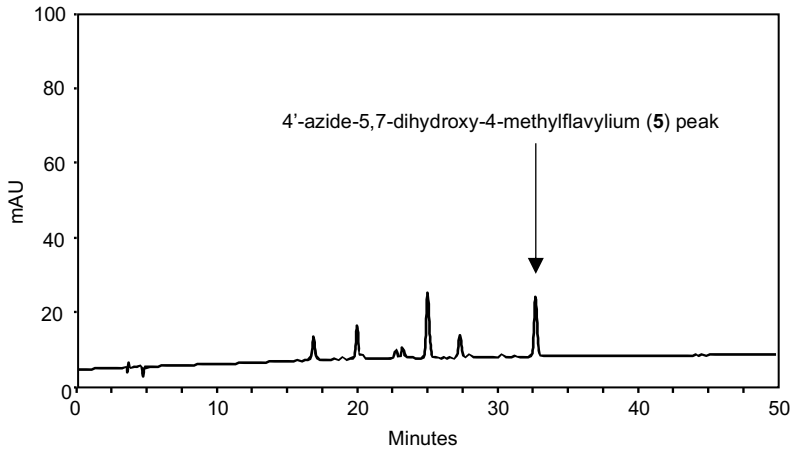

Figure 53: HPLC-DAD chromatogram of the dialysis water analysis after CHT25% conjugation with 4'-azide-5,7-dihydroxy-4-methylflavylium (**5**) dye, at λ = 455 nm.

As can be seen, there are several peaks in the dialysis water sample that absorb in the visible zone, indicating that running the calibration line through the UV-VIS spectrophotometer will be impossible because the result will be a sum of the absorbances of all the components visible in the HPLC-DAD chromatogram. The chromatographic peak highlighted at 33 minutes in figure 53 corresponds to the pigment peak in the sample.

For that reason, the processes was repeated, this time using HPLC-DAD analysis, using pigment stock solutions of 0.005, 0.01, 0.02, 0.04, 0.06 and 0.08 mM, which were prepared using a previously prepared stock solution of Flavylium pigment of

6.94 mM in a EtOH 0.001 M HCl solution, where a new calibration curve was plotted (figure 54).

Table 3: Concentration vs obtained maximum absorbance through HPLC analysis.

Concentration (mM)	Area
0.005	267888
0.01	627902
0.02	2838089
0.08	3943667

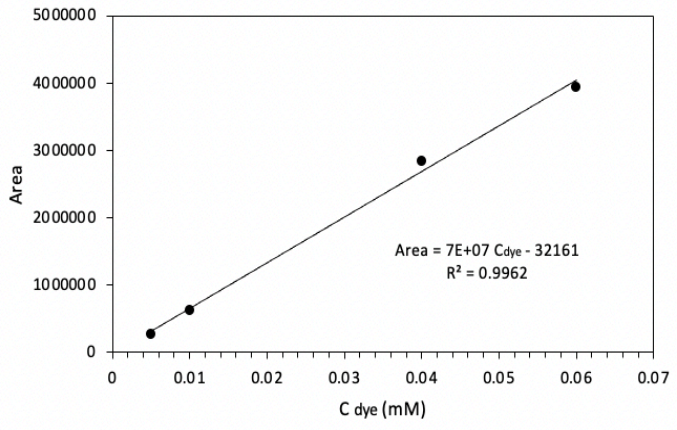

Figure 54: Calibration curve of 4'-azide-5,7-dihydroxy-4-methylflavylium pigment (**5**) executed by HPLC analysis.

Since two outliers were identified, at 0.02 and at 0.08 mM, these were eliminated from the calibration curve data processing. The area values identified on the HPLC (table 3) were used to calculate the calibration curve and relate to the 4'-azide-5,7-dihydroxy-4-methylflavylium pigment alone. As expected, the maximum absorbances are around 407 and 455 nm which are the typical values of this flavylium pigment. With this, a calibration line was drawn, the area corresponding only to the pigment in the dialysis water was also quantified, allowing the measuring of lost pigment in the dialysis process, in a known volume of solvent.

Table 4: Degree of dye conjugation to polymer and calibration curves in UV-VIS and HPLC-DAD

	Calibration curve	y value (λ = 455 nm)	Degree of substitution (%)	Free dye (%)
UV-VIS	A_{max} = 7.9264 C_{dye} + 0.0054	A_{max} (dialysis water) = 1.90	89.4	10.6
HPLC-DAD	Area = 7E+07 C_{dye} - 32161	Area $_{dye}$ (dialysis water) = 764168	**99.6**	**0.4**

$$\text{Degree of conjugation} = \frac{\text{total mass} - \text{mass in the dialysis water}}{\text{total mass}} \times 100 \qquad \text{(Equation 15)}$$

These results proved to be quite satisfactory, since only a small percentage of the pigment was released, meaning that the conjugation, in the case of HPLC-DAD analyses, was performed successfully (practically 100% of the pigment is covalently bonded to the CHT). Despite being presented, the results obtained through UV-VIS spectroscopy are not completely valid, due to the reasons mentioned above.

4.1.2. FTIR-ATR analysis

The FTIR-ATR analysis was done to determine whether or not the conjugation reaction occurred. Results of conjugate coupling with 4'-azide-5,7-dihydroxy-4-methylflavylium (**5**) ($FlavN_3$) precursor seems to indicate that in fact, the reaction occurred, since the peak corresponding to the azide group (2090 cm^{-1}) [79] disappeared, which might represent that the azide molecules from the pigment reacted through Click Chemistry. In addition, there is another peak that might prove that in fact the Click Chemistry reaction happened: there is small band marked at 945 cm^{-1} which is not present at the Flavylium or Chitosan spectra, however, it may indicate the formation of a new group throughout conjugation. Since these conclusions are not enough to prove that the triazole group was formed, ^{1}H NMR and NOESY analysis to the same conjugate was performed afterwards, figure 55.

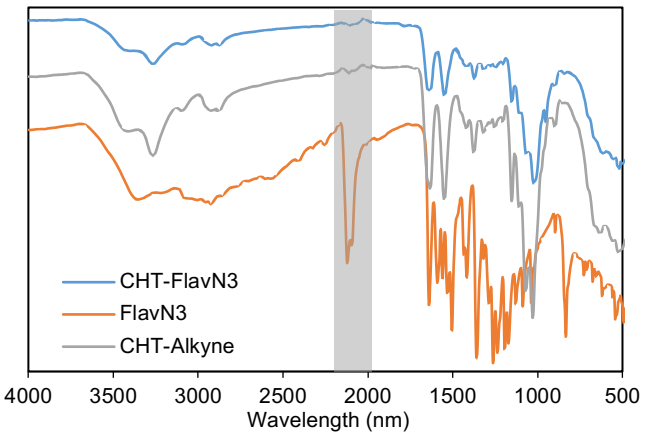

Figure 55: $FlavN_3$ (4'-azide-5,7-dihydroxy-4-methylflavylium) , CHT-Alkyne and CHT25%-Flavylium conjugate FTIR-ATR spectrum.

4.1.3. ^{1}H NMR analysis

After analysing the NMR spectra, figure 56, it is possible to assure that C-H triazole peaks appear between at 7-10 ppm [80]. According to the molecule, C-H triazole peaks does not have neighbouring protons and for that reason, the signal should appear as a singlet. However, there are several signals in this area that may be related to the proton of the triazole group however only through this technique it was not possible to identify it. Thus, a NOESY NMR analysis was performed.

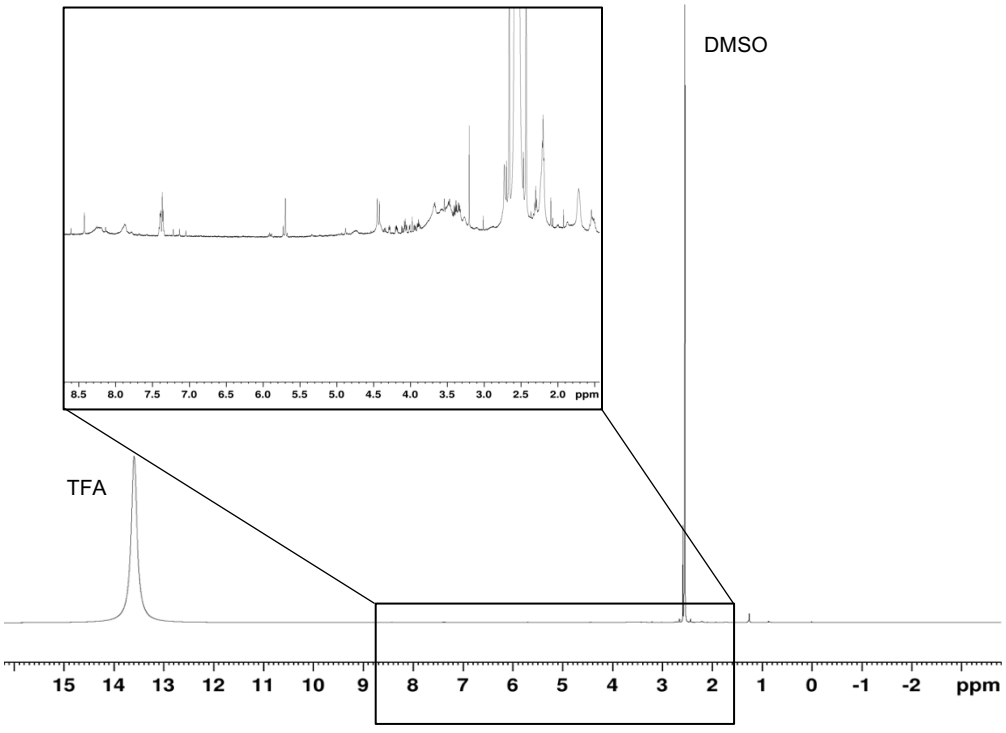

Figure 56: NMR 600 MHz analysis data of the CHT25%-Flavylium conjugate in DMSO-d6:TFA (9:1).

Figure 57 presented below is regarding to the aromatic region expansion of the ^{1}H NMR analysis which were performed to flavylium, the modified chitosan, as well as the conjugate.

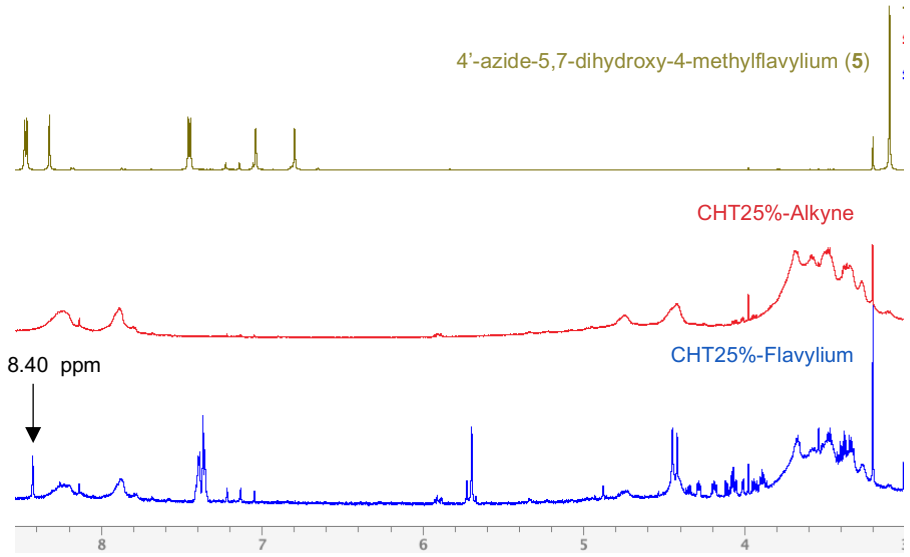

Figure 57: NMR analysis data of the isolated 4'-azide-5,7-dihydroxy-4methylflavylium (**5**), modified Chitosan (CHT25%-Alkyne) and CHT25%-Flavylium conjugate, with an expansion region in the zone of interest - the aromatic region.

It was observed that some peaks between 7 and 7.4 ppm corresponding to the Flavylium are present in the conjugate spectrum, which might indicate that the analyzed mixture actually has flavylium protons. In the same figure, it was also observed the peak at 8.40 ppm, which most likely corresponds to the triazole group, according to the literature [81]. Furthermore, this peak does not exist in the CHT25%-Alkyne spectrum.

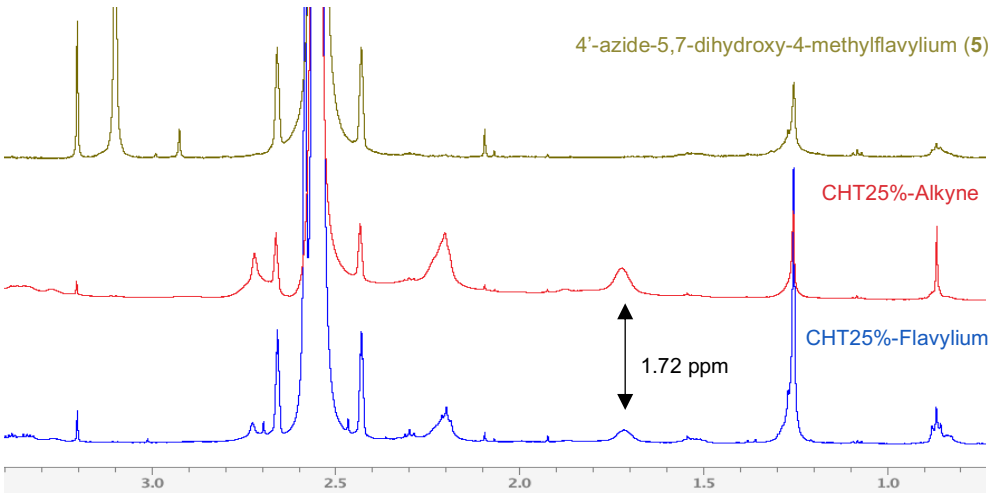

Figure 58: NMR analysis data of the isolated 4'-azide-5,7-dihydroxy-4-methylflavylium, modified Chitosan and CHT25%-Flavylium conjugate in the aliphatic region emphasizing the peak presented at 1.72 ppm.

Figure 58 showed a signal at 1.72 ppm, which might correspond to the alkyne group. After several analysis, we could conclude that this signal appears very often when a conjugate is produced with an excess of CHT25%-Alkyne used. When the pigment is covalently linked to Chitosan, the alkyne group peak decreases when comparing to the same peak in the CHT25%-Alkyne analysis. Also, when the alkyne peak decreases, it is evident the increase peak of the previously mentioned triazole group at 8.40 ppm, in the conjugate spectra, giving us further evidence of the conjugation of CHT25% with the Flavylium pigment.

4.1.4. DLS/Zeta potential analysis

Stock solutions of native polymers and conjugates (1 mg/mL) were prepared in acetate buffer pH 5.5 and measured at 0.1 mg/mL. The aim of this analysis was to confirm if whether or not the Flavylium dye significantly altered the positive charge of the Chitosan polymer in order to produce multi-layer membranes via electrostatic interactions. These electrostatic interactions are stronger if the opposite charges of the two polymers involved in the biofilm are as opposite as possible and so, the main goal of this study is to determine whether the electrostatic strength is high enough to create the biofilm.

The zeta-potential results showed that CHT25%-Alkyne has a positive average surface due to amino group protonation with a potential value of 23.3 ± 0.7 mV and ALG has a negative average charge due to the carboxyl group whose potential value is -24.5 ± 0.4 mV. Then, it was measured the value of the CHT25%-Flavylium, and it was obtained 32.9 ± 3.1 mV. These results revealed to be promising for ensuring electrostatic driven interactions by direct deposition on inert substrates, such as PP, with the goal of forming pH-responsive multi-layered membranes via Layer-by-Layer assembly technology. The measurements were performed in acetate buffer pH 5.5 since the LbL technique is carried out under the same conditions. Figure 59 display the results of this analysis.

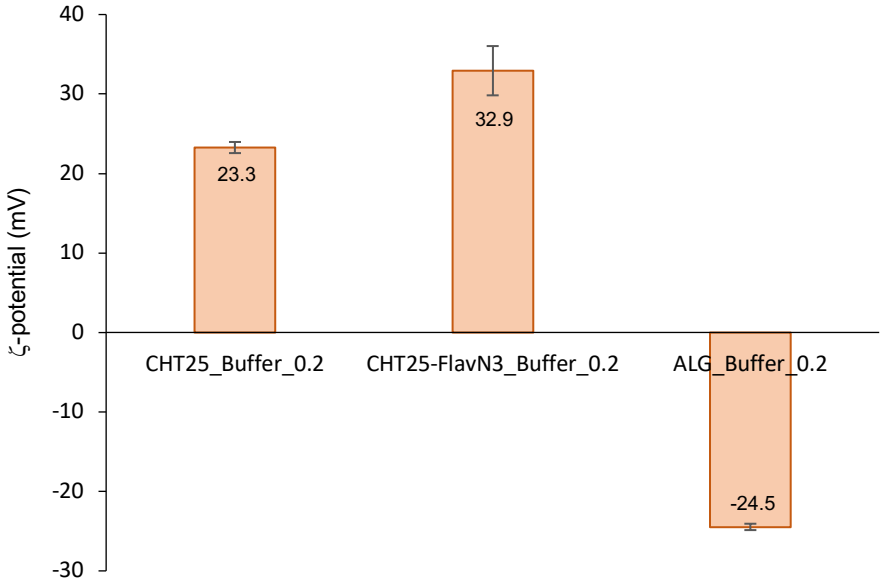

Figure 59: ζ-potential analysis of native CHT25%-Alkyne (CHT25_Buffer_0.2), CHT25%-Flavylium (CHT25-FlavN3_Buffer_0.2) conjugate and oppositely charged polysaccharide, Alginate (ALG_Buffer_0.2) solutions: 0.1 mg/mL, acetate buffer pH 5.5.

4.2. Pyranoflavylium-Chitosan conjugation

After all purification processes, this conjugate was also submitted to several characterization techniques, such as FTIR-ATR, Physical-Chemical equilibria, and DLS/Zeta Potential analysis.

4.2.1. FTIR-ATR analysis

For comparison, the CHT4%-PyFlav conjugate, polymer (CHT modified at 4 %), and the 10-azidepropyl-4'-hydroxypyranoflavylium (**10**) dye were studied separately (figure 60). The resemblance between the conjugate and the isolated polymer is quite strong, which makes sense given that just 4% of the Chitosan chain is replaced with the pigment, if considering that the conjugation occurred with a 100% yield. Yet in the fingerprinting zone, around 1200 cm^{-1}, usually belongs to an alkyl ketone group there is a small band that differs in the two spectra (CHT4% polymer and CHT4%-PyFlav conjugate), and this could represent the presence of the covalently bonded dye to the polymer. It is also important to emphasise that the azide band, present in the Pyranoflavylium dye spectra at 2090 cm^{-1} disappears in the conjugate spectra, which might indicate the covalently interaction between the polymer and the dye; however, this

information was not sufficient to confirm whether or not the conjugation occurred, and thus other characterization techniques are required.

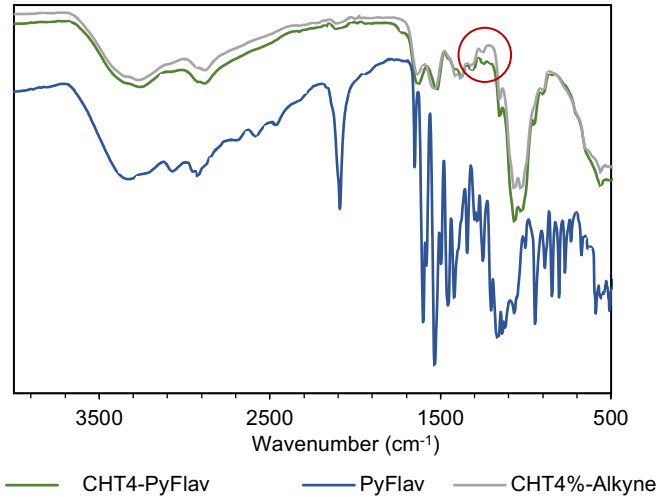

Figure 60: FTR-ATR analysis of the CHT4%-Pyranoflavylium (CHT4-PyFlav) conjugate.

4.2.2. UV-VIS spectroscopy

One important study in this work was the determination of pK_a values of the synthesized dyes and polymer-dye conjugate since it allowed us to check whether the pigment or conjugate has the capacity to change colour with pH variation. As it could be seen in figure 61 there is also the presence of an isosbestic point, however, with less predominance as the isolated pigment, which means that the conjugate's absorbance was lower than that of the isolated pigment. In the same figure it is also depicted the results of the titration performed on the CHT4%-PyFlav conjugate in Acetate Buffer (pH 3.6 at 2.7 mg/mL). The spectrophotometer blank was conducted with simply Acetate Buffer pH 3.6, and the titration was performed using a previously prepared 5 M NaOH solution. Buffer acetate was prepared according to previously published work [73].

It was tried the same method used to study the acidity constants of the free dye which is performed using 1 mL of 75% EtOH 0.1M HCl, 1 mL of stock solution and 1 mL of universal buffer pH 1 as seen previously, however this method did not work, since the Chitosan-Pyranoflavylium conjugate precipitated in the cuvette, when adding the NaOH solution, before reaching the equivalence point. Using the Acetate Buffer in this experiment, the same thing happens, however after the turning point of the conjugate,

which allowed to determine the pK_a value of this conjugate. Figure 62 depicts the results received after fitting the values acquired and then using the excel solver function.

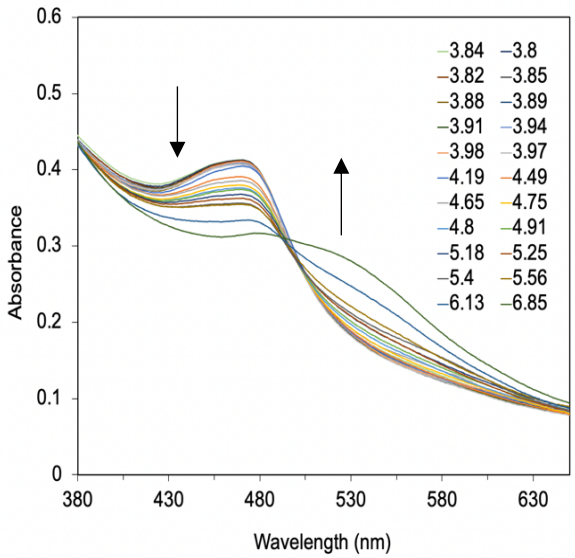

Figure 61: Maximum absorbance measurements using a UV-VIS spectrophotometer at several pH values of the Chitosan-Pyranoflavylium conjugate.

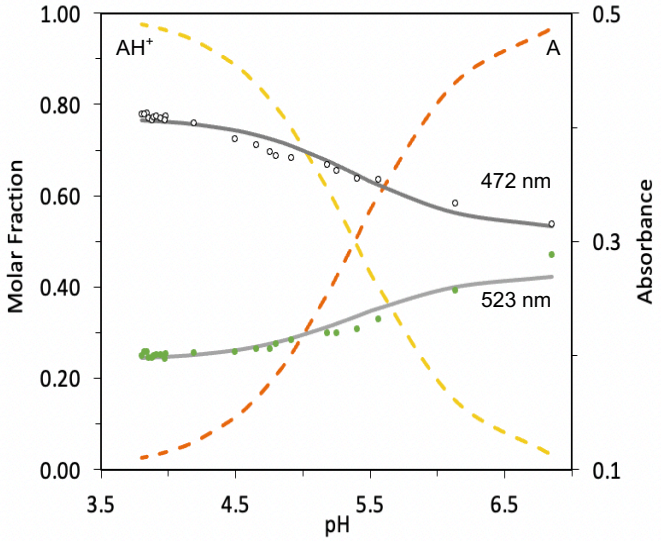

Figure 62: Achieved fitting of pKa using solver function of the Chitosan-Pyranoflavylium conjugate.

As the pH values rises the deprotonation of the OH group at the C-4' in the B-ring of the pyranoflavylium will occur converting the cationic species AH^+ to A species, as shown in figure 63. These chemical equilibria resulted in a shift of the colour of the conjugate (from yellow to pale orange) at pK_a value of 5.4.

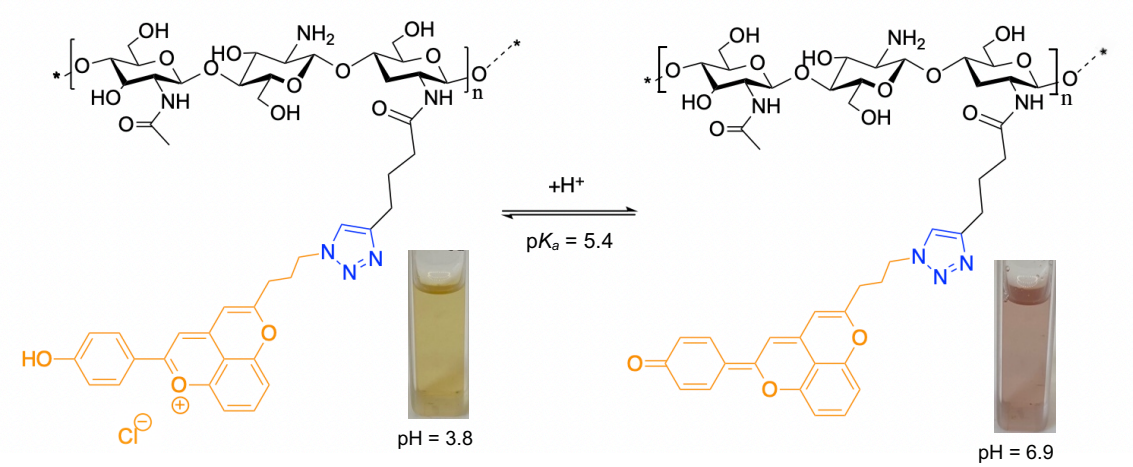

Figure 63: Chemical equilibria of the Pyranoflavylium-Chitosan conjugate with pH variation.

4.2.3. DLS/Zeta Potential analysis

Similar to the analyses performed on the CHT25%-Flavylium conjugate, stock solutions in Acetate Buffer pH 5.5 1 mg/mL were prepared and the samples were analyzed at diluted 0.1 mg/mL. CHT4%-Alkyne has a positive average value of 20.6 ± 0.5 mV, ALG has a negative average charge valued in -24.5 ± 0.4 mV and CHT4%-Pyranoflavylium as a value of 21.8 ± 0.5 mV. Figure 64 shows graphical representation of the obtained values.

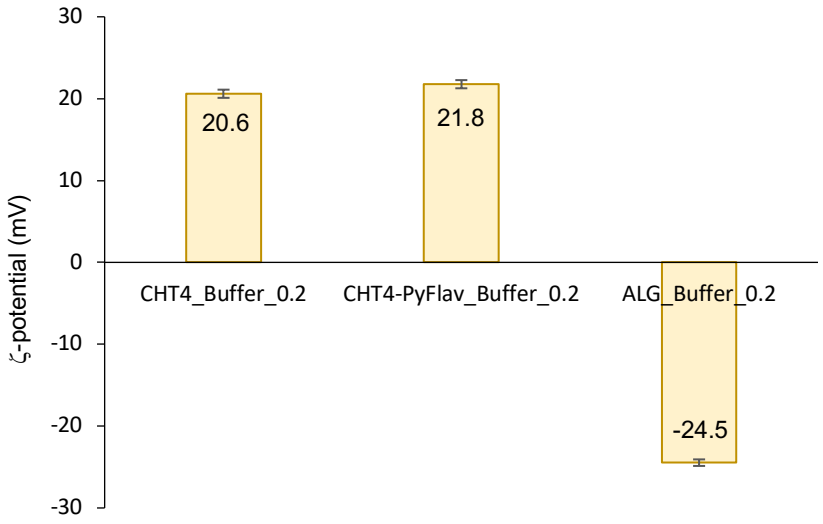

Figure 64: DLS analysis results of the CHT4%-Alkyne (CHT4_Buffer_0.2), CHT4%-Pyranoflavylium (CHT4-PyFlav_Buffer_0.2) conjugate and Alginate (ALG_Buffer_0.2).

It is also important to note that the conjugation of modified Chitosan with the Pyranoflavylium pigment does not significantly change the average charge values, however, it should not present a major problem, since the value of the Pyranoflavylium-Chitosan conjugate and Alginate have practically the same value, however, the average charge of Alginate is negative, as predicted, due to the presence of co-functional groups in this polymer: The more opposite these values are, the greater the electrostatic interaction between the two layers, producing more solid membranes.

5. Fabrication of multi-layered membranes

5.1. QCM-D

The assembly of CHT25%/ALG and CHT25%-Flavylium/ALG multi-layer growth by Layer-by-Layer assembly was investigated in situ using the QCM-D technique, which involves applying solutions containing the polymers consecutively onto a gold coated quartz crystal sensors electrode dissolved in acetate buffer solutions, with a concentration of 0.2 mg/mL at pH 5.5. Two 7-cycle tests were carried out: one with the CHT25%-Alkyne/Alginate as a control and another with CHT25%-Flavylium/Alginate as the film of interest. Between the depositions of both polymers in both tests, rising steps were carried out. Figure 65 shows a diagram of the conditions used in QCM-D.

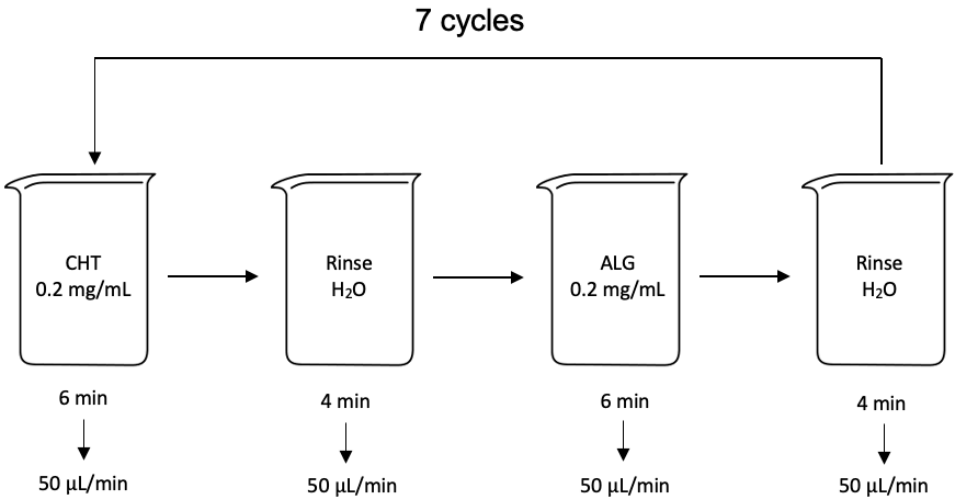

Figure 65: Specific conditions of the QCM-D technique.

CHT25%/ALG membranes

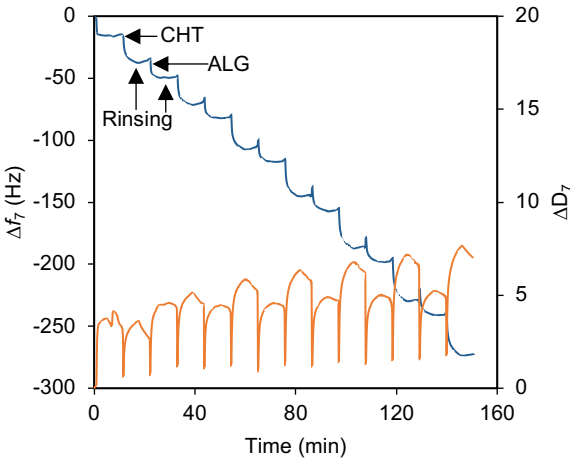

Figure 66: QCM-D monitoring of the control biofilm: Chitosan/Alginate.

CHT25%-Flavylium/ALG membranes

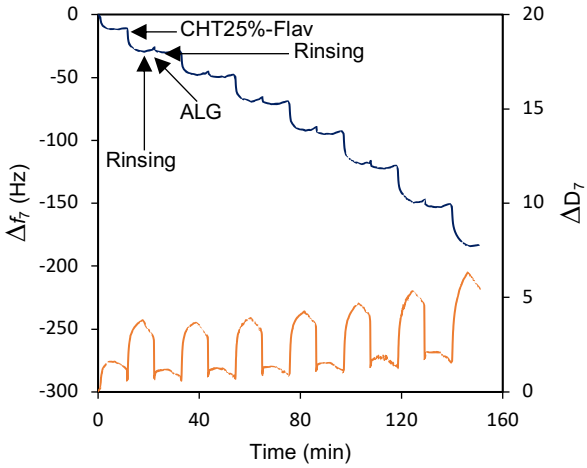

Figure 67: QCM-D monitoring of the functionalized biofilm: Chitosan-Flavylium/Alginate.

The QCM-D approach was used in this work to screen the potential built-up of multi-layered thin coatings of CHT and ALG. This technique detects changes in the hydrodynamic mass of the different layers (ng·cm^{-2}) as a result of the shift of the resonance frequency, but it also measures the viscoelastic characteristics by calculating the expended energy in the mechanical oscillation of the sensors [67].

After the adsorption of each successive material, the development of the multi-layered thin membranes is commonly demonstrated by dropping 50 μL of each solution minute by minute, as demonstrated in figures 66 and 67, witnessing a decrease in the normalized frequency shift (Δf_7) and an increase in the dissipation factor (ΔD_7). This outcome reflects not only the successful deposition of the polymers, resulting in an increase in absorbed mass at each deposition step, but also its effective incorporation and LbL growth. The decrease in frequency (Δf_7) is more pronounced in the control experience (CHT25%/ALG) than in the Chitosan-Flavylium / ALG experiment, indicating that deposition is more effective in the control experiment since the polymers develop stronger electrostatic interactions with each other. Normally, the progressive rise in ΔD_7 demonstrates the viscoelastic nature of the absorbed polymeric layers [82], which was not observable in these studies, concluding these materials could be lacking in viscoelasticity.

5.2. Layer-by-Layer assembly technology (LbL)

The previous experiments results obtained by the QCM-D technique allowed us to conclude the possibility to explore the synthetized conjugates to form membranes. Layer-by-Layer assembly technology was performed with collaboration with COMPASS group of CICECO of University of Aveiro.

This approach was used to deposit polyelectrolytes with opposing charges on a PP subtract. PP is thought to have negative charged surface, allowing it to retain positively charged polymers, for that reason the first dip of the PP substrate is into a positively charged solution which is the CHT25%-Flavylium conjugate solution. To perform this technique, it was used a home-made robot, showed in Figures 68 and 69.

Figure 68: Layer-by-Layer assembly robot, at CICECO – University of Aveiro.

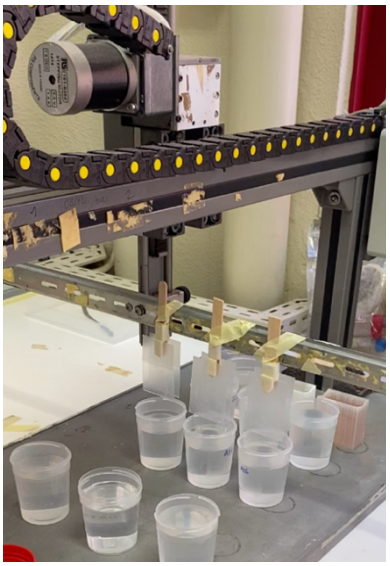

Figure 69: Polypropylene subtract in the dip coating process.

5.2.1. Robot operation

Through the robot is possible to programme the number of cycling, the dipping time and the distance between each sample. The robot was set to perform 200 cycles. Deposition was driven by electrostatic interactions between charged polymers. Electrostatic interaction is achieved by sequentially depositing alternate layers of

positively and negatively charged materials, over the PP substrate. As previously said, Alginate was used as a negatively charged polymer, since COO^- groups are present in its structure, which give it this negative surface charge. As positively charged polymer, the conjugate Chitosan-Flavylium was used, since CHT has only undergone substitution of amine groups by alkynes. To eliminate any polymer solution that is not attached to the substrate between dips, the substrate is rinsed that is carried out with the buffer solution. After the deposition, the free standing-membranes were formed at PP surface which were detached and kept in fridge until further use (figure 70).

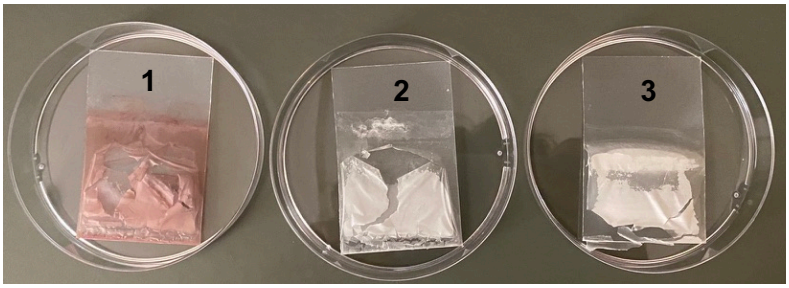

Figure 70: 1 – CHT25%-Flavylium/ALG membrane; 2 – CHT25%/ALG membrane; 3 – CHT/ALG membrane.

5.3. Membranes characterization

After the membrane fabrication, the membranes were characterised, considering their thickness, moisture content and water solubility. All of these analyses were based on previous research [43]. In terms of characterizing them at a deeper level, it was also performed a SEM analysis.

5.3.1. SEM analysis

SEM was used to characterize the morphology of the CHT-Flavylium membranes and also to measure the thickness of several areas. For this analysis to be carried out, pH indicator membranes were previously manufactured using 1 mg/mL solutions, as previously described. The results corroborate the results obtained by QCM-D, where we saw that the electrostatic deposition of the different layers was possible. Figures 71 and 72 present the results obtained by the SEM technique in a 60x and 2300x top view.

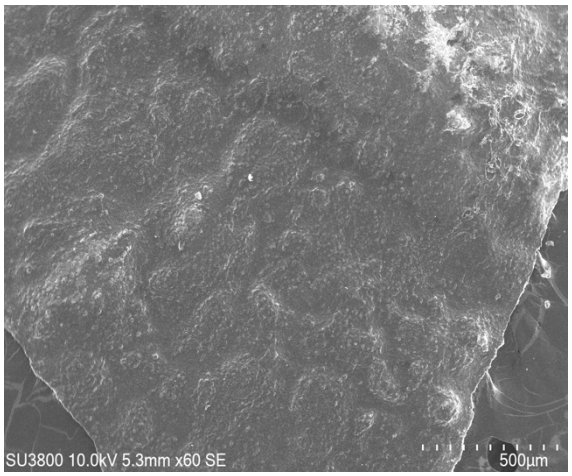

Figure 71: Top view, taken at 60x.

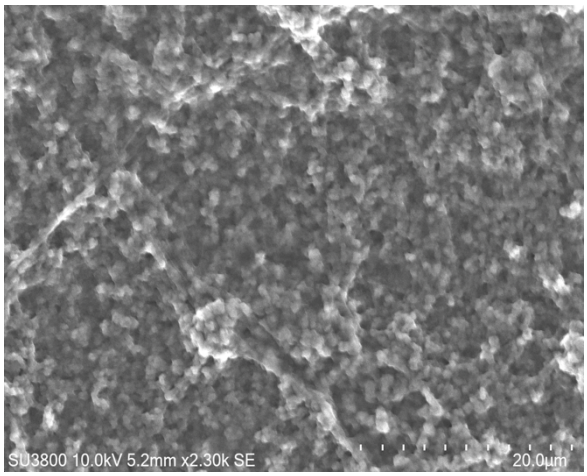

Figure 72: Top view, taken at 2300x.

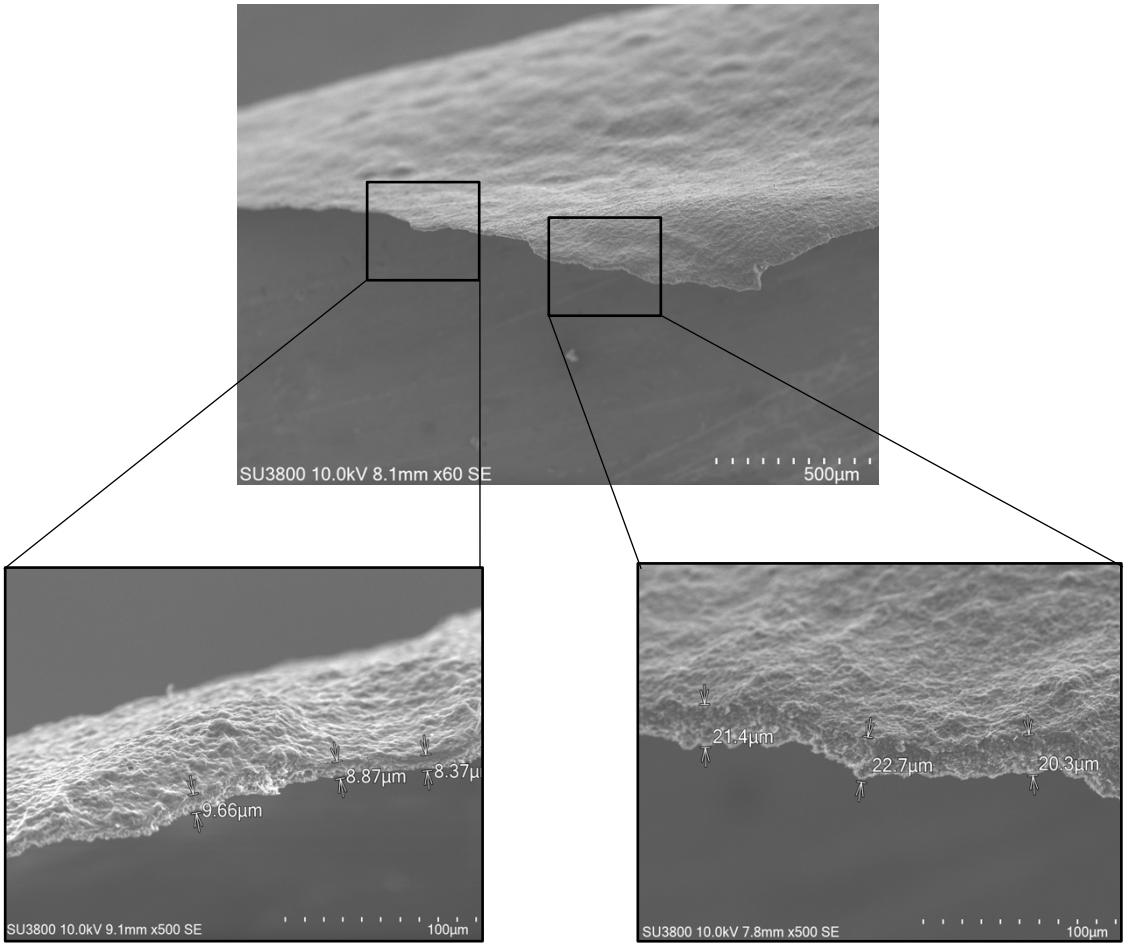

Figure 73: Different areas of the same membrane, emphasizing the different measurements in thickness.

SEM pictures did not show a uniform and homogenous membrane, because the measurements performed showed significant difference in the values obtained between different zones in a same small portion of the membrane (figure 73). This was a foregone conclusion given the small number of bilayers.

5.3.2. Thickness

The used equipment is presented in figure 74. The resulting membranes lack homogeneity since there are parts where more conjugate is kept and areas where there is little retention. The found and presented values, figure 75 and table 5, represent mean between 3 replicates, measured in 10 random positions.

Figure 74: TE 1250-0.1 F, Sauter coating thickness meter, with a CHT25%-Flavylium biofilm.

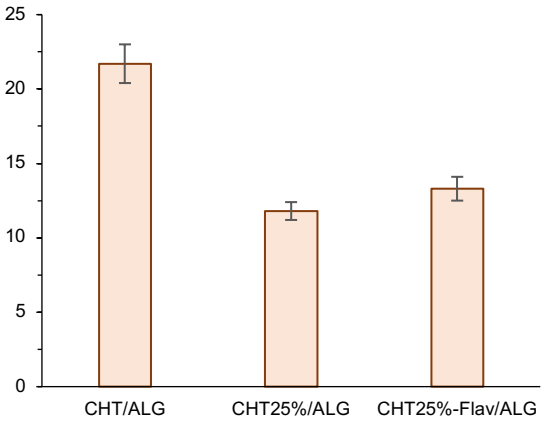

Figure 75: Thickness test results.

Table 5: Obtained numeric thickness values in 3 replicates and measured in 10 random spots with its respective standard error.

	Thickness (μm)
CHT/ALG	21.7 ± 1.3
CHT25%/ALG	11.8 ± 0.6
CHT25%-Flav/ALG	13.3 ± 0.8

As predicted, and comparing to the SEM results, once again it can be concluded that these membranes lack homogeneity, because the thicknesses vary greatly within the same small portion of membrane.

5.3.3. Moisture Content (MC) and Water Solubility (WS)

The parameters were calculated and measured according to the instructions mentioned in section 9, of Experimental Section. Table 6 shows the results obtained in these studies.

Table 6: Moisture Content (MC) and Water solubility (WS) numeric results are respective standard errors.

	MC (%)	WS (%)
CHT/ALG	11.8 ± 2.7	16.3 ± 5.7
CHT25%/ALG	8.0 ± 2.0	54.8 ± 4.3
CHT25%-Flav/ALG	5.3 ± 3.0	61.1 ± 3.5

Unfortunately, it can be concluded that these membranes also lack robustness: many of the membranes broke, particularly the thinnest parts (they do not retain a homogeneous thickness, as previously observed through thickness and SEM studies). The studies for construction of membranes with greater robustness and high homogeneity are ongoing, in order to be able to incorporate them into intelligent packaging.

5.4. Chromatic variation of membranes in buffer solution with different pH values

The goal of this study was to find out if membranes (figure 76) are pH-responsive when exposed to different buffer solutions, if they are resistant to the presence of water, and if their mass change when exposed to these solutions. It is important also to estimate the quantity of pigment that is released out after the membranes have been separated from the PP substrate and immersed in buffer solutions from pH 4-8 (figure 77).

Figure 76: CHT25%-Flavylium membranes.

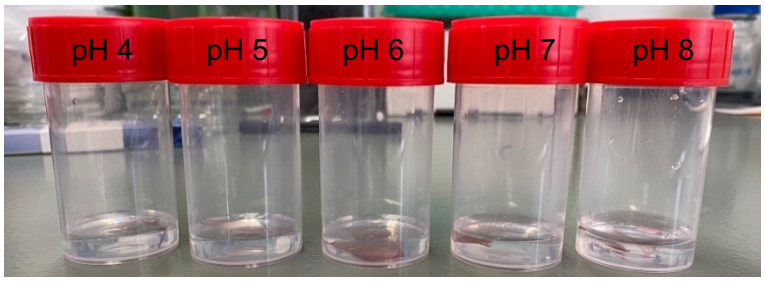

Figure 77: Membranes submerged in buffer solutions of different pH values.

No evident colorimetric change was observed during the first 24 hours, but there was no breakdown or leaching, indicating that the pigment did not release to the buffer solution, which still confirms that flavylium is covalently bonded to chitosan. After 24h, the membranes were taken out of the bottles and the result is shown in figure 78.

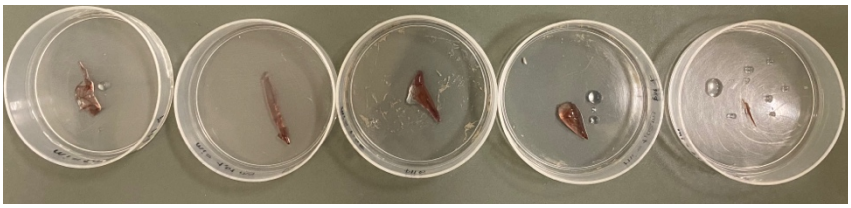

Figure 78: Aspect of membranes after 24 hours of immersion in buffer solutions.

6. Membranes synthesis by casting

In order to compare the membranes synthesized via LbL approach, membranes were also produced by the casting technique, which were already described in several other works. The comparison was performed in terms of thickness, morphology, and effectiveness.

To begin, 10 mg of the CHT25%-Flavylium conjugate and 10 mg of ALG were dissolved in 2% CH_3COOH solutions and Milli-Q H_2O, respectively. These solutions were left to stir for a few hours before being combined and put on petri plates. The plates were dried in a 40 °C oven for 72 h, figure 79. It was prepared two solutions, with the same conditions, except one was supplemented with 30% glycerol, which is a plasticizer agent that proved to be helpful to ensure pH sensor effectiveness elsewhere [43]. The absence of glycerol the higher inter/intramolecular hydrogen bonding in the polymer chain resulting in a tighter net, preventing the penetration of water molecules both in the polymeric chain and in the pigment and, as a result, preventing the interaction of H^+ and OH ions with the film also. As a result, the pigment has greater difficulty interacting with these molecules, inhibiting the film from changing colour in a different environment with varying pH levels. Actually, the presence of plasticizer causes a considerable variation in the thickness and colour of the membranes, the formation of pores, which increased the permeability of the membranes to water as well as the surface contact area [8343].

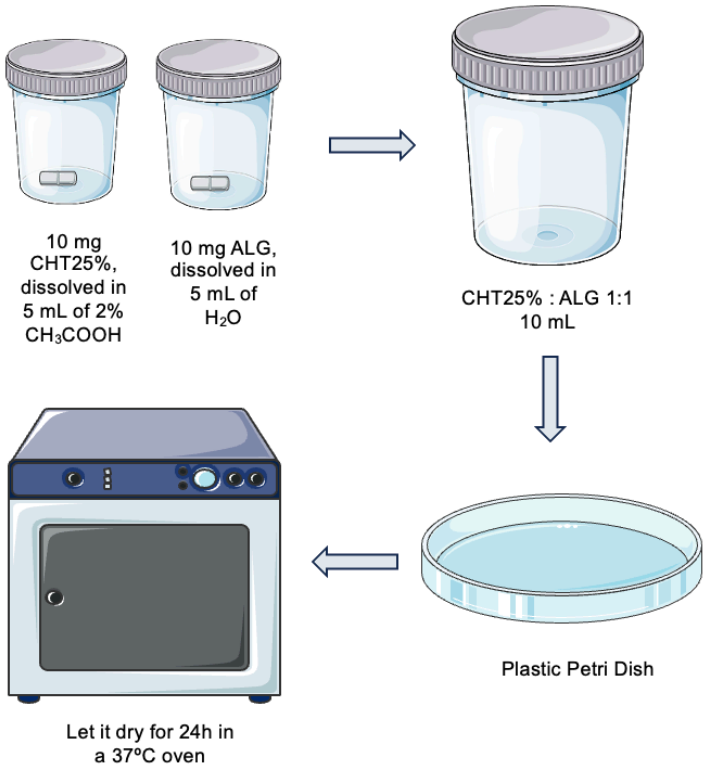

Figure 79: Schematic procedure of casting membranes.

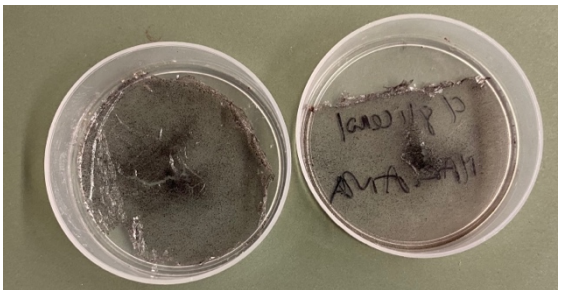

Figure 80: Obtained results: 1) No Glycerol 2) 30% Glycerol.

As we can see, in Figure 80, the membranes obtained by casting were difficult to be detached from the Petri dish, but after some time, small portions were removed and exposed to pH 3.6 and 7 buffer solutions (figure 81).

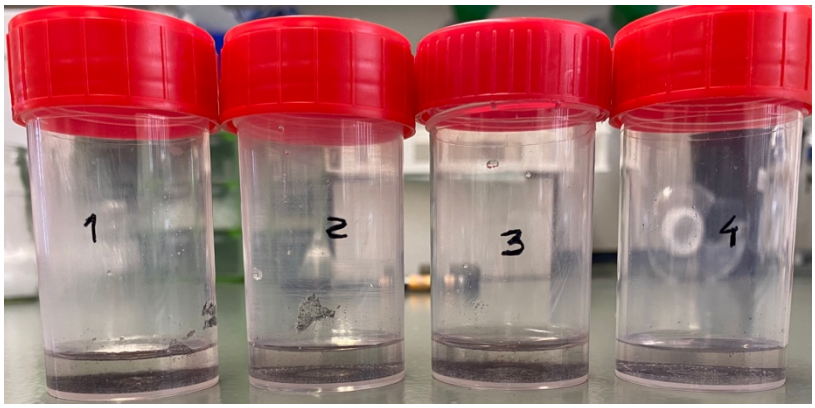

Figure 81: Results obtained after the emergence of membranes in buffer solutions. 1) no glycerol membrane immersed in buffer solution pH 3.6; 2) no glycerol membrane immersed in buffer solution pH 7; 3) 30% glycerol membrane immersed in buffer solution pH 3.6; 4) 30% glycerol membrane immersed in buffer solution pH 7.

It was observed that when the membranes came into touch with the buffer solutions, they instantly disintegrated, suggesting that the casting approach used in these membranes would not be a feasible option since it was not robust enough to be in contact with aqueous solutions, hence, they are not viable to be in contact with an aqueous environment. This highlights the potential of membranes fabricate by LbL to be applicable as smart materials for their use in water-rich environments.

IV. Conclusions

The synthesis of pyrano-3,7-deoxyanthocyanin derivative pigments were successfully performed, with yields between 2-10%. All pigment structures were confirmed and characterized by HPLC, LC-DAD/ESI-MS, FTIR-ATR and ^{1}H NMR. Physical-chemical properties and the pK_a values were also determined through UV-VIS spectroscopy of 4'-azide-5-hydroxy-4-methylflavylium (**3**), 4'-azide-5,7-hydroxyflavylium (**5**) and 10-azidepropyl-4'-hydroxypyranoflavylium (**10**). Compounds (**5**) and (**10**) proved to be of high interest for application as pH indicators membranes for the detection of food spoilage since a change in colour (which means change of the equilibrium state) of the pigments was observed throughout the variation in pH values.

The immobilization of the pigments was performed covalently using Click-Chemistry methodologies and the success of these reactions was confirmed by ^{1}H NMR and FTIR-ATR, mostly by the azide peak decrease and the appearance of the triazole proton peak. Unfortunately, the physical-chemical properties and pK_a values of CHT25%-Flav conjugate were not achieved despite all efforts: the solution containing the conjugate precipitated when pH values raised before the equilibrium point was reached. However, it was possible to determine these parameters for CHT4%-PyFlav conjugate revealing great chromatic variation within the desired pH range. Afterwards, the ability to fabricate multi-layer membranes using the CHT25%-Flav conjugate was evaluated using the QCM-D and DLS techniques, where it was found that the conjugate and the ALG had the potential to establish electrostatic interactions between themselves, thus forming the membrane through LbL assembly technology. After their fabrication, they were characterized by SEM, Thickness, Moisture Content and Water Solubility, where it was concluded that these membranes lack homogeneity most likely due to the scarce layers or due to precipitation of the solution containing the conjugate at the time of construction. When compared to the other techniques, for example casting, the LbL membranes showed a good performance, as they presented satisfactory results, considering their hydrophilic character.

As a general conclusion, it can be stated that the results obtained were satisfactory, since the tasks established to carry out this project were successfully completed, and it was possible to synthesize these membranes despite the difficulties encountered.

V. Future perspectives

The main objective of this project was the development of flavylium-based multi-layered membranes and to study their chromatic properties for application as pH sensors in smart food packaging. In future work, it is pretended to optimize all the syntheses carried out during this work, so that their yield and purity can be improved and the application of these techniques can be implemented by the industry. Another goal is to screen and synthesize other high valuable flavylium-based pigments and conjugates with different biopolymers.

Due to the promising results obtained for the CHT4%-PyFlav conjugate, it is pretended to study the experimental conditions of the LbL fabrication process in order to produce robust CHT4%-PyFlav/ALG membranes, which because of lack of time, it was not possible to pursue. Therefore, it is pretended to conduct a systematic study of the LbL conditions namely polymer concentrations, deposition time, number of cycles, among others. Then, FTIR, SEM analysis, swelling index studies, mechanical properties, and barrier tests, that were not considered so far, will be carried out.

The last step would be to test the flavylium-based membranes on real samples (milk, meats, fish) to validate their pH responsiveness. Then, it will be important to create partnerships with food industry players to implement new ways of creating smart packaging, where they can provide us with their products to carry out the final studies.

References

(1) Bertelli, A.; Biagi, M.; Corsini, M.; Baini, G.; Cappellucci, G.; Miraldi, E. Polyphenols: From Theory to Practice. *Foods* 2021, 10(11), 2595. https://doi.org/10.3390/foods10112595.

(2) Pandey, K. B.; Rizvi, S. I. Plant Polyphenols as Dietary Antioxidants in Human Health and Disease. *Oxidative Medicine and Cellular Longevity* 2009, 2 (5), 270–278. https://doi.org/10.4161/oxim.2.5.9498

(3) Libro, R.; Giacoppo, S.; Rajan, T. S.; Bramanti, P.; Mazzon, E. Natural Phytochemicals in the Treatment and Prevention of Dementia: An Overview. *Molecules* 2016, 21(4), 518. https://doi.org/10.3390/molecules21040518.

(4) Bhosale, P. B.; Ha, S. E.; Vetrivel, P.; Kim, H. H.; Kim, S. M.; Kim, G. S. Functions of Polyphenols and Its Anticancer Properties in Biomedical Research: A Narrative Review. *Translational Cancer Research* 2020, 9(12), 7619–7631. https://doi.org/10.21037/tcr-20-2359.

(5) Michalska, M., Gluba, A., Mikhailidis, D. P., Nowak, P., Bielecka-Dabrowa, A., Rysz, J., & Banach, M. (2010). The role of polyphenols in cardiovascular disease. *Medical science monitor : international medical journal of experimental and clinical research*, 2020, 16(5), RA110–RA119.

(6) Sun, C.; Zhao, C.; Guven, E. C.; Paoli, P.; Simal-Gandara, J.; Ramkumar, K. M.; Wang, S.; Buleu, F.; Pah, A.; Turi, V.; Damian, G.; Dragan, S.; Tomas, M.; Khan, W.; Wang, M.; Delmas, D.; Portillo, M. P.; Dar, P.; Chen, L.; Xiao, J. Dietary Polyphenols as Antidiabetic Agents: Advances and Opportunities. *Food Frontiers* 2020, 1(1), 18–44. https://doi.org/10.1002/fft2.15.

(7) Wang, S.; Moustaid-Moussa, N.; Chen, L.; Mo, H.; Shastri, A.; Su, R.; Bapat, P.; Kwun, I. S.; Shen, C. L. Novel Insights of Dietary Polyphenols and Obesity. *Journal of Nutritional Biochemistry* 2014, 25(1), 1–18. https://doi.org/10.1016/j.jnutbio.2013.09.001.

(8) Bhullar, K. S.; Rupasinghe, H. P. V. Polyphenols: Multipotent Therapeutic Agents in Neurodegenerative Diseases. *Oxidative Medicine and Cellular Longevity* 2013, 2013, 1–18. https://doi.org/10.1155/2013/891748.

(9) De, L. A.; Alvarez-Parrilla, E.; González-Aguilar, G. A. Fruit and Vegetable Phytochemicals : Chemistry, Nutritional Value and Stability; Wiley-Blackwell: Ames (Iowa), 2009.

(10) Šamec, D.; Karalija, E.; Šola, I.; Vujčić Bok, V.; Salopek-Sondi, B. The Role of Polyphenols in Abiotic Stress Response: The Influence of Molecular Structure. *Plants* 2021, 10(1), 118. https://doi.org/10.3390/plants10010118.

(11) Garrido, J.; Borges, F. Wine and Grape Polyphenols - A Chemical Perspective. *Food Research International*. 2013, 54(2), 1844–1858. https://doi.org/10.1016/j.foodres.2013.08.002.

(12) Khoo, H. E.; Azlan, A.; Tang, S. T.; Lim, S. M. Anthocyanidins and Anthocyanins: Colored Pigments as Food, Pharmaceutical Ingredients, and the Potential Health Benefits. *Food & Nutrition Research* 2017, 61 (1), 1361779. https://doi.org/10.1080/16546628.2017.1361779.

(13) Khoo, H. E.; Azlan, A.; Tang, S. T.; Lim, S. M. Anthocyanidins and Anthocyanins: Colored Pigments as Food, Pharmaceutical Ingredients, and the Potential Health Benefits. *Food & Nutrition Research* 2017, 61 (1), 1361779. https://doi.org/10.1080/16546628.2017.1361779.

(14) Pina, F.; Melo, M. J.; Laia, C. A. T.; Parola, A. J.; Lima, J. C. Chemistry and Applications of Flavylium Compounds: A Handful of Colours. *Chemistry Society Review* 2012, *41* (2), 869–908. https://doi.org/10.1039/c1cs15126f.

(15) Castañeda-Ovando, A.; Pacheco-Hernández, M. de L.; Páez-Hernández, M. E.; Rodríguez, J. A.; Galán-Vidal, C. A. Chemical Studies of Anthocyanins: A Review. *Food Chemistry* 2009, 113(4), 859–871. https://doi.org/10.1016/j.foodchem.2008.09.001.

(16) Dangles, O.; Fenger, J. A. The Chemical Reactivity of Anthocyanins and Its Consequences in Food Science and Nutrition. *Molecules* 2018, 13(8). https://doi.org/10.3390/molecules23081970.

(17) Turturică, M.; Oancea, A. M.; Râpeanu, G. Anthocyanins: naturally occurring fruit pigments with functional properties. *Food Technology* 2015, 39(1), 9-24. Corpus ID: 100513018.

(18) Castañeda-Ovando, A.; Pacheco-Hernández, M. de L.; Páez-Hernández, M. E.; Rodríguez, J. A.; Galán-Vidal, C. A. Chemical Studies of Anthocyanins: A Review. *Food Chemistry* 2009, 113(4), 859–871. https://doi.org/10.1016/j.foodchem.2008.09.001.

(19) Qian, B. J.; Liu, J. H.; Zhao, S. J.; Cai, J. X.; Jing, P. The Effects of Gallic/Ferulic/Caffeic Acids on Colour Intensification and Anthocyanin Stability. *Food Chemistry* 2017, *228*, 526–532. https://doi.org/10.1016/j.foodchem.2017.01.120.

(20) Rytel, E.; Tajner-Czopek, A.; Kita, A.; Kucharska, A. Z.; Sokół-Łętowska, A.; Hamouz, K. Content of Anthocyanins and Glycoalkaloids in Blue-Fleshed Potatoes and Changes in the Content of α-Solanine and α-Chaconine during Manufacture of Fried and Dried Products. *International Journal of Food Science Technology* 2018, *53* (3), 719–727. https://doi.org/10.1111/ijfs.13647.

(21) Furtado, P.; Figueiredo, P.; Chaves das Neves, H.; Pina, F. Photochemical and Thermal Degradation of Anthocyanidins. *Journal of Photochemistry and Photobiology A: Chemistry* 1993, 75 (2), 113–118. https://doi.org/10.1016/1010-6030(93)80191-b

(22) Berké, B.; Chèze, C.; Vercauteren, J.; Deffieux, G. Bisulfite Addition to Anthocyanins: Revisited Structures of Colourless Adducts. *Tetrahedron Letters* 1998, 39 (32), 5771–5774. https://doi.org/10.1016/s0040-4039(98)01205-2.

(23) Arias, N.; Teresa, · M; Leixuri, M. ·; Iñaki, A. ·; María, M. ·; Portillo, P. The Combination of Resveratrol and Quercetin Enhances the Individual Effects of These Molecules on Triacylglycerol Metabolism in White Adipose Tissue. *European Journal of Nutrition* 2015, *55(1)*, 341–348. https://doi.org/10.1007/s00394-015-0854-9.

(24) Teissedre, P. L.; Jourdes, M. Tannins and Anthocyanins of Wine: Phytochemistry and Organoleptic Properties. Natural Products: Phytochemistry, Botany and Metabolism of Alkaloids, Phenolics and

Terpenes; *Springer Berlin Heidelberg* 2013; 2255–2274. https://doi.org/10.1007/978-3-642-22144-6_73.

(25) Dufourc, E. J. Wine Tannins, Saliva Proteins and Membrane Lipids. *Biochimica et Biophysica Acta - Biomembranes*. 2021, 1863(10), 183670. https://doi.org/10.1016/j.bbamem.2021.183670.

(26) Thompson, R. S.; Jacques, D.; Haslam, E.; Tanner, R. J. N. Plant Proanthocyanidins. Part I. Introduction; the Isolation, Structure, and Distribution in Nature of Plant Procyanidins. *Journal of Chemistry Society, Perkin Transactions* 1972, *1*, 1387. https://doi.org/10.1039/p19720001387.

(27) Liu, S.; Laaksonen, O.; Yang, W.; Zhang, B.; Yang, B. Pyranoanthocyanins in Bilberry (Vaccinium Myrtillus L.) Wines Fermented with Schizosaccharomyces Pombe and Their Evolution during Aging. Food Chemistry 2020, 305, 125438–125438. https://doi.org/10.1016/j.foodchem.2019.125438.

(28) Cruz, L.; Teixeira, N.; Silva, A. M. S.; Mateus, N.; Borges, J.; Freitas, V. de. Role of Vinylcatechin in the Formation of Pyranomalvidin-3-Glucoside−(+)-Catechin. *Journal of Agricutural and Food Chemistry* 2008, 56(22), 10980–10987. https://doi.org/10.1021/jf8021496.

(29) Rentzsch, M.; Schwarz, M.; Winterhalter, P.; Blanco-Vega, D.; Hermosín-Gutiérrez, I. Survey on the Content of Vitisin A and Hydroxyphenyl-Pyranoanthocyanins in Tempranillo Wines. *Food Chemistry* 2010, *119* (4), 1426–1434. https://doi.org/10.1016/j.foodchem.2009.09.023.

(30) Gomes, V.; Pires, A. S.; Fernandes, I.; Mateus, N.; de Freitas, V.; Cruz, L. Synthesis of Novel Pyrano-3,7-Deoxyanthocyanin Derivatives and Study of Their Thermodynamic, Photophysical and Cytotoxicity Properties. *Journal of Photochemistry and Photobiology A: Chemistry* 2021, *415*. https://doi.org/10.1016/j.jphotochem.2021.113313.

(31) Sousa, J. L. C.; Gomes, V.; Mateus, N.; Pina, F.; de Freitas, V.; Cruz, L. Synthesis and Equilibrium Multistate of New Pyrano-3-Deoxyanthocyanin-Type Pigments in Aqueous Solutions. *Tetrahedron* 2017, *73* (41), 6021–6030. https://doi.org/10.1016/j.tet.2017.08.051.

(32) Rentzsch, M.; Schwarz, M.; Winterhalter, P. Pyranoanthocyanins – an Overview on Structures, Occurrence, and Pathways of Formation. *Trends in Food Science & Technology* 2007, 18 (10), 526–534. https://doi.org/10.1016/j.tifs.2007.04.014.

(33) Balasubramanian, R.; Kumutha, • K; Sarojadevi, • M; Sarojadevi, M. Mechanical, Thermal and Electrical Properties of Polyimides Containing 1, 2, 3-Triazole Ring Prepared by Click Reaction. *Polymer Bulletin* 2016, *73(2)*, 309–330. https://doi.org/10.1007/s00289-015-1488-z.

(34) Kappe, C. O.; Van der Eycken, E. Click Chemistry under Non-Classical Reaction Conditions. *Chemistry Society Reviews* 2010, 39 (4), 1280–1290. https://doi.org/10.1039/b901973c.

(35) Rojas-Sánchez, L.; Sokolova, V.; Riebe, S.; Voskuhl, J.; Epple, M. Covalent Surface Functionalization of Calcium Phosphate Nanoparticles with Fluorescent Dyes by Copper-Catalysed and by Strain-Promoted Azide-Alkyne Click Chemistry. *ChemNanoMat* 2019, *5* (4), 436–446. https://doi.org/10.1002/cnma.201800509.

(36) Nwe, K.; Brechbiel, M. W. Growing Applications of “Click Chemistry” for Bioconjugation in Contemporary Biomedical Research. Cancer Biotherapy and Radiopharmaceuticals 2009, 24 (3), 289–302. https://doi.org/10.1089/cbr.2008.0626.

(37) Worrell, B. T.; Malik, J. A.; Fokin, V. V. Direct Evidence of a Dinuclear Copper Intermediate in Cu(I)-Catalyzed Azide-Alkyne Cycloadditions. *Science* 2013, *340* (6131), 457–460. https://doi.org/10.1126/science.1229506.

(38) Ahlquist, M.; Fokin, V. V. Enhanced Reactivity of Dinuclear Copper(I) Acetylides in Dipolar Cycloadditions. *Organometallics* 2007, *26* (18), 4389–4391. https://doi.org/10.1021/om700669v.

(39) Himo, F.; Lovell, T.; Hilgraf, R.; Rostovtsev, V. V.; Noodleman, L.; Sharpless, K. B.; Fokin, V. V. Copper(I)-Catalyzed Synthesis of Azoles. DFT Study Predicts Unprecedented Reactivity and Intermediates. *Journal of the American Chemical Society* 2005, *127* (1), 210–216. https://doi.org/10.1021/ja0471525.

(40) Jankovič, D.; Virant, M.; Gazvoda, M. Copper-Catalyzed Azide-Alkyne Cycloaddition of Hydrazoic Acid Formed in Situ from Sodium Azide Affords 4-Monosubstituted-1,2,3-Triazoles. *Journal of Organic Chemistry* 2022, *87* (6), 4018–4028. https://doi.org/10.1021/acs.joc.1c02775.

(41) Wu, C.; Li, Y.; Sun, J.; Lu, Y.; Tong, C.; Wang, L.; Yan, Z.; Pang, J. Novel Konjac Glucomannan Films with Oxidized Chitin Nanocrystals Immobilized Red Cabbage Anthocyanins for Intelligent Food Packaging. *Food Hydrocolloids* 2020, *98, 105245*. https://doi.org/10.1016/j.foodhyd.2019.105245.

(42) Zhao, L.; Liu, Y.; Zhao, L.; Wang, Y. Anthocyanin-Based PH-Sensitive Smart Packaging Films for Monitoring Food Freshness. *Journal of Agriculture and Food Research* 2022, 9, 100340. https://doi.org/10.1016/j.jafr.2022.100340

(43) Gomes, V.; Pires, A. S.; Mateus, N.; de Freitas, V.; Cruz, L. Pyranoflavylium-Cellulose Acetate Films and the Glycerol Effect towards the Development of PH-Freshness Smart Label for Food Packaging. *Food Hydrocolloids* 2022, 127, 107501. https://doi.org/10.1016/j.foodhyd.2022.107501.

(44) Pires, A. S.; Gomes, V.; Neves, D.; Mateus, N.; de Freitas, V.; Cruz, L. Colorimetric PH-Responsive Biomaterials Based on Pyranoflavylium-Biopolymer Hybrid Conjugates. *ACS Applied Polymer Materials* 2022, 4 (7), 4961–4971. https://doi.org/10.1021/acsapm.2c00514.

(45) Namazi, H. Polymers in Our Daily Life. *BioImpacts*. Tabriz University of Medical Sciences 2017, 7(2), 73–74. https://doi.org/10.15171/bi.2017.09.

(46) Lee, K. Y.; Mooney, D. J. Alginate: Properties and Biomedical Applications. *Progress in Polymer Science* 2012, 37 (1), 106–126. https://doi.org/10.1016/j.progpolymsci.2011.06.003.

(47) Li, P.; Dai, Y.-N.; Zhang, J.-P.; Wang, A.-Q.; Wei, Q. Chitosan-Alginate Nanoparticles as a Novel Drug Delivery System for Nifedipine. International Journal of Biomedical Science 2008, 4(3), 221-228. PMID: 23675094.

(48) Grøndahl, L.; Lawrie, G.; Anitha, A.; Shejwalkar, A. Applications of Alginate Biopolymer in Drug Delivery. *Biointegration of Medical Implant Materials* 2019, 375–403. https://doi.org/10.1016/B978-0-08-102680-9.00014-7.

(49) Brownlee, I. A.; Allen, A.; Pearson, J. P.; Dettmar, P. W.; Havler, M. E.; Atherton, M. R.; Onsøyen, E. Alginate as a Source of Dietary Fiber. *Critical Reviews in Food Science and Nutrition* 2005, 45 (6), 497–510. https://doi.org/10.1080/10408390500285673.

(50) Kuo, C. K.; Ma, P. X. Ionically Crosslinked Alginate Hydrogels as Scaffolds for Tissue Engineering: Part 1. Structure, Gelation Rate and Mechanical Properties. *Biomaterials* 2001, 22 (6), 511–521. https://doi.org/10.1016/s0142-9612(00)00201-5.

(51) Lee, K. Y.; Mooney, D. J. Alginate: Properties and Biomedical Applications. *Progress in Polymer Science* 2012, 37 (1), 106–126. https://doi.org/10.1016/j.progpolymsci.2011.06.003.

(52) Dekamin, M. G.; Peyman, S. Z.; Karimi, Z.; Javanshir, S.; Naimi-Jamal, M. R.; Barikani, M. Sodium Alginate: An Efficient Biopolymeric Catalyst for Green Synthesis of 2-Amino-4H-Pyran Derivatives. *International Journal of Biological Macromolecules* 2016, 87, 172–179. https://doi.org/10.1016/j.ijbiomac.2016.01.080. .

(53) Mohammadi, A.; Daemi, H.; Barikani, M. Fast Removal of Malachite Green Dye Using Novel Superparamagnetic Sodium Alginate-Coated Fe_3O_4 Nanoparticles. *International Journal of Biological Macromolecules* 2014, *69*, 447–455. https://doi.org/10.1016/j.ijbiomac.2014.05.042.

(54) Bierhalz, A. C. K.; da Silva, M. A.; Kieckbusch, T. G. Natamycin Release from Alginate/Pectin Films for Food Packaging Applications. *Journal of Food Engineering* 2012, *110* (1), 18–25. https://doi.org/10.1016/j.jfoodeng.2011.12.016.

(55) Lee, K. Y.; Mooney, D. J. Alginate: Properties and Biomedical Applications. *Progress in Polymer Science* 2012, 37 (1), 106–126. https://doi.org/10.1016/j.progpolymsci.2011.06.003.

(56) Nilsen-Nygaard, J.; Strand, S. P.; Vårum, K. M.; Draget, K. I.; Nordgård, C. T. Chitosan: Gels and Interfacial Properties. *Polymers*. 2015, 7(3), 552–579. https://doi.org/10.3390/polym7030552.

(57) Cheung, R. C. F.; Ng, T. B.; Wong, J. H.; Chan, W. Y. Chitosan: An Update on Potential Biomedical and Pharmaceutical Applications. *Marine Drugs* 2015, 13(8), 5156–5186. https://doi.org/10.3390/md13085156.

(58) Ressler, A. Chitosan-Based Biomaterials for Bone Tissue Engineering Applications: A Short Review. *Polymers* 2022, 14(16), 3430. https://doi.org/10.3390/polym14163430.

(59) Morin-Crini, N.; Lichtfouse, E.; Torri, G.; Crini, G. Applications of Chitosan in Food, Pharmaceuticals, Medicine, Cosmetics, Agriculture, Textiles, Pulp and Paper, Biotechnology, and Environmental Chemistry. *Environmental Chemistry Letters* 2019, 17(4), 1667–1692. https://doi.org/10.1007/s10311-019-00904-x.

(60) Zhang, M.; Zhang, F.; Li, C.; An, H.; Wan, T.; Zhang, P. Application of Chitosan and Its Derivative Polymers in Clinical Medicine and Agriculture. *Polymers* 2022, 14(5), 958. https://doi.org/10.3390/polym14050958.

(61) Kedir, W. M.; Abdi, G. F.; Goro, M. M.; Tolesa, L. D. Pharmaceutical and Drug Delivery Applications of Chitosan Biopolymer and Its Modified Nanocomposite: A Review. *Heliyon* 2022, 8(8), 10196. https://doi.org/10.1016/j.heliyon.2022.e10196.

(62) Shariatinia, Z. Pharmaceutical Applications of Chitosan. *Advances in Colloid and Interface Science* 2019, 263, 131–194. https://doi.org/10.1016/j.cis.2018.11.008.

(63) Kumar, M. N. V. R. A Review of Chitin and Chitosan Applications. *Reactive and Functional Polymers* 2000, 46(1), 1-27. https://doi.org/10.1016/S1381-5148(00)00038-9.

(64) Amaral, I. F.; Cordeiro, A. L.; Sampaio, P.; Barbosa, M. A. Attachment, Spreading and Short-Term Proliferation of Human Osteoblastic Cells Cultured on Chitosan Films with Different Degrees of Acetylation. *Journal of Biomaterials Science Polymer Edition* 2007, *18* (4), 469–485. https://doi.org/10.1163/156856207780425068.

(65) Lieder, R.; Darai, M.; Örlygsson, G.; Sigurjonsson, O. E. Solution Casting of Chitosan Membranes for in Vitro Evaluation of Bioactivity. *Biological Procedures Online* 2013, 15 (1), 11. https://doi.org/10.1186/1480-9222-15-11.

(66) Qu, B.; Luo, Y. A Review on the Preparation and Characterization of Chitosan-Clay Nanocomposite Films and Coatings for Food Packaging Applications. *Carbohydrate Polymer Technologies and Applications* 2021, 2(3), 100102. https://doi.org/10.1016/j.carpta.2021.100102.

(67) Monteiro, L. P. G.; Borges, J.; Rodrigues, J. M. M.; Mano, J. F. Unveiling the Assembly of Neutral Marine Polysaccharides into Electrostatic-Driven Layer-by-Layer Bioassemblies by Chemical Functionalization. *Marine Drugs* 2023, *21* (2), 92-92. https://doi.org/10.3390/md21020092.

(68) Cazorla-Luna, R.; Martín-Illana, A.; Notario-Pérez, F.; Ruiz-Caro, R.; Veiga, M. D. Naturally Occurring Polyelectrolytes and Their Use for the Development of Complex-Based Mucoadhesive Drug Delivery Systems: An Overview. *Polymers* 2021, 13(14), 2241. https://doi.org/10.3390/polym13142241.

(69) da Silva Júnior, W. F.; de Oliveira Pinheiro, J. G.; Moreira, C. D. L. F. A.; de Souza, F. J. J.; de Lima, Á. A. N. Alternative Technologies to Improve Solubility and Stability of Poorly Water-Soluble Drugs. *Multifunctional Systems for Combined Delivery, Biosensing and Diagnostics* 2017, 281–305. https://doi.org/10.1016/B978-0-323-52725-5.00015-0.

(70) Cruz, L.; Basílio, N.; de Freitas, V. Color Stabilization of Cyanidin-3-Glucoside-Based Dyes by Encapsulation with Biocompatible PEGylated Phospholipid Micelles. *Dyes and Pigments* 2020, 181, 108592. https://doi.org/10.1016/j.dyepig.2020.108592.

(71) Gomes, V.; Mateus, N.; De Freitas, V.; Cruz, L. Synthesis and Structural Characterization of a Novel Symmetrical 2,10-Bis-Styryl-1-Benzopyrylium Dye. *Synlett* 2018, *29* (10), 1390–1394. https://doi.org/10.1055/s-0036-1591978.

(72) Küster, F. W.; A. Thiel. Tabelle per Le Analisi Chimiche e Chimico-Fisiche. *Hoepli,* 1982, 12th edn. ISBN: 978-88-203-2357-8.

(73) AAT Bioquest. Acetate Buffer (pH 3.6 to 5.6) Preparation and Recipe | AAT Bioquest. Aatbio.com. https://www.aatbio.com/resources/buffer-preparations-and-recipes/acetate-buffer-ph-3-6-to-5-6.

(74) Perrin, C. L.; Chang, K. L. The Complete Mechanism of an Aldol Condensation. *Journal of Organic Chemistry* 2016, *81* (13), 5631–5635. https://doi.org/10.1021/acs.joc.6b00959.

(75) Gomes, V.; Guimarães, M.; Gonçalves, G.; de Freitas, V.; Cruz, L. Bioinspired Synthesis and Physical-Chemical Properties of a New 10-Methylpyrano-4′-Hydroxyflavylium Chloride Salt. *Synlett* 2020, *31* (4), 334–338. https://doi.org/10.1055/s-0039-1690744.

(76) Gomes, V.; Pires, A. S.; Fernandes, I.; Mateus, N.; de Freitas, V.; Cruz, L. Synthesis of Novel Pyrano-3,7-Deoxyanthocyanin Derivatives and Study of Their Thermodynamic, Photophysical and Cytotoxicity Properties. *Journal of Photochemistry and Photobiology A: Chemistry* 2021, *415*. https://doi.org/10.1016/j.jphotochem.2021.113313.

(77) Berland, H.; Andersen, Ø. M. Characterization of a Natural, Stable, Reversible and Colourful Anthocyanidin Network from Sphagnum Moss Based Mainly on the Yellow Trans-Chalcone and Red Flavylium Cation Forms. *Molecules* 2021, *26* (3), 709. https://doi.org/10.3390/molecules26030709.

(78) Sousa, J. L. C.; Gomes, V.; Mateus, N.; Pina, F.; de Freitas, V.; Cruz, L. Synthesis and Equilibrium Multistate of New Pyrano-3-Deoxyanthocyanin-Type Pigments in Aqueous Solutions. *Tetrahedron* 2017, *73* (41), 6021–6030. https://doi.org/10.1016/j.tet.2017.08.051.

(79) Pandey, P.; Farha, O. K.; Spokoyny, A. M.; Mirkin, C. A.; Kanatzidis, M. G.; Hupp, J. T.; Nguyen, S. T. A “Click-Based” Porous Organic Polymer from Tetrahedral Building Blocks. *Journal of Material Chemistry* 2011, *21* (6), 1700–1703. https://doi.org/10.1039/c0jm03483e.

(80) Mungalpara, D.; Kelm, H.; Valkonen, A.; Rissanen, K.; Keller, S.; Kubik, S. Oxoanion Binding to a Cyclic Pseudopeptide Containing 1,4-Disubstituted 1,2,3-Triazole Moieties. *Organic Biomolecule Chemistry* 2017, *15* (1), 102–113. https://doi.org/10.1039/C6OB02172G.

(81) Liu, Z.; Liao, Q.; Yang, D.; Gao, Y.; Luo, X.; Lei, Z.; Li, H. Well-Defined Poly(N-Isopropylacrylamide) with a Bifunctional End-Group: Synthesis, Characterization, and Thermoresponsive Properties. *Des Monomers Polymers* 2013, *16* (5), 465–474. https://doi.org/10.1080/15685551.2012.747165.

(82) Marx, K. A. Quartz Crystal Microbalance: A Useful Tool for Studying Thin Polymer Films and Complex Biomolecular Systems at the Solution - Surface Interface. *Biomacromolecules* 2003, 4(5), 1099–1120. https://doi.org/10.1021/bm020116i.

(83) Ardila-Diaz, L. D.; de Oliveira, T. V.; Soares, N. de F. F. Development and Evaluation of the Chromatic Behavior of an Intelligent Packaging Material Based on Cellulose Acetate Incorporated with Polydiacetylene for an Efficient Packaging. *Biosensors (Basel)* 2020, *10* (6), 59. https://doi.org/10.3390/bios10060059.